Spring 1996

Observation of Shelfwater Overrunning the Southern Slope Sea

Ajoy Kumar
Old Dominion University

OBSERVATION OF SHELFWATER OVERRUNNING THE SOUTHERN SLOPE SEA

by

Ajoy Kumar
Master of Science, 1987
University of Madras, India
Bachelor of Science, July, 1985
University of Madras, India

A Dissertation submitted to the Faculty of
Old Dominion University in Partial Fulfillment of the
Requirements for the Degree of

DOCTOR OF PHILOSOPHY

OCEANOGRAPHY

OLD DOMINION UNIVERSITY
May, 1996

Approved by:

Dr. G. T. Csanady (Director)

Dr. Larry P. Atkinson (Member)

Dr. William C. Boicourt (Member)

Dr. Arnoldo Valle-levinson (Member)

ABSTRACT

OBSERVATION OF SHELFWATER OVERRUNNING THE SOUTHERN SLOPE SEA.

Ajoy Kumar
Old Dominion University, 1996
Director: Dr. Gabriel T. Csanady

Analyses of two years (1992 and 1993) of high resolution (1.47 km^2) sea surface temperature satellite images of the southern Mid-Atlantic Bight (MAB), showed that unusually extensive overhang of shelf water occurs episodically, and coherently over along shelf distances of several hundred kilometers. These episodes are dubbed *overrunning* of the Slope Sea by shelf water. The overrunning volume has a "face" and a "back" (southern and northern limit). It transports substantial quantities of shelf water southward, and does not retreat onto the shelf, but eventually joins the western edge of the Gulf Stream in the vicinity of Chesapeake Bay.

The correlation between satellite and *in situ* surface temperature , the location of shelf-slope front, and the relation of surface temperature to the deeper water mass were explored in order to quantify the overrunning episodes. The satellite extracted temperature profile agreed well with *in situ* surface temperature and coincident Expendable Bathythermographs (XBT) transects. The combined analyses of satellite imagery and various *in situ* data further demonstrated that the shelf water that overrun the Slope Sea are not mere surface features but can reach depths between 40 $\sim$ 60 m.

Results confirm previous concepts on shelf circulation, shelf-slope exchange, fate

of shelf water. They also sheds new light on shelfwater budget: overrunning of Slope Sea and southwest transport by upper slope current constitutes an important conduit for shelf water transport.

Further analyses of potential causes for the overrunning events showed that wind stress due to winter storms moved the shelf–slope front and with it shelf water offshore to distances $\sim$ 10 to 40 km. The offshore displacement of shelf water also appeared to be realted to the onshore veering of the Gulf Stream near Cape Hatteras. This veering of the Stream caused sea level to rise near Cape Hatteras producing a blocking effect on the shelf circulation. Such a blocking effect of the southwestward flow of shelf water in the MAB appeared to be the reason for the overruning of shelf water off New Jersey. In addition, the excess fresh water discharge from the St. Lawerence is also observed to be related to the flooding of shelf water off New Jersey.

ACKNOWLEDGEMENTS

These years at the Oceanography Department at ODU have brought numerous trials, errors and achievements, both in the personal and scientific life. This whole process of learning could not have been achieved without the help of many people and I'm delighted to acknowledge them.

During the last five years, my advisor, Dr. Gabe Csanady has given me continuous encouragement and guidance. He has taught me to focus on what ever I am doing and to see new simple ideas from every angle of oceanographic data especially from satellite imagery. To Joyce Csanady, I owe my sincere thanks for making me feel at home and always there to share and laugh at many of the things I did. To both of them, I am grateful for all these years of support, patience and guidance.

To Dr. Larry Atkinson I am grateful for the guidance, help and support he provided me all these years. Dr. Arnoldo has always been helpful and patient in answering my questions and I sincerely thank him for his support and timely help. I also wish to thank Dr. Eileen Hofmann, Dr. John Klinck, Dr. Denny Kirwan and Dr. William Boicourt for their help and concern for my work during the last few years. I am grateful to Boyd for all his help with the computer system.

I am indepted to Dr. Schwab, for providing me with the program to analyze SST imagery and Dr. Krasnopolsky and Dr. Breaker for providing me the program for estimation of surface velocities from satellite imagery. I also thank Mary Hollinger for her help in providing the CoastWatch SST images and Erik Gottlieb and Grayson

Wood for Oleander XBT data.

I thank all my fellow students and friends especially Andry, Andras, Ana, Jose, Lisa Hommel, Lisa Drake, Pete Becker, Sangki, Surya, Vittal and Yvette for their friendship and encouragement. I also wish to thank all my Indian friends especially and families especially Ravindran for their upport and help.

Finally, I wish to express my sincere gratitude and respect to my mother and all my six brothers for their love, support and encouragement all these years. I am especially grateful to my mother and wish to dedicate this dissertation to her.

The work described in this dissertation has been funded by the Commonwealth Center for Coastal Physical Oceanography.

TABLE OF CONTENTS

PAGE

LIST OF FIGURES viii

Chapter

1. INTRODUCTION 1

2. SCIENTIFIC BACKGROUND: THE MID-ATLANTIC BIGHT SHELF AND THE SLOPE SEA 5

2.1 CIRCULATION IN THE MAB 16

2.2 SHELF-SLOPE EXCHANGE PROCESSES IN THE MAB 17

3. SEA SURFACE TEMPERATURES (SST) FROM SATELLITES 22

3.1 INSTRUMENTATION 22

3.2 PROCESSING OF SST IMAGES 25

3.3 ACCURACY OF MEASUREMENTS 27

3.4 ACCURACY OF SST DATA USED IN THIS WORK 29

4. SEASONAL CYCLE OF SURFACE TEMPERATURE OVER THE SHELF AND SLOPE 35

4.1 DATA ACQUISITION AND PROCESSING 35

4.1.1 SORTING AND CONTOURING 35

4.1.2 DATA COVERAGE 37

PAGE

4.2 DISCUSSION OF THE CONTOURED SST IMAGES 37
4.2.1 1992 37
4.2.2 1993 41
4.3 TIME HISTORY OF SURFACE TEMPERATURE 54

5. RELATIONSHIP BETWEEN SATELLITE SST AND *in situ* DATA 69
5.1 DATA 69
5.2 OBSERVATIONS 71

6. ANALYSIS OF SHELF WATER OVERRUNNING IN THE SOUTHERN SLOPE SEA 87
6.1 ESTIMATION OF ALONGSHELF VELOCITY 87
6.2 VOLUME CALCULATIONS 93
6.3 TRANSPORT 96
6.4 POTENTIAL FORCING MECHANISMS 98
6.4.1 EFFECT OF WIND STRESS 98
6.4.2 EFFECT OF FRESH WATER DISCHARGE 102
6.4.3 PRESSURE GRADIENT EFFECT 104

7. CONCLUSIONS 117

BIBLIOGRAPHY 120

VITA 128

LIST OF FIGURES

FIGURE PAGE

1. Map showing location of Mid–Atlantic Bight. The major bathymetry contours and canyons are also shown 6

2. Temperature/salinity correlation for January 1976, Conrad 19-05. The following symbols represent bottle data, defined by their bathymetric location: $\triangle$ –inner shelf water; + - middle shelf water; 0 - outer shelf water. The small dots are STD profiles 7

3. As in Figure 1 but for May 1977, Cape Henlopen, 77-01. The small dots are CTD profiles 9

4. As in Figure 1 but for July 1975, Conrad 19-01 11

5. Temperature/salinity correlation for October 1974, Vema 32-01, from Gordon et. al., (1976). These data are from STD profiles. The inset T-S scatter for a single station is not discussed 12

6. Temperature (°C), salinity (%) and density ($\sigma_t$units) shelf/slope transect made south of Long Island in January 1976, Conrad 19–05. Numbers across the top refers to STD stations 14

PAGE

7. As in Figure 5 but for August 1977, Knorr ACE-III.
Numbers across the top refers to CTD stations 15

8. Position of NDBC buoys used for comparison with satellite SST. The stars represented by P shows the location from which the overrunning distances are determined, The stars represented by G, is the location from which the Gulf Stream thermal front distances are measured, D is the location of the tide gauge (referenced in chapter 6) 31

9. Comparison between satellite SST and buoy (44009) SST 32

10. Comparison between satellite SST and buoy (44012) SST 33

11. Comparison between satellite SST and buoy (44014) SST 34

12. Color plate showing SST images 43

13. Color plate showing SST images 44

14. Color plate showing SST images 45

15. Color plate showing SST images 46

16. Color plate showing SST images 47

17. Color plate showing SST images 48

18. Color plate showing SST images 49

PAGE

19. Color plate showing SST images 50

20. Color plate showing SST images 51

21. Color plate showing SST images 52

22. Color plate showing SST images 53

23. The MAB region showing the four SST transects 56

24. Sample of profiles extracted from a SST image 57

25. Sample of profiles extracted from a SST image 58

26. Sample of profiles extracted from a SST image 59

27. Sample of profiles extracted from a SST image 60

28. Time series of surface temperature on the inner shelf extracted from SST profiles along the four Transects (1992) 61

29. Time series of surface temperature at the mid shelf 62

30. Time series of surface temperature on the outer shelf 63

31. Time series of surface temperature in the slope region 64

32. Time series of surface temperature on the inner shelf extracted from SST profiles along the four transects 65

PAGE

33. Time series of surface temperature at the mid shelf 66

34. Time series of surface temperature on the outer shelf 67

35. Time series of surface temperature in the slope 68

36. The surface temperature, salinity and satellite extracted temperature across a transect from NY to Bermuda during February, 1992. The bottom section shows temperature contours constructed from XBT data in the underlying water mass. The full lines with rapid variation is satellite SST 76

37. As in Figure 36 but for February, 1993 77

38. As in Figure 36, but for March, 1992 78

39. As in figure 36, but for April 1992 79

40. As in figure 36, but for April, 1993 80

41. As in figure 36, but for May, 1993 81

42. Color plate showing SST image 82

43. Oleander transect on 1–2 May showing the signature of the Outer Shelf Current 83

44. As in figure 36, but for June, 1992 84

PAGE

45. As in figure 36, but for August, 1992 85

46. As in figure 36, but for November, 1992 86

47. SST image with velocity vectors obtained from feature tracking superimposed in the image. The shades of red represent Gulf Stream water. Shades of yellow and green the slope water mass and shades of blue the shelf water mass. The red arrows represent surface velocity determined from feature tracking. The arrow shown in a box on the right hand side shows a scale of 0.20 ms^{-1} for the surface velocity 89

48. Cummulative shelf water volume between the 100 m isobath and the satellite determined position of the shelf-slope front. The three shaded portions during 1992 represent the shelf water volume during the three overrunning episodes of 1992 97

49. Coherence^2 and Phase of wind stress 106

50. Time series Wind Vectors for buoy 44008, 1992 107

51. Time series Wind Vectors for buoy 440014, 1993 108

52. Time series wind stress for buoy 44008, 1992 109

53. Time series wind stress for buoy 44014, 1993 110

PAGE

54. Wind induced Ekman transport for 1992 and 1993 111

55. St. Lawerence River discharge 112

56. Chesapeake Bay discharge 113

57. A four-month-long time series(for 1992 and 1993)
of the surface position of the Gulf Stream and shelf
water on a line extending directly offshore from the
shelf break(100 m isobath) 114

58. A four-month-long time series of Sea level
variation measured at Duck, North Carolina for 1992.
The straight lines represent periods when the thermal
position of the Gulf Stream was near (less than 10 km)
from the shelf break 115

59. A four-month-long time series of Sea level variation
measured at Duck, North Carolina for 1993 116

1 INTRODUCTION

The seaward boundary of the Mid–Atlantic Bight (MAB) continental shelf is the shelf–slope front which intersects the surface far offshore of the shelf break [*Halliwell and Mooers*, 1979]. This narrow and highly dynamic region is recognized by sharp gradients in water properties between shelf and slope waters. The front generally intersects the bottom near the shelf edge [*Wright*, 1976].

The shelf water volume in the MAB is circumscribed by the coast and the shelf–slope front. *Wright and Parker* [1976], estimated that about half of the volume of shelf water from Cape Cod to Cape Hatteras lies in the surface wedge outside of the 100 m isobath and the shelf–slope front. *Mountain* [1991] in his analysis of the volume of shelf water in the MAB and Georges Bank determined the position of the shelf–slope front from satellite imagery. He suggested that changes in the location of the shelf–slope front at the surface, as determined by satellite imagery, could account for approximately 50% of the variance in the shelf water volume. In addition, he observed that the offshore position of the front is highly variable and can account for 50–80% of the interannual changes in the volume of shelf water in the MAB.

A potentially important reason for understanding the offshore extent of the shelf–slope front and the accompanied changes in shelf water volume in the MAB arises due to its effect on the phytoplankton population and carbon and nitrogen budgets. In winter and early spring, the wedge of shelf water between the shelf break and the shelf–slope front may contain $>2\mu$m NO_3, and it is reasonable to assume that phytoplankton blooms develop far seaward of the shelf break [Wirick, 1994].

This dissertation conforms to the journal model Journal of Geophysical Research.

Even though the primary production in these offshore blooms occurs over the slope, it is shelf production because it is initially fueled by nutrients transported from the shelf. Finally, much of the carbon fixed in this wedge must sink through the shelf–slope front into slope water. Therefore, it is necessary to include all of the shelf water and not be limited to water lying over the continental shelf in the budgets (eg. carbon and nitrogen) for the MAB.

The majority of outflow of shelf water from the MAB is thought to occur across the frontal boundary, so that relatively little shelf water transits the entire bight to exit at Cape Hatteras. A number of processes can contribute to the transfer of shelf water into the slope region. Some shelf water does leave the shelf at Cape Hatteras and is observed along the northern edge of the Gulf Stream [*Ford et al.*, 1952]. Gulf Stream Rings and eddies appear to entrain large amounts of shelf water from the shelf region [*Morgan and Bishop*, 1977; *Bisagni*, 1983; *Garfield and Evans*, 1989]. Instabilities in the shelf–slope front generate shelf–break eddies which can result in parcels of shelf water being separated from the shelf [*Ramp et al.*, 1983; *Garvine et al.*, 1988]. Modeling studies also indicate a steady cross–isobath transport of water past the shelf edge associated with bottom friction [*Wang*, 1982; *Chapman et al.*, 1986]. The relative importance of the various transfer processes and of the different pathways of shelf water to slope water and ultimately to the deep North Atlantic remains to be elucidated.

Satellite SST images are an important new source of information for understanding circulation and exchange processes on continental shelves since it provides a detailed method of sampling. The shelf and slope regions have water masses with strong horizontal gradients and dynamical features with scales larger than a few kilometers which are ideally suited for study by infrared satellite images. Quantities estimated from the satellite data set combined with *in situ* data collected during hydrographic

surveys are of great importance in many oceanographic applications including that of shelf–slope exchange and shelf water budgets [*Emery and Mysak*, 1980; *Njoku et al.*, 1985].

The strong horizontal gradients in the southern MAB for most of the year are readily identified in satellite images and lend themselves to such a study. A series of fairly clear SST maps separated by only a few days portray motions and realignment of boundaries between different water masses in the MAB. In the southern MAB the main boundaries separate shelf, slope and Gulf Stream waters. The shelf water–slope water boundary in particular is frequently found well offshore of the 100 m isobath (the conventional separation line between "shelf" and "slope"). We have called such large excursions of the front, *overrunning* of slope water by shelf water. The frequency and extent of such overrunning (of slope water by shelf water) and the behavior of distinct shelf water parcels in slope water yield important clues to shelf circulation, shelf–slope exchange, fate of shelf water and sheds new light on shelf water budget.

The thesis is organized in the following manner. A review of the MAB shelf and slope hydrography, circulation and shelf–slope exchange processes are presented in Chapter 2. Since the principal data set used in this study is sea surface temperature fields (SST), a detailed summary of the processing methods and accuracy of satellite determined SST are presented in Chapter 3. Chapter 4 describes and analyses two years (1992 and 1993) of SST images of the southern MAB. The relationship between the satellite and *in situ* data are explored in Chapter 5. The main objective of the thesis is to analyze and determine the overrunning of shelf water into the slope region. Chapter 6 gives estimate of the velocity, volume and transport of the overrun shelf water. This Chapter also examines the potential forcing mechanisms that cause the shelf water to overrun the slope region due to wind, freshwater discharge and changes in the circulation due to sea level slope variation caused by the veering of the Gulf

Stream. The conclusions are found in Chapter 7.

2 SCIENTIFIC BACKGROUND: THE MID-ATLANTIC BIGHT SHELF AND THE SLOPE SEA

The MAB extends from the southwest corner of Georges Bank to Cape Hatteras, N. C. (Figure 1) and has been extensively studied from the time of *Bigelow* [1933]. Recent reviews of its physical oceanography can be found in *Allen et al.* [1983] and in *Brink* [1987]. The MAB shelf topography is simple and smooth over its 800 km length, indented with canyons including the Hudson Canyon . The width of the shelf from the shore to the shelf break is about 100 km, except that it broadens in the New York Bight (to 150 km) and narrows near Cape Hatteras (to 50 km). The depth of the shelf break decreases from 150 m south of Georges Bank to 50 m off Cape Hatteras. Wedged in between the shelf water and the Gulf Stream is the distinctive slope water mass named by *Iselin* [1936]. The strip of ocean containing slope water is about 200 km wide and 1600 km long, stretching from Cape Hatteras to the Grand Banks, between the Gulf Stream and the continental shelf. It is called the "Slope Sea" by *Csanady and Hamilton* [1988].

The winter T/S diagram of the shelf–slope waters of the MAB exhibits the 'seven' shape characteristic of this region (Figure 2). The portion of the T/S curve below the 'elbow', the temperature and salinity maximum near 14° and 35.6%, is slope water, seaward of the shelf–slope front and deeper than 200 m. This part of the curve is the freshened modification of the North Atlantic Central water (NACW) as discussed by *Mclellan* [1957]. Below the T and S maximum, four components of deep water are noticeable: the NACW component of relatively rapid salinity decrease down to the 8° to 9° C isotherm (100 to 300 m); the Irminger Atlantic water with slightly decreasing gradients between the 8° to 4° C isotherm near 1000 m; a region of small salinity gradient reversal between Labrador Sea Water at 1000 m and the Mediterranean

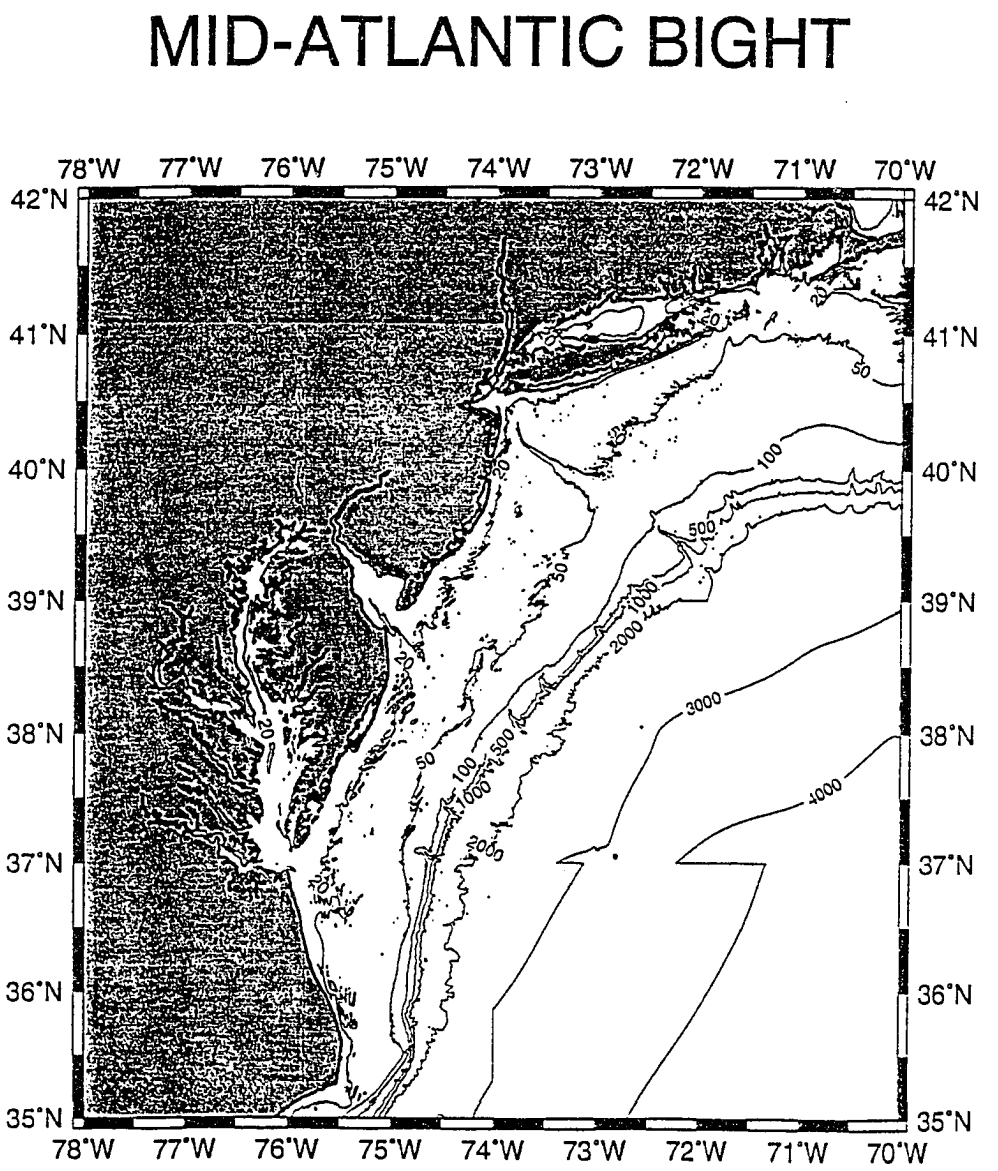

Figure 1: Map showing location of Mid–Atlantic Bight. The major bathymetry contours and canyons are also shown.

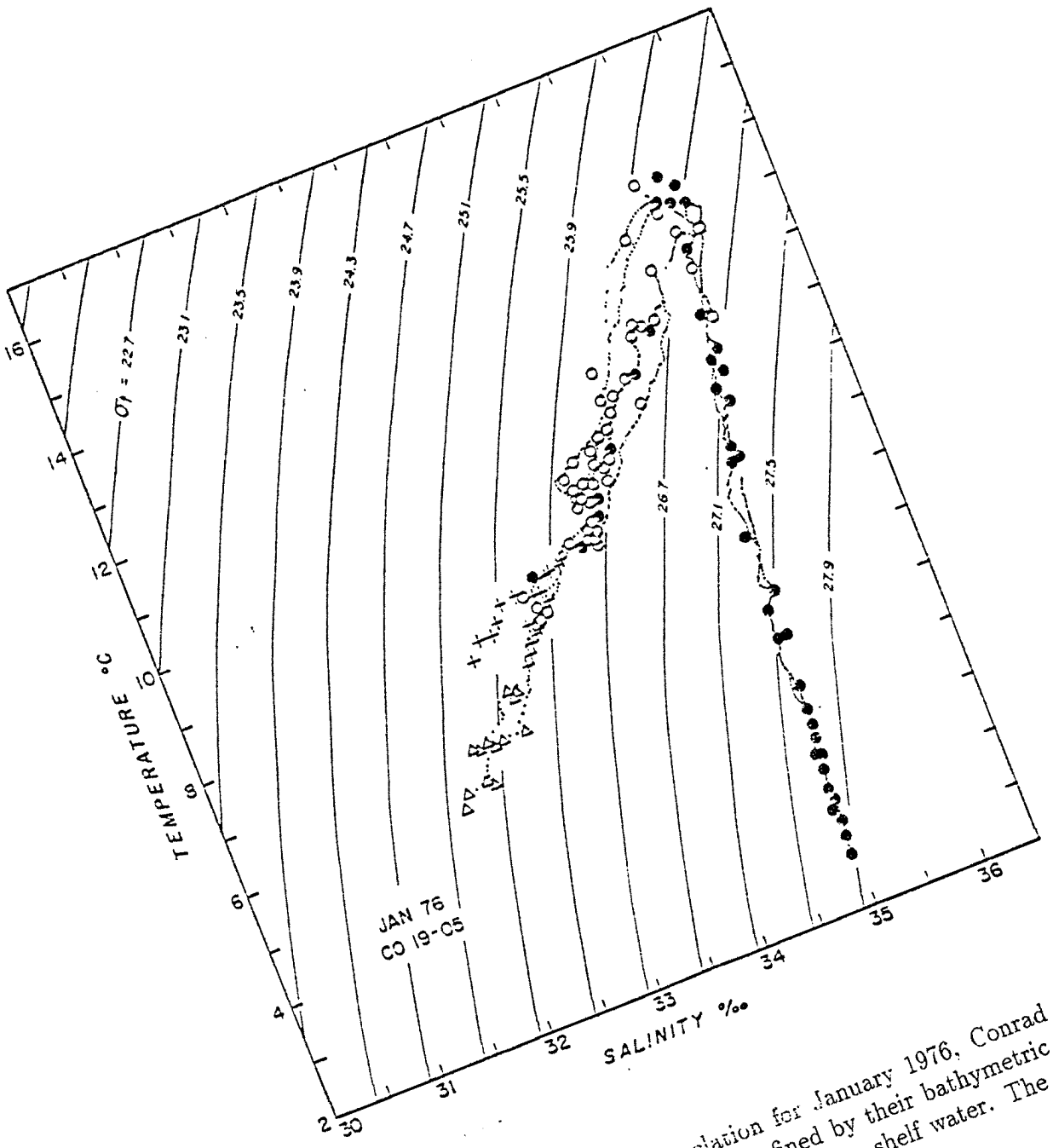

Figure 2: Temperature/salinity correlation for January 1976, Conrad 19-05. The following symbols represent bottle data, defined by their bathymetric location: Δ- inner shelf water; + - middle shelf water; 0 - outer shelf water. The small dots are STD profiles.

component of North Atlantic Deep Water (NADW); and below 2000 m, a region of decreasing salinity to the sea floor with temperature and salinity slightly above that of the northern component of NADW [*Gordon et al.,* 1976].

The 'elbow' in the T/S curve is a junction between the cold and slightly fresher slope water and the cold and fresher shelf water masses, called as the 'Upper Slope Water thermostad' [*Wright and Parker,* 1976]. The temperature maximum identity of this feature is destroyed in summer, but the salinity maximum remains intact. The temperature and salinity maximum of this feature can vary due to the influence of four components; the seasonal influence of the atmosphere, by the continental shelf water, Gulf Stream ring and alongshore advective effects from upstream sources.

The straight line of the T/S curve from the salinity maximum to the inner shelf (6° C, 32%) is composed of water from the upper slope, from the shelf–slope frontal region, and from middle and inner shelf regions. This part of the curve is indicative of the uniformity of the processes which mix shelf and slope waters in winter.

The vernal progression of T/S characteristics in the MAB begins in late March to early April with increased net solar radiation, increased river runoff and decreasing wind stress. This marks the transition from horizontal to vertical density stratification and is usually complete by late June. By May, the surface shelf and slope waters will start to freshen and warm up as the effectiveness of the vernal buoyancy input is enhanced by the increasing vertical stratification and reduced vertical mixing (Figure 3). Over the shelf the seasonal pycnocline separates the buoyant surface water from the remnant winter water near the bottom called the 'cold pool'. The sharp shelf–slope frontal zone is the area enclosed between 34 to 35% and 6 to 13° C. This zone is represented by low density of data points due to the relatively small volume of water. The influence of freshwater discharge is mostly confined to the lighter surface layers. The low salinities over the slope suggest seaward spreading of shelf surface

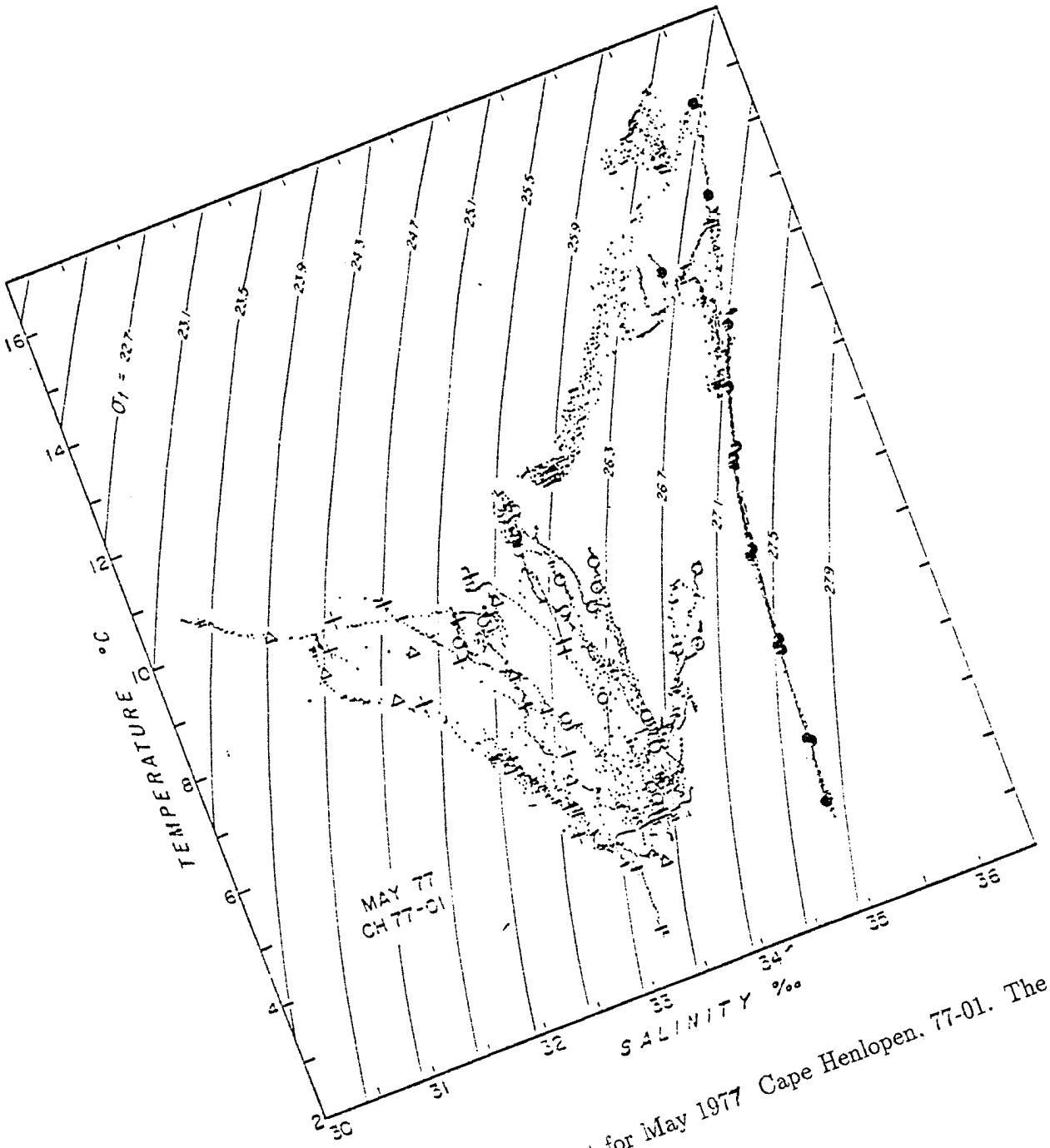

Figure 3: As in Figure 1 but for May 1977 Cape Henlopen, 77-01. The small dots are CTD profiles.

water. Isopycnal (constant density surfaces) contact is now established between the shelf and slope waters as compared to the winter regime of isopycnal isolation.

By July, the summertime T/S characteristics in the MAB are fully developed, with a strong thermocline of about 18° C at mid-shelf (Figure 4). The T/S points show two groups; the low salinity component above the cold pool over the inner and middle shelf and the high salinity component of surface slope water. The shelf-slope front signature is indicated by the low number of data points between these two regions. The reduced salinity over the slope region is caused by seaward spreading of freshened shelf water. The salinity maximum in the shelf region (marked as B) is the mid depth shoreward intrusion of slope water.

By October, the cooling of the sea surface and increasing wind stress contribute to the deepening of the surface mixed layer, erosion and deepening of the seasonal thermocline, warming and shrinking of the cold pool and an eventual destruction of the two layer structure (Figure 5). Numerous inversions in the temperature and salinity field are indicative of the breakdown of summer stratification. The shelf and slope waters are intergrated via mixing and overturning processes.

By late October and early November, the vertical mixing leads to a thermal collapse of the T/S envelope and warming of the bottom water on the shelf to the yearly maximum [*Beardsley and Flagg,* 1978]. After this the shelf and slope waters start to cool together until the winter time thermal front is reestablished as well as the 'figure seven' T/S characteristic of the MAB.

The relatively cool and fresh shelf water is separated from the warmer and saltier continental slope water by the baroclinic shelf-slope front. This thermohaline feature is discernible from around Georges Bank to Cape Hatteras and slopes downward (with depth) and shoreward from its manifestation over the inner slope to where it

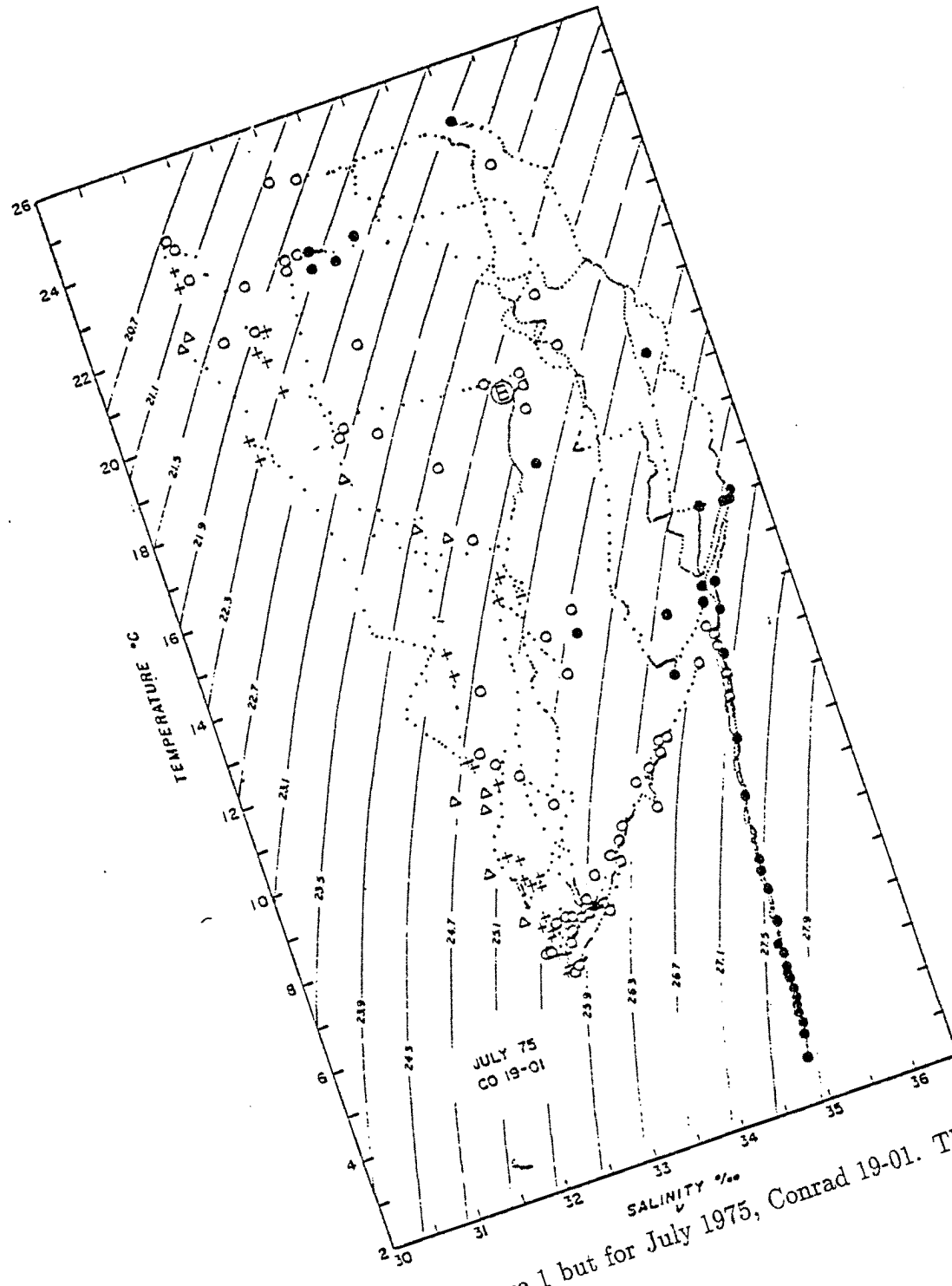

Figure 4: As in Figure 1 but for July 1975, Conrad 19-01. The small dots are STD profiles.

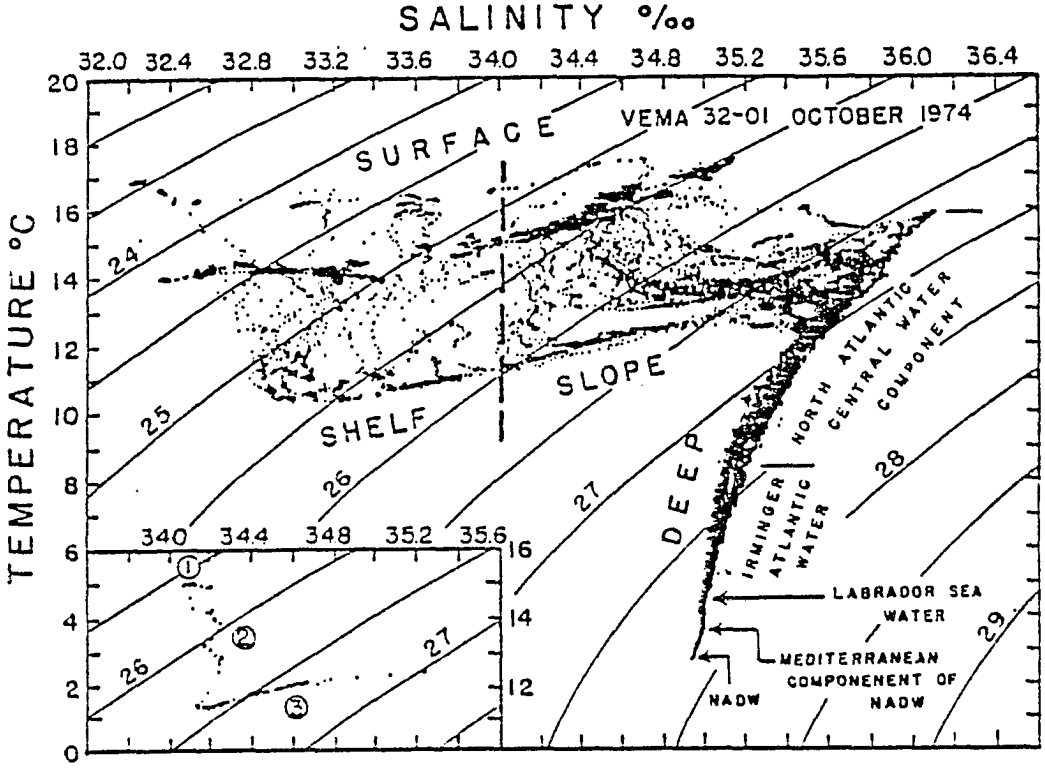

Figure 5: Temperature/salinity correlation for October 1974, Vema 32-01, from Gordon et. al., (1976). These data are from STD profiles. The inset T-S scatter for a single station is not discussed.

intersects the bottom at about the 90 m isobath. The surface of the front is subjected to a host of higher frequency perturbations apart from the seasonal changes which give it the highly convoluted surface appearance and offshore and alongshore scales of 50 km and 80 km respectively [*Halliwell and Mooers,* 1979].

The winter structure of the shelf–slope frontal regime consists of the vertically mixed shelf waters divided from the well mixed to weakly stratified slope waters (Figure 6). The horizontal density gradient is directed offshore throughout the water column and there is no isopycnal contact between shelf and slope waters. The degree of compensation of the salinity field by the temperature field is not enough to erase the winter time density signature.

The summer time manifestation of the shelf–slope front is dominated by the seasonal thermocline, a feature of the highly stratified regime (Figure 7). Above 50 m the front shows highly complex thermohaline features, whose shape is discernible in the salinity field. Isopycnal contact is now established between the shelf and slope waters. Strong density compensating gradients in temperature and salinity exist on the isopycnal surfaces. A shallow, surface mixed layer of freshened shelf water extends out over the slope. This signature is more discernible in the salinity field because the seasonal heating usually erases the thermal contrast. A seasonal pycnocline extends across the front, but is shallower and more intense over the shelf than over the slope. A mid–depth saline intrusion in the shelf water pycnocline seem to be fed by the slope water. The cold pool maintains its thermal signature throughout the summer. The foot of the front can be displaced shoreward by bottom intrusions. These intrusions are observed more often in summer than in winter.

A feature of the Slope Sea is the formation of slope water pycnostad (deep mixed layer) due to convective overturning and boundary mixing in winter by storms and low air temperatures [*Csanady and Hamilton,* 1988]. A dramatic example of pycnostad

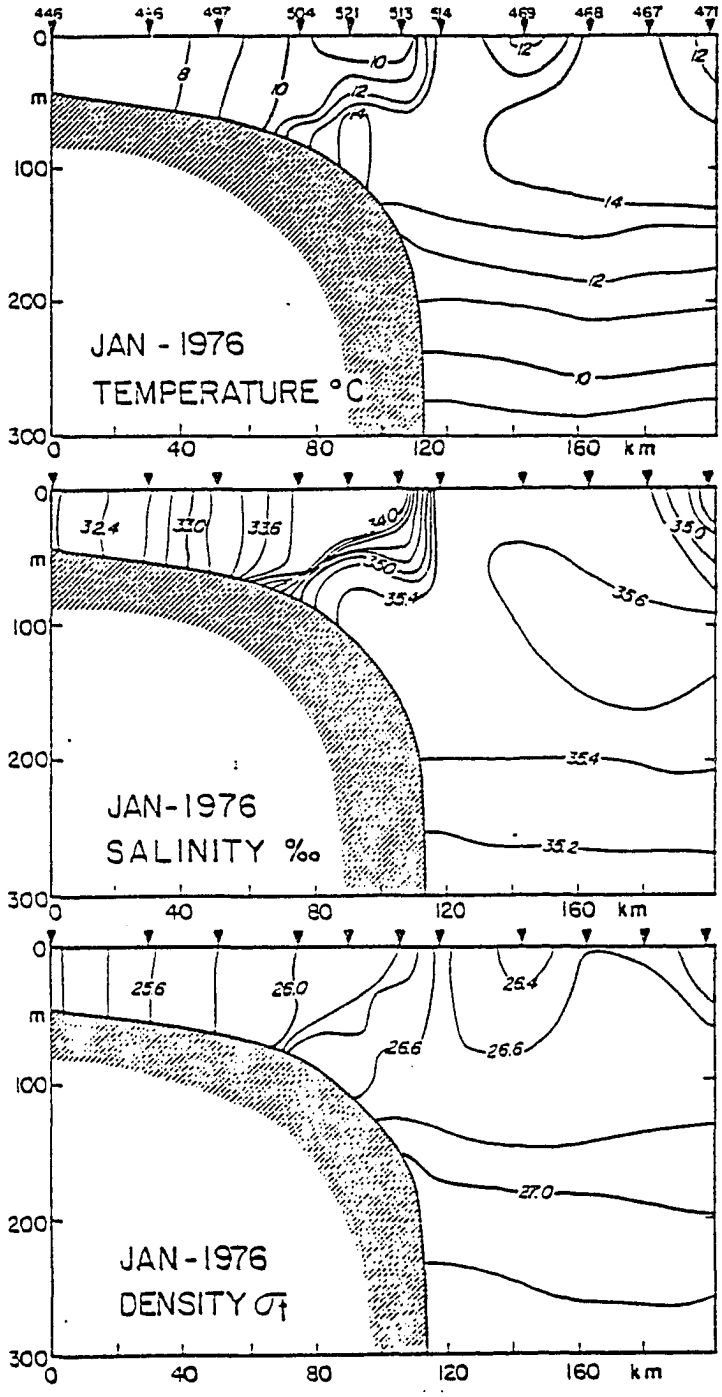

Figure 6: Temperature (°C), salinity (%) and density (σ_t units) shelf/slope transect made south of Long Island in January 1976, Conrad 19–05. Numbers across the top refers to STD stations.

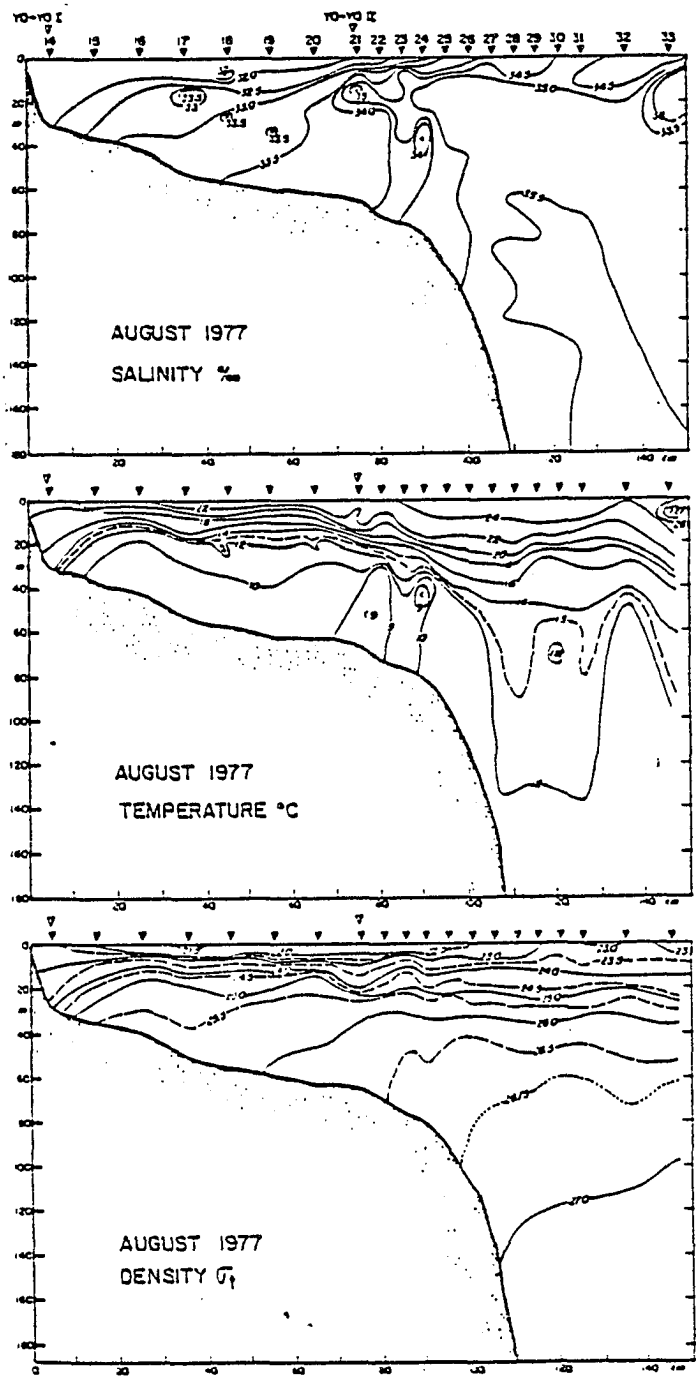

Figure 7: As in Figure 5 but for August 1977, Knorr ACE-III. Numbers across the top refers to CTD stations.

formation off Nova Scotia is the sudden increase of the σ_t = 26.8–27.0 layer depth from a few meters to about 200 m [*Horne,* 1978]. The pycnostad is found throughout the Slope Sea in winter but not in late autumn. It extends from the shelf-edge to the Gulf Stream with a typical salinity of 35.5 and a temperature near 12° C. The pycnostad is capped by a seasonal thermocline in May and its signature completely disappears by late Autumn. The disappearance is enhanced by saline Sargasso Sea intrusions along isopycnals at 10–20 m depth from under the Gulf Stream [*Rossby,* 1936; *McLellan,* 1957]. These intrusions are warmer, saltier and slightly lighter than the pycnostad that develops from them later in the winter.

2.1 Circulation in the MAB

The understanding of the general circulation of the MAB shelf and slope water is important to explain shelf-slope exchange processes. The shelf water in the MAB is part of a coastal current that seems to originate near Greenland [*Chapman and Beardsley,* 1989]. The coastal current carrying fresh water from Labrador rivers flows south and west along the continental margin, past the Gulf of St. Lawerence into the Gulf of Maine [*Fairbanks,* 1982]. In the Gulf of Maine, the deep mean inflow of slope water through the Northeast Channel mixes with the near shore flow around the tip of Nova Scotia. The resulting water is carried by the mean circulation around Georges Bank and then westward past Nantucket Shoals into the MAB. The combined flow of 0.40 Sv provides the mean southwestward transport into the MAB and shows large seasonal and interannual variation [*Mountain,* 1991]. Within the MAB, the mean southwest flow towards Cape Hatteras has an average speed of 0.03–0.04 m s^{-1} [*Beardsley and Flagg,* 1976].

The slope water circulation consists of a closed gyre in the western 'Slope Sea' driven by a combination of local wind forcing, water discharge from the Labrador Current and the Gulf Stream [*Csanady and Hamilton, 1988].* On the western side

of the Slope Sea gyre, the Mid-Atlantic Slope and Rise (MASAR) and Shelf Edge Exchange Processes (SEEP) programs have shown an upper slope current. The slope current has a predominantly southwestward mean flow of about 0.15 m s^{-1} but speeds of up to 0.40 m s^{-1} have also been observed. The total southwestward transport by the slope current off New Jersey was of the order of 3.75 Sv but was only intermittently observed off Chesapeake Bay because of the influence of Gulf Stream discharged water [*Churchill and Cornillon, 1991a*].

Bane et al. [1990] showed that the slope currents respond to remote forcing by the Gulf Stream. Large shifts in the Gulf Stream position take place when the Stream interacts with a ring. These effects are then transmitted to the shelf break currents and cause changes in the structure and strength of the Slope Sea gyre. When the Gulf Stream is near the shelf break the currents are 0.30–0.40 m s^{-1} and when it is 300 km or so away, the currents are nearly zero.

The slope water flow on the northeastern side of the Slope Sea is headed off by the southward intrusion of the Labrador Current [*Csanady and Hamilton, 1988*]. The slope water then turns southward and rejoins the Gulf Stream, eventually escaping eastward as part of the North Atlantic Current. Some slope water is also entrained in the retroflecting Labrador Current flowing eastward. The total slope water transport on the northeastern side of the Slope Sea is about 10 Sv moving eastward but its final fate is unclear.

2.2 Shelf-slope exchange processes in the MAB

Shelf-slope exchange occurs along the entire length of the MAB and constitutes an important mechanism to transfer heat, salt and nutrients between the shelf and slope waters. The study of exchange and mixing of shelf and slope waters have gained

importance recently for at least two reasons [*Churchill et al., 1993*]. The first is the concern for the transport of contaminant to and from the continental shelf and the other is the transport of plankton to different hostile and hospitable environments. Knowledge of this exchange process is incomplete [*Garfield and Evans, 1987*].

The shelf water leaves the shelf all along the shelf-slope front and near Cape Hatteras and a number of processes that transport the shelf water into the slope region in the MAB are identified. The movement of the shelf-slope front in the MAB plays an important part in the exchange of shelf water [*Garvine et al., 1988*]. In simplified models, the front usually intersects the surface within 50 km offshore of the shelf break (200 m isobath in the MAB) and just inshore of the shelf edge at the bottom. But large surface displacements of 100 to 300 km are observed to take place [*Halliwell and Mooers, 1979*]. The bottom intersection of the front is found to vary only within 16 km of the shelf break [*Wright, 1976*]. These surface excursions of the frontal position account for nearly 50% of the variability of the shelf water volume found in the MAB [*Mountain, 1991*].

Shelf Water has been known to be entrained from the western end of the Slope Sea eastward, along the northern boundary of the Gulf Stream [*Ford et al., 1952; Kupferman and Garfield, 1977; Fisher, 1972; Csanady and Hamilton, 1988*]. The entrainment and subsurface flow structure of the shelf and slope waters along the Gulf Stream edge has been recently shown [*Churchill et al., 1989; Lillibridge et al., 1990*] to be a complex and variable process often reaching depths of about 100 m on the Gulf Stream side. The entrainment into warmer saline Gulf Stream can cause salt finger mixing at its upper surface and mixing by diffusive layering below [*Lillibridge et al., 1990*]. The subsurface entrained water has a high level of chlorophyll, fluorescence and dissolved oxygen and a species of diatom assemblage distinct to the shelf species. The total annual export of biogenic carbon was estimated as 10^6 kg C yr^{-1} and the

total transport due to water entrainment as 0.15 Sv [*Lillibridge et al., 1990].*

Another mechanism of shelf–slope exchange is related to warm–core rings (WCR). WCR entrain large amounts of shelf water [*Evans et al., 1985; Garfield and Evans, 1987; Joyce et al., 1992].* When the inshore edge of the ring comes in contact with the shelf-slope front, long filaments or streamers of shelf water are drawn offshore, wrapping anticyclonically around the WCR [*Ramp, 1986]. Morgan and Bishop [1977],* calculated the shelf water transport by a streamer entrained by a WCR from hydrographic data. Assuming three ring interaction per year each lasting for 90 days, they obtained a transport of 0.006 Sv. *Bisagni [1983]* calculated the shelf water transport by a Gulf Stream entrained streamer from the velocity of satellite-tracked drogues, the width of the streamer and an assumed depth of 50 m. He also assumed three ring interaction per year but only 50% of the time and obtained a transport of 0.06 Sv. *Garfield and Evans [1987]* also obtained a single instantaneous value for streamer entrainment from hydrography and satellite-tracked drogue for the Gulf of Maine region. Then, using a seven year collection of SST, they found that streamer entrainment occurred 69 +/– 20% of the time. Thus, they obtained a transport of 0.18 Sv. During 1970–1976, *Halliwell and Mooers [1979]* observed twenty eddies between Georges Bank and Cape Hatteras using weekly satellite-derived charts of surface temperature fronts. These eddies have a lifespan of about half a year and tended to shrink in size and propagate faster as they approached Cape Hatteras. Near the shelf break the eddies tend to force near-surface shelf water offshore, seen as cold tongues in satellite images. Some of these tongues were observed to be about 50 m thick and 50 km wide and suggest that the cold tongues observed in satellite images cannot be dismissed as arbitrarily thin. These estimates show the variable nature of the inflow and outflow of shelf water in the MAB and the assumption made by different people.

Garvine et al. [1988] used a combination of buoy tracking, intensive hydrography,

SST and moored current meters to resolve the structure of shelf break eddies that were present most of the time at the shelf-slope front. These eddies were mistaken as 'lenses' of shelf water in the Upper slope region [*Cresswell,* 1967; *Wright* 1976; *Houghton and Marra* 1983]. There was no presence of Gulf Stream eddies or rings at the time. The shelf break eddies, with a wave length of 33 km, deformed the front into a 'backward breaking' wave. This feature caused plumes of lighter shelf water to protrude well over the outer slope contradicting the interpretation by *Cresswell and Wright* as detached parcels of shelf water. These eddies have a potential to enhance the diffusivity for across-front diffusion of heat and salt. *Garvine et al.* [1988] compare these shelf break eddies to the 'squirts' found on the California shelf [*Davis,* 1985; *Hood et al.,* 1990] as the prime agents of cross-shelf exchange. But the difference is that, the Californian shelf is about 20 km wide and the filaments that develop are transported offshore within a few days. Whereas, in the broad MAB shelf, the eddies, which form in the front, translate westward alongshore. Also the flow fields along the Californian shelf were related to the onset or relaxation of upwelling winds. *Garvine et al.* [1988] reported almost negligible winds during their observations.

SST images show large outbreaks of shelf water over the slope region, which are not related to eddies or filaments [*Garfield and Evans,* 1987]. These outbreaks are often found in the area around Northeast Channel and seem to originate from the Scotian shelf and the eastern end of Georges Bank. They appear as large tongues of shelf water on satellite imageries, flooding from the frontal area into the slope water. Small outbreaks may retreat back into the shelf water, but larger ones seem to be persistent and continuous with the shelf water, and appear to mix with the slope water. These outbreaks are observed 29% of the time and did not appear to be associated with Gulf Stream rings and eddies.

Mountain [1991] has calculated the annual mean cycle and the interannual vari-

ability of the volume of shelf water in the MAB between 1977–1987. The offshore extent of the shelf water is determined from the mean position of the shelf-slope front taken from satellite imagery. The volume is determined from the along shelf distance of this frontal position and an assumed average thickness of 40 m. In fact, the extent of the frontal position is variable and can introduce considerable errors in this type of calculation. The volume of shelf water, exhibits a significant annual cycle (55%), with a distinct spring maximum. Large interannual changes are observed in the volume of shelf water in the MAB (2-3 $\times$ 10^3 km^3). The changes in the interannual volume of shelf water in the MAB has been related to the fresh water discharge from the St. Lawerence that advects into the Gulf of Maine and which later constitute the major part of inflow into the MAB. The majority of outflow from the MAB occur uniformly all along the entire length of the shelf-slope front.

Results from the recently concluded SEEP-II experiment also confirm that significant amount of shelf water leaves the shelf well north of Cape Hatteras to be absorbed by the Slope Sea [*Biscaye et al.,* 1994]. The shelf water that is transported is about 40–50 m deep and can extend 50–100 km offshore of the shelf break. SST images of this region also suggest southward-propagating, finite amplitude waves with a wavelength of about 60 km, phase speed of about 0.25 m s^{-1} and a period of about 66 h.

3 SEA SURFACE TEMPERATURE (SST) RETRIEVAL FROM SATELLITES

Recent progress in advanced very high resolution radiometry and improved algorithms for retrieval of Sea Surface Temperature (SST) from infrared images have made remotely sensed temperature fields a more reliable and useful method in oceanography, meteorology and fisheries studies [*Minnett,* 1991]. Synoptic SST images are now easily accessible from archived sources through internet and dial up modem within two or three hours of acquisition. SST images are available from different sources, each of them using various algorithms and processing methods. Therefore, it is necessary to summarize the algorithms and processing methods used in this study. This chapter gives an account of SST products available through CoastWatch program of National Oceanic and Atmospheric Administration (NOAA).

3.1 Instrumentation

The images covering coastal areas in the Great Lakes, East Coast and Gulf of Mexico, are processed and distributed nationally through Internet. The data are obtained by instruments carried on the TIROS-N/NOAA series of satellites, designed to operate in a near polar sun-synchronous orbit. The present operating series of satellites include NOAA-7, NOAA-8, NOAA-9, NOAA-10, NOAA-11 and NOAA-12. The payload on these satellites includes the Advanced Very High Resolution Radiometer (AVHRR) and TIROS Operational Vertical Sounder (TOVS). NOAA and National Environmental Satellite, Data, And Information Service (NESDIS) operates two Command and Data Acquisition stations, one in Wallops Island, Virginia and one in Fairbanks, Alaska. These stations receive both recorded and direct readout environmental data from the satellite and send it to Suitland, Maryland, via satellite relay. When the satellite is out of contact with either of the ground stations, the data is recorded

at Lannion, France. The orbital period of the satellite is about 102 minutes which produces 14.1 orbits per day. The suborbital tracks do not repeat on a daily basis since the number of orbits per day is not an integer. But the local solar time of the satellite's passage is essentially unchanged for any latitude.

The AVHRR is a cross-track scanning radiometer which features four or five spectral channels. The AVHRR flown aboard NOAA-6, NOAA-8, and NOAA-10 has four channels, and the AVHRR aboard NOAA-7, NOAA-9, NOAA-11 and NOAA-12 has five channels. The channels in the AVHRR have a basic resolution of 1.1 km at nadir in the visible (0.55-0.90 μm), the reflected-infrared (0.725-1.10 μm), thermal infrared (3.55-3.93 μm) and the infrared bands (10.50-11.50 and 11.50-12.50 μm). At infrared wavelengths water is essentially opaque and it is often assumed that the ocean radiates like a blackbody. Wavelengths in the range 3-15 μm are most useful for oceanic studies, because radiant power peaks in the range of 9.3-10.7 μm, and atmospheric absorption minima are found at 3.5, 9.0 and 11.0 μm . At these wavelengths sufficient radiant power is available for substantial detector response and the optical properties of the atmosphere permit detection of sea surface temperature. The 3.5-5 μm window is least affected by absorption by water vapor and the relative sensitivity is here about three times larger than at 10 μm . But surface reflectivity is also three times greater, undermining the usefulness of the 3.5 μm channel for SST determination. Therefore the signal available for measurement is largest in the 10-12 μm window and forms the basis for temperature retrieval algorithms.

The AVHRR thermal and visible data values are calibrated to temperatures and albedos respectively. For the thermal band the energy measured by the sensor is computed as

$$E_i = S_i C + I_i \tag{1}$$

where E_i is the energy value in mW m^2 sr cm^{-1}, C is the input data value ranging

from 0 to 1023 counts, S_i is the scaled slope and I_i is the scaled intercept values. The conversion to brightness temperature from energy is performed using the inverse of Planck's radiation equation

$$T(E_i) = \frac{C_2\nu}{ln(1 + \frac{C_1\nu^3}{E_i})} \tag{2}$$

where T is the temperature (K), ν is the central wave number and C1 and C2 are constants.

The percent albedo (A_i) as measured by channel i in the visible band is computed as follows:

$$A_i = G_iC + H_i \tag{3}$$

where C is the input data value, G_i is the scaled slope and H_i is the scaled intercept values.

The percent albedo is then converted to spectral radiance by (4).

$$R = A_i\frac{F}{100\pi W} \tag{4}$$

where R is the spectral radiance in W m^{-2} μm sr, F is the integrated solar spectral irradiance in W m^{-2} and W is the equivalent width of the spectral response function in μm.

The infrared channels are calibrated in-flight using the view of a stable blackbody and space as a reference. The analog data output from the sensors is digitized on board the satellite to 10-bit precision. The digitized data are transmitted from the satellite in real-time as High Resolution Picture Transmission (HRPT) data, and selectively recorded on board the satellite for subsequent playback as either Local Area Coverage (LAC) or Global Area Coverage (GAC) data.

The raw data is then quality controlled, assembled into discrete data sets, with Earth location and calibration information appended (not applied). This data set is

called the Level 1b data and is archived for further processing.

3.2 Processing of SST Images

The AVHRR Level 1b data is the input for the processing and production of sea surface temperature images. First step in the processing is Target construction, in which the AVHRR data of good quality are used to construct a 11 x 11 pixel target array. Next the data is divided into day and night targets using the satellite zenith angle (SZA). The night time target is processed if the SZA is less than 45° and a day time target is processed if the SZA is less than 53°. In the Land/Sea test the pixels over land are eliminated with a land/sea tag data base.

Blocks of 2 x 2 unit arrays of AVHRR pixels within the 11 x 11 target are passed through various cloud tests which include the thermal-IR uniformity test, average unit array values, thermal-IR cloud tests and the uniform low stratus test. Basically, the reflectance from cloud free areas is less than 10% compared to the 50% from the clouds. By assigning a threshold, most of the large clouds are eliminated. At night a combination of three infrared channel ratio (5) are used to eliminate the radiance from small patches of clouds.

$$\frac{T_{3.7} - T_{11}}{T_{11} - T_{12}} \tag{5}$$

where the subindices indicate the AVHRR channels. The radiance from subresolution clouds is a combination of cold cloud temperature and the warm SST. This will increase the ratio (5) because this radiance is more sensitive to 3.7 μm than at 11 or 12 μm . With thick non transmissive clouds, the emissivity at 3.7 μm is lower than at 11 or 12 μm and the ratio decreases in value. After the cloud screening only about 10% of the target arrays remain.

In any spectral interval, thermal radiation emitted by the sea surface is absorbed

by atmospheric constituents and remitted at all levels in the atmosphere. This is described by the radiative transfer equation

$$I_i = B_i(T_s)\tau_i + B_i(\bar{T}_i)(1 - \tau_i) \tag{6}$$

where I_i is the radiance at the top of the atmosphere, B(T) is the Planck function at temperature T, τ_i is the transmittance of the atmosphere and $\bar{T}$ is the atmospheric temperature at some level i. The atmospheric absorption at the three infrared channels occurs at very low levels and as a result the mean atmospheric temperature T is the same in these channels. Also $\bar{T}$ is nearly equal to T_s, the sea surface temperature. Since atmospheric absorption is primarily due to water vapour, the transmittance can be approximated by $\tau_i = e^{-kX} = 1 - k_i X$, where k_i is the absorption coefficient and X is a function of the water vapour amount. With these approximations the temperature difference due to water vapour absorption in one channel can be obtained by a linear regression of the brightness temperature of two different window channels as

$$T_s - Ti = [k_i/(k_j - k_i)](T_i - T_j) \tag{7}$$

In practice, $(T_i - \bar{T}_s)$ are regressed against $(T_i - T_j)$ for various combinations of window channels using atmospheric models and equations of the form (8) are obtained.

$$Ts = (T_i + C_3)(T_i - T_j) + C_4 \tag{8}$$

where C's are the regression coefficients. These coefficients are determined for different regions by comparison against *in situ* buoy data. The brightness temperatures decrease with high values of water vapour and for large satellite zenith angle (SZA) during the night. The measurement accuracies are improved in later algorithms by the input of a term $(\sec(\theta) - 1)$ to correct for satellite zenith angles. The algorithms function better in mid-latitudes where the atmospheric absorption due to water vapour is less [*Wick et al.*, 1992]. Presently used algorithms also use a non-linear form of the Multi Channel Sea Surface Temperature (MCSST) algorithm to correct for the non-linear response of the sensor.

For the Coastwatch SST images used in this study a triple window MCSST equation (9) is used.

$$MCSST = 1.03603(T_{11}) + 0.89286(T_{3.7} - T_{12}) + \quad (9)$$
$$0.52006(T_{3.7} - T_{12})(SEC - 1.0) - 282.37397$$

where $T_{3.7}$, T_{11} and T_{12} are the brightness temperatures in Degrees Kelvin for the 3.7, 11 and 12 μm AVHRR channels respectively and SEC is the secant of the satellite zenith angle.

3.3 Accuracy of measurements

The AVHRR measures the 'skin' temperature of the ocean surface, which is the radiation from the upper few millimeters of the ocean surface. On account of evaporation, the ocean has a cool skin, being approximately 0.1°-0.5°K colder than the water immediately (1 mm say) below. The *in situ* sea surface temperature that is measured commonly refers to the bucket temperature of the samples taken from ships or to the ship's cooling water temperature or to the temperature measured from drifting and moored buoys. The bulk temperature measurements range from about 1 m to nearly 5 m depth depending on the type of instrument used.

The ocean surface is cooled or heated as the result of a combination of air-sea fluxes, horizontal and vertical advection and mixing within the ocean. Winds above 10 m s^{-1} tend to mix the surface layers and reduce the difference between skin and bulk temperature. During the day solar radiation can produce a shallow (order of 1 m deep), warm, near-surface layer with a surface skin that is warmer than the water at a depth of several meters. During the night, this shallow warm layer cools making the skin temperature cooler than the temperature just a few meters below. Hence the difference between the skin and bulk temperature ranges anywhere from -0.5° K to

0.9° K. These differences have to be kept in mind when comparing remotely sensed SST with bulk temperatures.

The MCSST technique using AVHRR data discussed above is widely and operationally used for the determination of SST. The MCSST based algorithms had been extensively tested, modified and compared with other methods for its accuracies. *McClain et al.* [1985], have compared the MCSST data with *in situ* Pazan ship data for different seasons. They computed standard deviations of 0.5–0.6° C and biases between 0.3–0.4° C. *Schluessel et al.* [1987], have used *in situ* skin temperature measured from radiometers and subsurface data to compare with the satellite data. The MCSST method gave a mean difference ranging from 0.55 to 0.73° C in comparison with the *in situ* skin temperatures and a difference between -0.25° and 0.6° C with subsurface measurements. When the MCSST was used with additional atmospheric corrections with data from the High-Resolution Infrared Sounder (HIRS), the temperature difference reduced to between 0.22° to 0.33° C. MCSST data are also compared with *in situ* data from comprehensive ocean-atmosphere data (COADS) for the period 1982-1988 [*Bates and Diaz,* 1991]. The comparison shows the MCSST values lower than COADS by 0.19° to 0.64° C, with a standard deviation ranging from 0.03° to 0.45° C.

The general conclusion of these studies is that the MCSST algorithms are capable of producing surface temperatures accurate to within 0.3° C and rms deviations of about 0.5° C [*McClain et al.,* 1985; *Schluessel et al.,* 1987]. The chief among the limitations of the MCSST is lack of retrievals in areas of persistent cloud cover, but the AVHRR with its high resolution is still the best among all the available sensors. Atmospheric aerosols from volcanic eruptions have been shown to greatly increase the attenuation of the infrared signal. Eruptions from El Chichon, iciano in Mexico, has particularly affected the MCSST's in the northern tropics and subtropics [*McClain*

et al., 1985]. Another possible error is from the uncertainty in the pixel/ship co–location [*Schluessel et al.,* 1987]. But this error is not very large because the surface temperature seldom shows gradients of 0.5° C per pixel.

The old problem of skin/bulk temperature difference still remains. Again this difficulty is reduced to a great extent by the incorporation into the MCSST of temperature-dependent bias correction derived from satellite/buoy match data. This correction presumably compares the average skin versus the 1 m depth *in situ* temperature but the main problem will always remain in this type of retrieval mechanisms [*McClain et al.,* 1985]. The match up between skin and bulk temperature also has improved with a little smoothing of the images and the new non-linear form of MCSST in use nowadays. The other method to properly account for the differences is by using a four-dimensional data assimilation scheme [*Bates and Diaz,* 1991]. *Reynolds* [1988], explains another method, a 'blended analysis' between *in situ* and satellite data which eliminates most of the biases mentioned above. Even with these limitations, the SST obtained from remotely sensed platforms are useful in many oceanographic applications.

3.4 Accuracy of SST data used in this work

We have compiled a 'match up' data base consisting of AVHRR data and *insitu* sea surface temperature measurements corresponding to the time of the satellite measurements. We used reasonably clear SST images of the MAB region from January to June 1992. All the images are obtained during the night time pass of the satellite and the night-time MCSST algorithm and corrections are applied. Thus the error due to warming of the sea surface by solar radiation is reduced. As mentioned earlier, all images are passed through a filter to smooth the unwanted pixels and a cloud/land mask applied to eliminate such areas from our comparison with *in situ* data. Tem-

perature from three by three pixel boxes centered at each *in situ* location is extracted from each image where possible and an average value obtained for comparison with buoy data.

The *in situ* data used here are obtained from US National Data Buoy Center (NDBC) moored buoys located in the MAB region for the year 1992. The are a total of three buoys that fall within the area of the image (Figure 8). The buoy temperatures are averaged over every three hours.

The *in situ* records are matched with the date of the AVHRR extractions. Since only night time images are compared, the time frame of all the images fall within the interval of buoy observations. Thus all the AVHRR extractions fall within the same three hour averaged buoy time. The extracted AVHRR and buoy values are used in the calculation of rms and bias.

The comparison between satellite SST and buoy SST for the three buoys are shown in Figure 9, Figure 10 and Figure 11. The mean square deviation (MSD) for each of the buoys 44009, 44012 and 44014 are 0.348312, 0.321837 and 0.278191 respectively. This gives a root mean square deviation (RMSD) for the whole data set of 0.5622395°. The bias for each of the above buoys in that order yields 0.357917, 0.334490 and 0.199487° C . The bias for the whole data set is 0.297298° C.

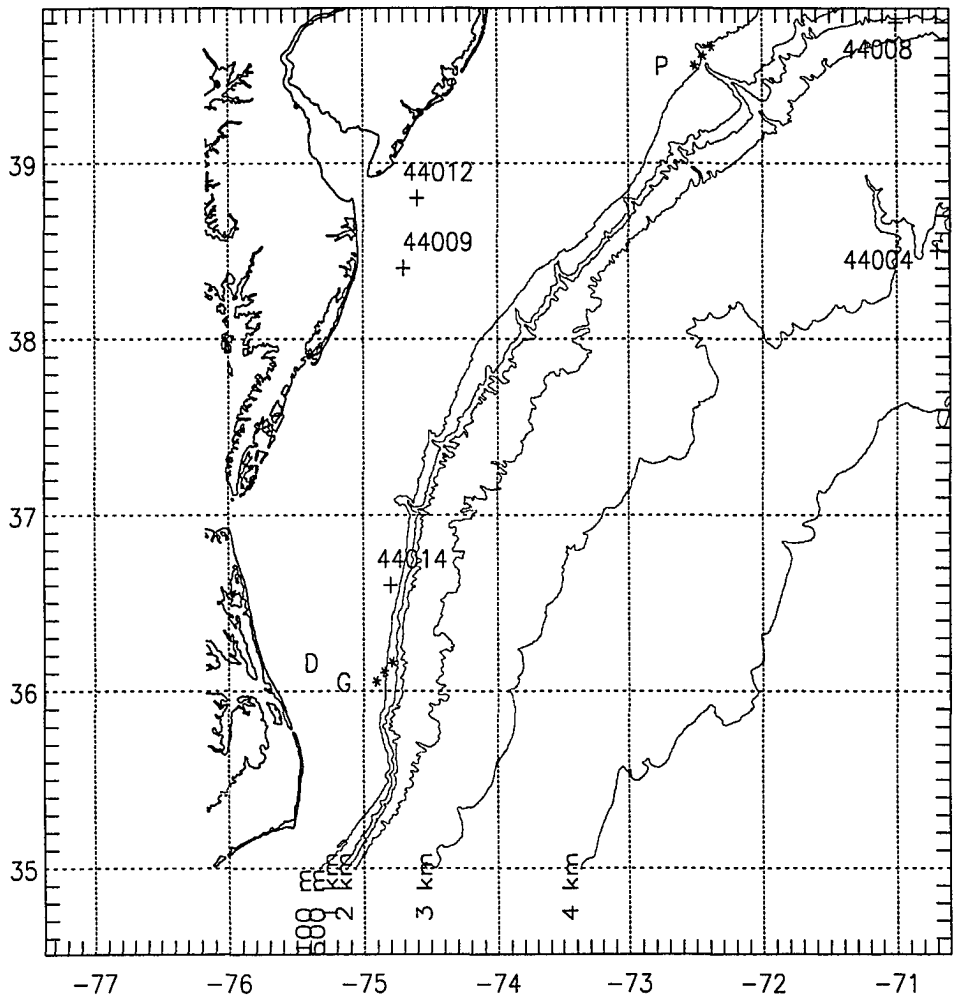

Figure 8: Position of NDBC buoys used for comparison with satellite SST. The stars represented by P shows the location from which the overrunning distances are determined. The stars represented by G, is the location from which the Gulf Stream thermal front distances are measured. D is the location of the tide gauge (referenced in chapter 6).

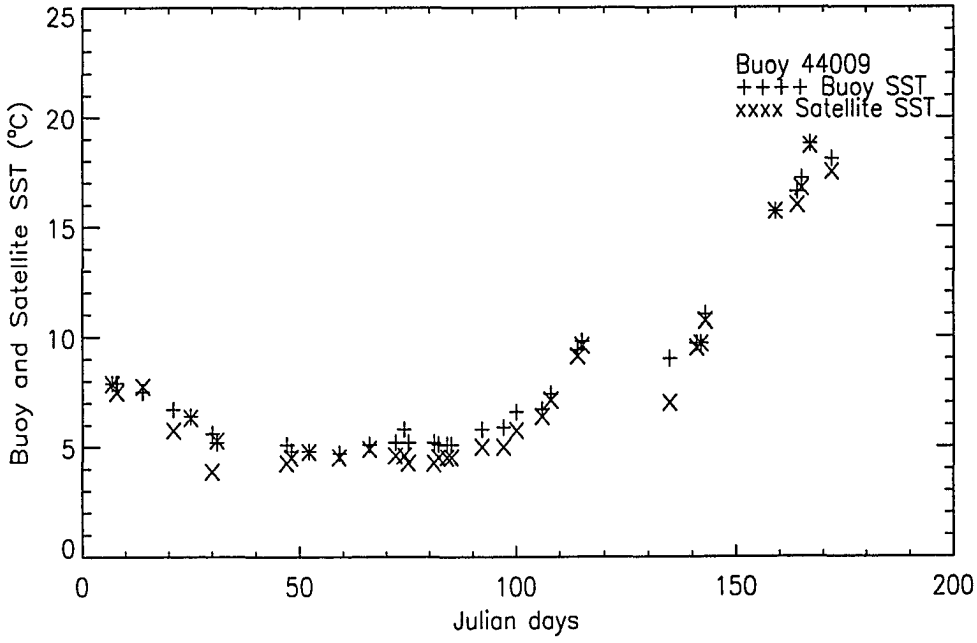

Figure 9: Comparison between satellite SST and buoy (44009) SST.

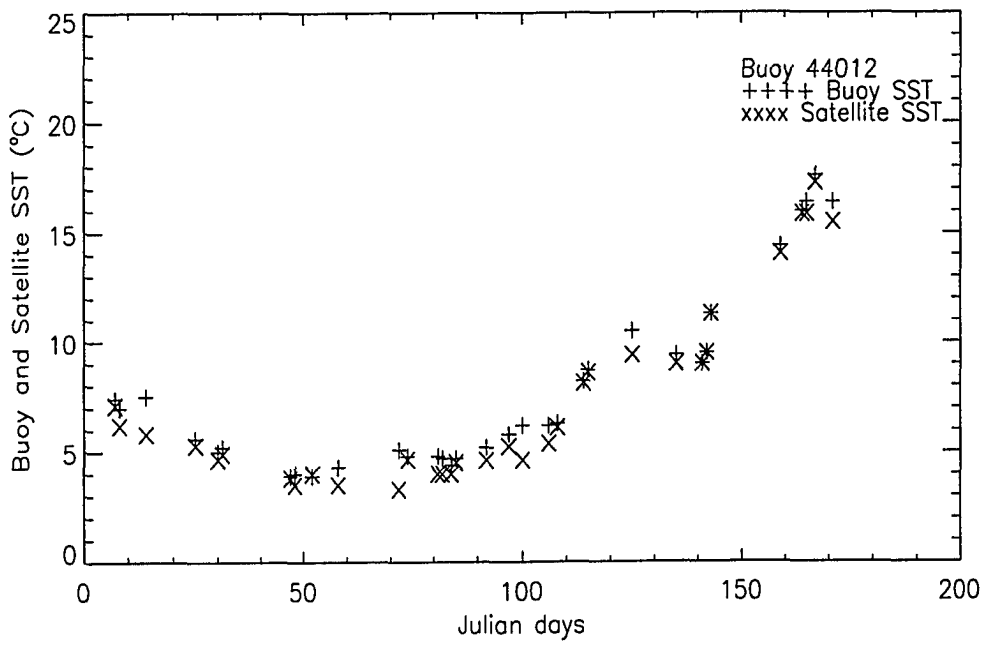

Figure 10: Comparison between satellite SST and buoy (44012) SST.

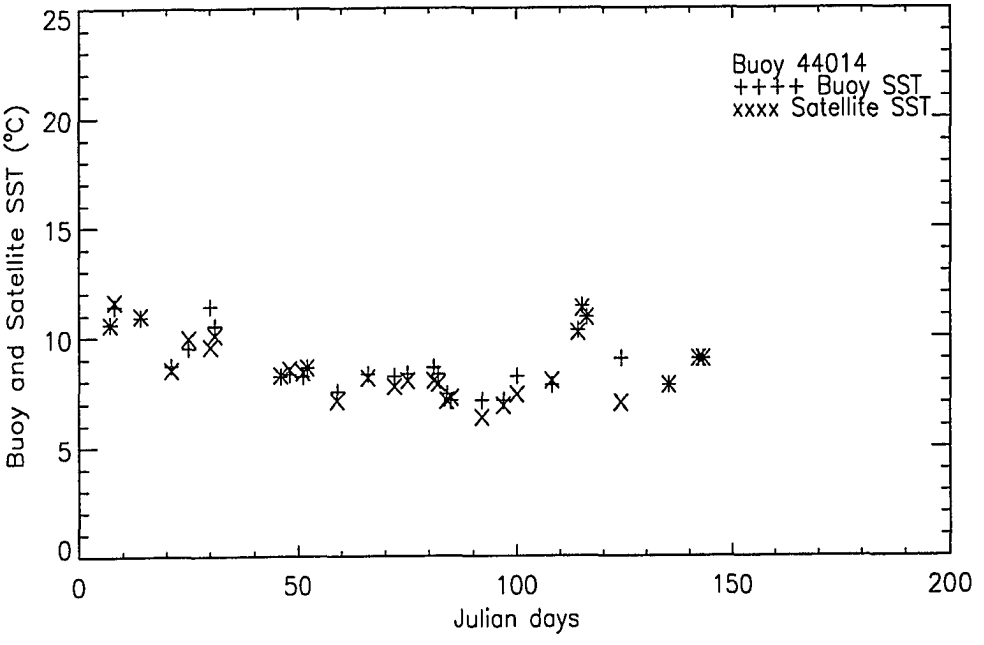

Figure 11: Comparison between satellite SST and buoy (44014) SST.

4 SEASONAL CYCLE OF SURFACE TEMPERATURE OVER THE SHELF AND SLOPE

Sea Surface Temperature in the MAB is subject to various seasonal forcing including solar heating, wind forcing, cooling by winter storms, freshwater input, alongshore transport over the shelf and slope, displacement of water mass by meanders and eddies of the Gulf Stream. The response of the shelf and slope waters to these forcings produce a dramatic change in the seasonal hydrography. From winter to summer the shelf and slope waters progress from relatively homogeneous in the vertical to highly stratified. In this section, a two year (1992 and 1993) narrative of events follows beginning a first step in the analysis of a complete set of usable, high resolution sea surface temperature satellite imageries of the southern MAB.

4.1 Data Acquisition and Processing

The National Environmental Satellite, Data and Information Service provides CoastWatch with near real-time mapped SST products from its polar-orbiting satellite. CoastWatch, a component of NOAA's Coastal Ocean Program, maintains an archive of all SST images from May 1991 onwards. From this archive, all the SST images for 1992 and 1993 are obtained via file transfer protocol (FTP). The AVHRR provides 2 images per day of the study area, one at night and the other during the day. Since night time passes of the satellite reduces the error due to solar heating, all images presented here were acquired during the night.

4.1.1 Sorting and Contouring

The first task was to sort out the usable list of images. The SST images have a major problem with cloud cover, which makes them unusable and unreliable in many

cases. Therefore, all the images are individually inspected for clouds and only those images that are reasonably free from clouds used in this study. In the end, about 100 reasonably clear images for 1992 and about 60 for 1993 are retained for further analysis.

The SST images are then color coded, with each color covering a temperature interval of 2°C. The presence of water masses with strong horizontal gradients for most of the year in the MAB made the color code useful in distinguishing the various features. Clouds and land are coded black in all the SST images to contrast them with other false colors representing various temperature intervals.

The next process in the analysis required contouring the SST images. The coastline is first contoured to exclude land areas and small islands. Since the satellite does not pass over the same track each time, the images had to be registered individually to a fixed coastline to exactly match the land-sea boundary. Latitudes and longitudes are drawn and labeled on each image. A one degree grid (white dots, Figures 12 to 22) is overlaid on the images. The bathymetry is also indicated on each image: for simplicity only the 100 m isobath is shown, which is marked by the white line off the coast on each of the images (Figures 12 to 22). The 100 m isobath is the conventional separation line between the "shelf" and the "slope".

As discussed in Chapter 3 , Expendable Bathythermographs (XBT) and surface salinity data, coincident with the satellite data, are obtained from Oleander Ship of Opportunity program. The hydrographic stations are shown as white stars on each image (Figures 12 to 22).

Finally, surface temperatures fields are contoured with the 10°C isotherm to identify the extent of the shelf water. The center isotherm, in Oleander data, of the shelf water-slope water surface front was 12°C in early January, dropping to 10°C by

late January, and remaining at that temperature at least to mid-March. Therefore, the 10°C isotherm separating colder shelf water (green tones) from warmer shelf water (light blue, near 12°C) is emphasized with a thick black line on the SST images.

4.1.2 Data Coverage

Hundred SST images for 1992 and sixty images for 1993 reflect approximately 5 images per month. The frequency of useful SST images in the summer months is less due to decrease in thermal contrast and frequent cloud cover. The SST image has a resolution of 1.1 km at the nadir. Each image extended from longitude 71 to 77 and latitude 34.5 to 40 degrees. The temperatures shown in false color ranged from 0 to 32°C, with black representing 0°C (land and clouds) and white 32°C in the color.

4.2 Discussion of the contoured SST images

A sequence of adequately clear images spanning the two years 1992 and 1993 are shown in eleven plates attached to this Chapter. The following is a running commentary emphasizing their most notable features.

4.2.1 1992

On 8 January 1992 (image a01) low sea surface temperature of about 4–8°C (shades of green) is evident near the coast, progressively increasing to warmer temperatures (shades of blue) of 10 and 12°C in the slope region. The Gulf Stream (bright red) is partly obscured by clouds. The 10° isotherm (thick black line) shows the shelf water–slope water surface front ("front" from here on) to be well within the 100m isobath (white line). The SST image also clearly shows shelf water entrainment to

the Gulf Stream at Cape Hatteras. In the north, shelf water is seen, albeit partly covered by clouds, over the slope region.

The SST image on 31 January (a02) shows the front hugging the 100 m isobath from New Jersey to Virginia, where shelf water turns towards the Gulf Stream. This is presumably the undisturbed state of the front. In sharp contrast, the northeast corner of the image shows shelf water overrunning the Slope Sea to a distance of about 100 km off New Jersey. An anticyclonic eddy is also visible, just ahead of the shelf water in the slope region.

The next three images (a03 to a05) display the movement of the "face" of the shelf water mass that overrun the slope region. The face has progressed southwestward by 50 km from 3 February to 10 February and by nearly 120 km by 17 February. The anticyclonic eddy has progressed similarly, projecting shelf water ahead on its journey southwestward. Eddy activity appears to mix some of the shelf water as seen by the light blue enclosures within the overrun shelf water. On the 17 February, the anticyclonic eddy is connected to the Gulf Stream by a 'streamer' of shelf water. The anticyclonic eddy has almost disappeared by 21 February (a06). Shelf Water off Delaware almost reache the Gulf Stream. Most of the Slope Sea is covered by shelf water. Again, the Gulf Stream can be observed to entrain shelf water off Cape Hatteras.

On 28 February (a07), a part of the shelf water volume appears mixed with the slope water as seen by the light blue patches on the image. The large volume of shelf water has now progressed southwestward and has reached off Chesapeake Bay. Filaments from the Gulf Stream are connected to the shelf water at various points before being entrained by the Gulf Stream. Somewhat smaller but still substantial overhanging of shelf water persists and is noticeable all along the front at the end of March (22 March, a08)

The SST image on 1 April (a09) shows a large blotch of overrunning shelf water being entrained by the Gulf Stream off Chesapeake Bay. This may have accumulated from the sustained transport seen on March 22. Mixing between shelf and slope waters is evident in the north by the appearance of 14°C (dark blue) along with the 10°C (green) and 12°C (light blue shades) of water.

On 9 April (a10), a second episode of shelf water overrunning has started from the north. Large areas of shelf water once again flood the northern portion of the image, off New Jersey. Entrainment of the blotch of shelf water still persists off Chesapeake Bay. The image on 15 April (a11) shows the progression of the second episode of overrunning. The face has traveled about 80 km southwest. The face also has connected to a filament of the Gulf Stream. Large areas of shelf water still persist in the slope region off Chesapeake Bay, eventually to be entrained by the Gulf Stream.

As spring progresses, heating of shallow coastal waters become evident, while the outer shelf current transports colder waters from the north (24 April, a12). A temperature minimum (8°C) occurs at the shelf edge, between 100 and 500 m isobaths. It also signifies the end of the second episode of overrunning. The shelf water has mixed with the slope water, as seen by the 12°C water mass and is being entrained by the Gulf Stream. Patches of remnant shelf water can be seen in the slope region.

The images of May 5 to June 7 (a13–a15) show a wedge of cold water reaching down to almost Cape Hatteras over the outer shelf (between say, mid–shelf and the shelf–edge front). This is unlikely to be well–mixed water to the bottom (Oleander May1–2 proves that it is not, although density differences are slight) so that advection from the north is at best partially responsible.

On May 5 (a13), at Delaware Bay, the surface minimum temperature is 7°C. The

shelf water feeds into the Gulf Stream off Chesapeake Bay. Again mixing of 10-13°C waters can be seen in the north. On 21 May (a14) the temperature in the midshelf region has increased to nearly 12°C (light green). Temperature has also increased in the Slope Sea to around 18°C and the thermal contrast between the waters of the Slope Sea and the Gulf Stream starts to disappear.

On 7 June (a15), the outer shelf current remains visible albeit at a temperature of about 14°C. The temperature in the mid shelf region is cooler (12°C) than in the inner and outer shelf regions (16°C). Entrainment of the shelf waters by the Gulf Stream is also clearly seen.

During summer the shelf waters in the MAB warm up rapidly and the thermal gradient between the shelf and slope waters disappears. The 20°C isotherm is contoured by the black line on the images of 29 June (a16). Temperatures all over the shelf are more than 20° except for the slightly cooler waters over the mid and outer shelf. The Gulf Stream can be seen in shades of white in this image, representing temperatures of more than 30°C at this time of the year.

On the 11 July (a17) image, the temperatures have risen further all over the shelf (more than 22°C). An elongated strip of water cooler than 22°C is enclosed by the 22°C contour lines at the shelf edge. Another feature is the cooling of the coastal waters near New Jersey. The cooling of the coastal and inner shelf has progressed up to the Chesapeake Bay on the SST image 2 August (a18). Cool waters (less than 22°C) can be seen in the slope regions off New Jersey. By the 8 of August (a19), the cooling of the mid and outer shelf waters are noticeable by the progression of the elongated strip contoured by the 22°C isotherm.

As Fall commences, the shelf water in the MAB starts to cool rapidly. The SST images on the 12 and 13 September (a20 and a21), contoured by the 24°C isotherm,

show the cooling of the shelf region during early fall.

On 2 October (a22), the outer shelf current advects cooler water from the north as shown by the 22°C isotherm. The temperatures close to the coast off Delaware also have cooled to below 20°C. The warmer mid–shelf waters separate the layers of *in situ* cooling at the coast from cold water advection at the shelf edge. By the 7 of October (a23) the whole shelf is cooled to below 20°C. The 20°C isotherm hugs the shelf edge from New Jersey to Chesapeake Bay. By the 24 of October (a24), the shelf has cooled further to less than 18°C. The 18° isotherm (black line) follows the shelf edge, slightly off the shelf. Entrainment by the Gulf Stream can also be seen in the last two images.

As the season progresses the shelf and slope waters cool gradually and thermal contrast between these waters begin to reappear. On the 26 October (a25) image, the shelf water has cooled to about 16°C up to the Maryland coast and the mouth of the Chesapeake Bay.

On the SST images of 9 and 10 November (a26 and a27), the rapid cooling of the shelf is clearly observable. Within 24 hours the shelf water has cooled from 15 to 12°C off Delmarva peninsula. By the 6 of December (a28), the gradients between the shelf, slope and Gulf Stream (obscured by clouds) have reappeared. The dark area (mostly black) over most of the slope region and the Gulf Stream in the last 4 SST images are clouds typical of this time of the year.

4.2.2 1993

The SST images in 1993 follow the same seasonal cycle as in 1992. The lower number of images during 1993 is because of large cloud cover in many of them in the region of the study area especially during summer. Even then the main features described

in 1992 are again seen in 1993 and a description of events follow.

The SST image on 24 January (b01), 1993 shows the front (10°C isotherm) hugging the 100 m isobath from New Jersey to the Chesapeake Bay. Coastal waters are noticeably cooler than the outer shelf. Shelf Water overrunning into the slope region can be seen some 150 km off New Jersey. This overrunning has started a week earlier than in 1992. On 3 February (b02), the overrunning has remained in the same position. But by the 15 February (b03), the overrunning has progressed half way along the Delmarva peninsula, some 200 km southwestward, remaining there on 19th February(b04).

On 12 March (b05), the overrunning has covered much of the Slope Sea and connects to filaments of the Gulf Stream. The entrainment of shelf water can also be observed on this image. The slope water makes its reappearance by the 22 March (b06). The shelf water starts to clear from the Slope Sea on 4 April (b07) and by the 8 April (b08) only patches of overrunning are visible. Limited overrunning all along the shelf edge can be observed in the 23 April (b09) image. The Slope Sea has reappeared on the SST image and shelf water entrainment off Hatteras is also noticeable on this image.

In 1993, spectacular images of the outer shelf current can be observed. Three temperature layers, 10° (green), 12° (light blue) and 14°C (blue) are noticeable over the outer shelf region on the SST image of 8 May (b10). The cold waters, presumedly advected from the north appear to warm up on its journey towards the southwest. This outer shelf current signature persists on the images of May10 (b11), May11 (b12) and May16 (b13). The image on the 11 and 16 of May also illustrate the entrainment of the cool shelf waters advected by the outer shelf current by the Gulf Stream.

First signs of cooling at the coast are noticed on the image of 4 October (b14).

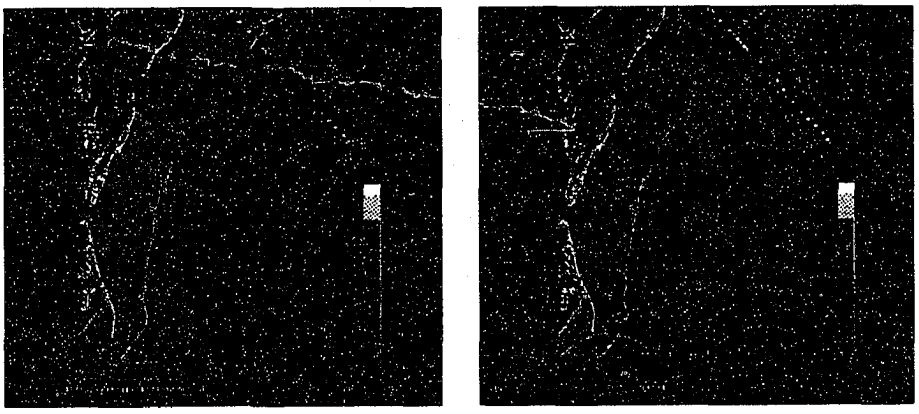

a01. 8 January, 1992.

a02. 31 January, 1992.

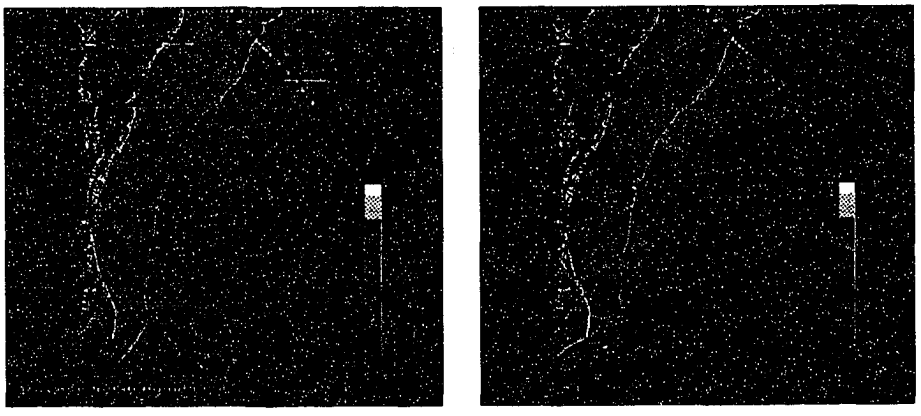

a03. 3 February, 1992.

a04. 10 February, 1992.

Figure 12: Color plate showing SST images.

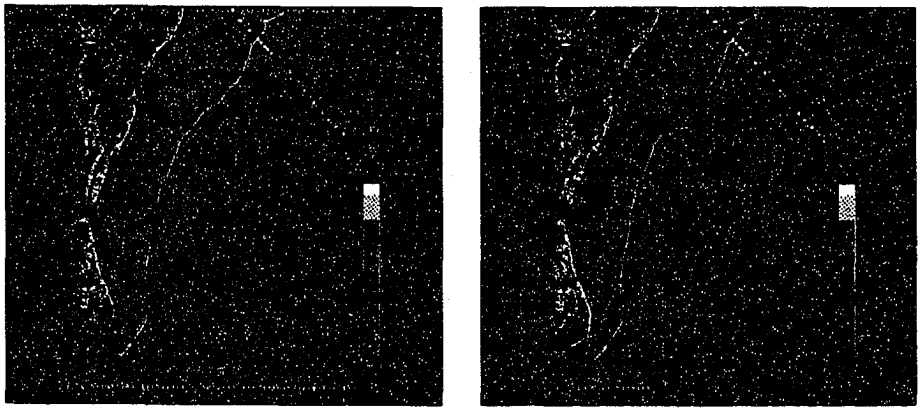

a05. 17 February, 1992.

a06. 21 February, 1992.

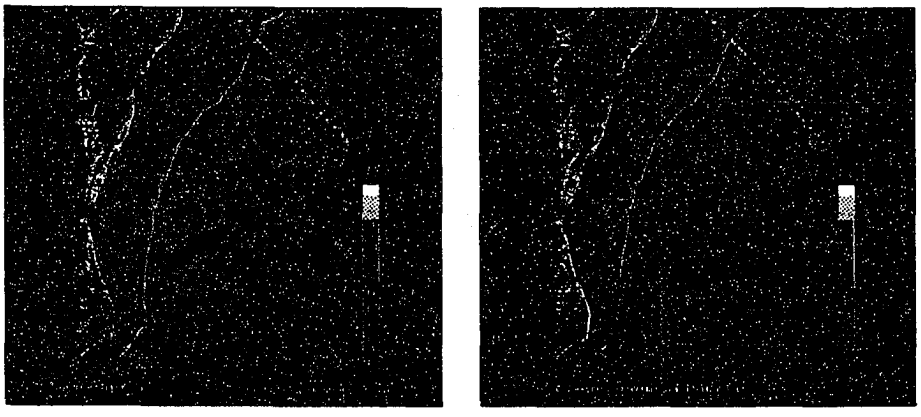

a07. 28 February, 1992.

a08. 22 March, 1992.

Figure 13: Color plate showing SST images.

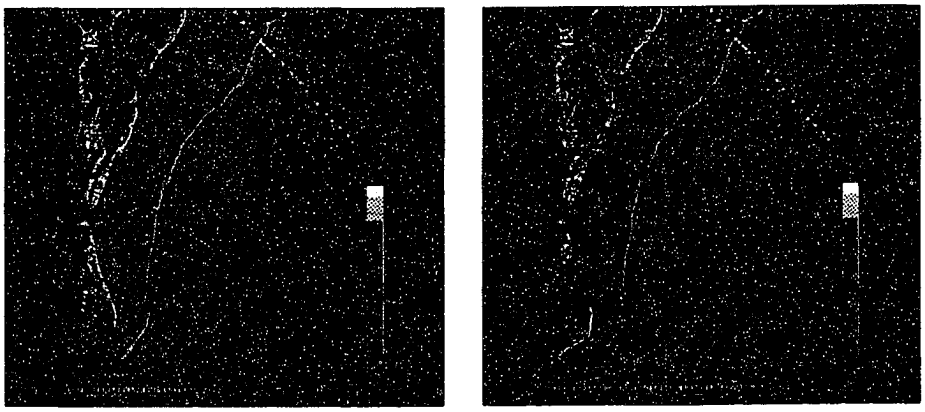

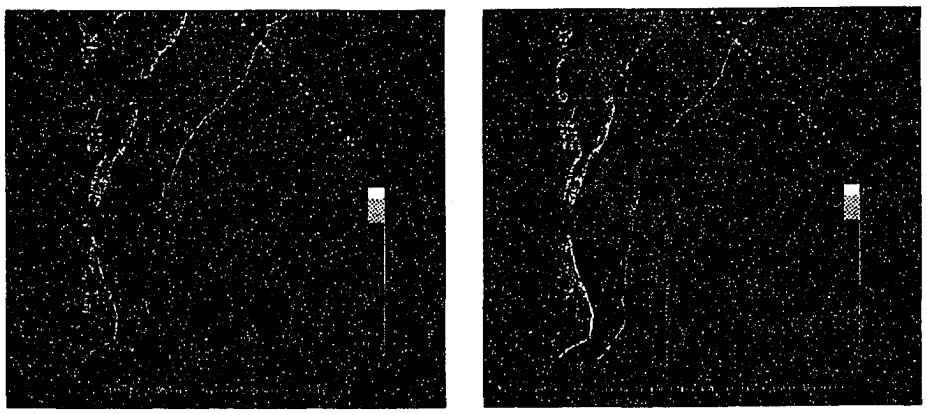

Figure 14: Color plate showing SST images.

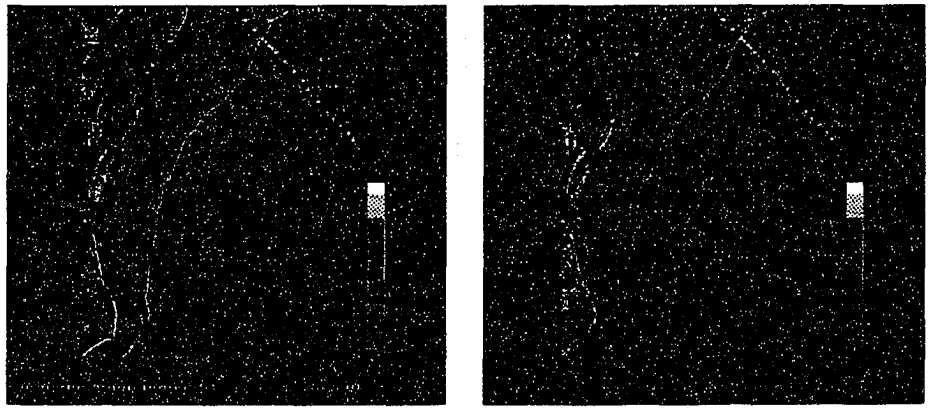

a13. 5 May, 1992.

a14. 21 May, 1992.

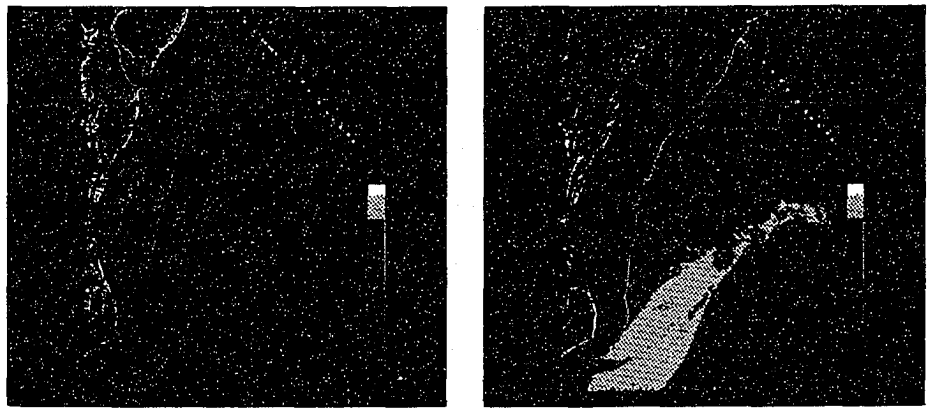

a15. 7 June, 1992.

a16. 29 June, 1992.

Figure 15: Color plate showing SST images.

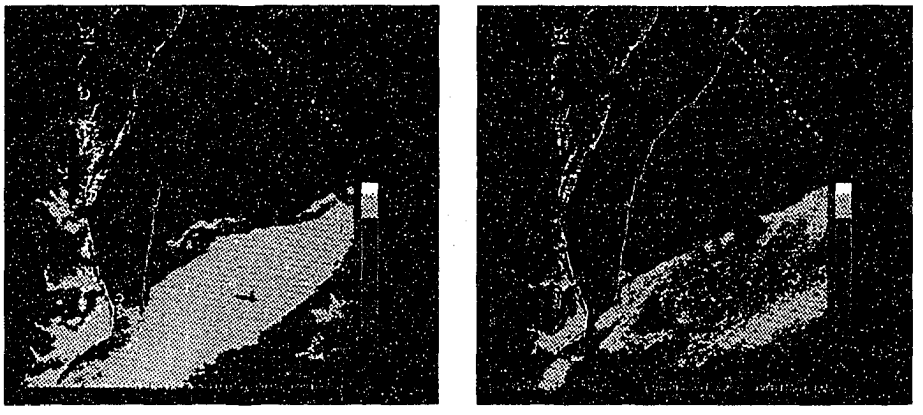

a17. 11 July, 1992.

a18. 2 August, 1992.

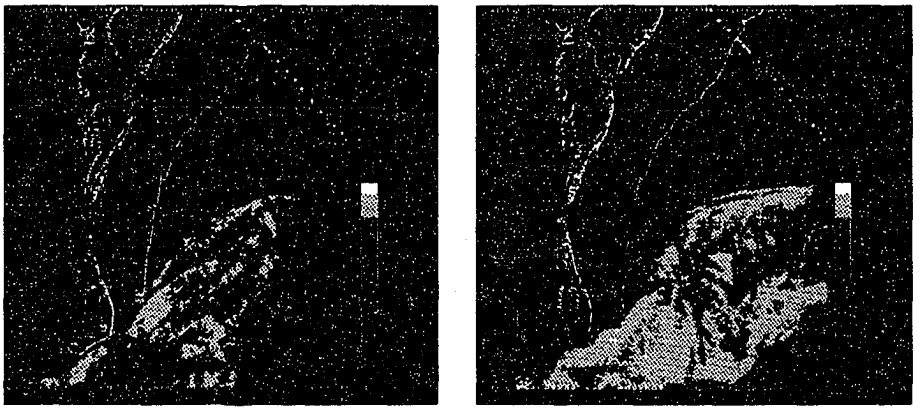

a19. 8 August, 1992.

a20. 12 September, 1992.

Figure 16: Color plate showing SST images.

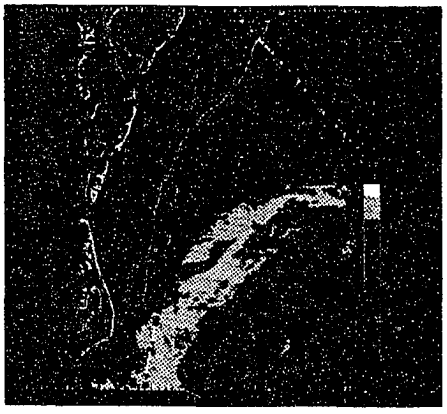

a21. 13 September, 1992.

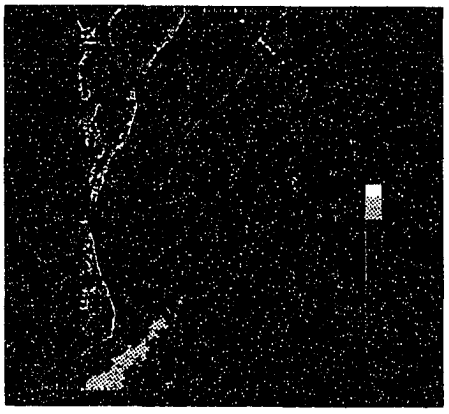

a22. 2 October, 1992.

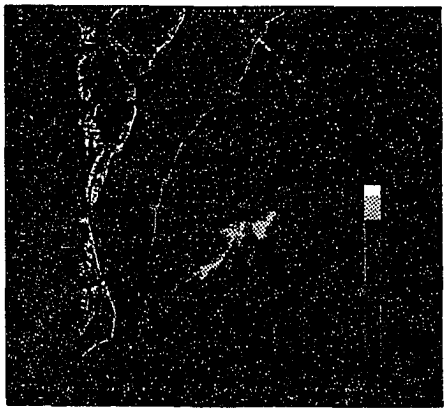

a23. 7 October, 1992.

a24. 24 October, 1992.

Figure 17: Color plate showing SST images.

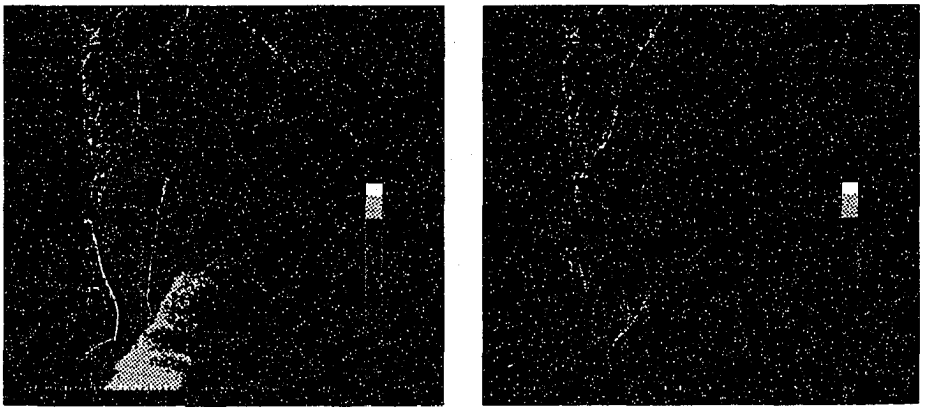

a25. 26 October, 1992.

a26. 9 November, 1992.

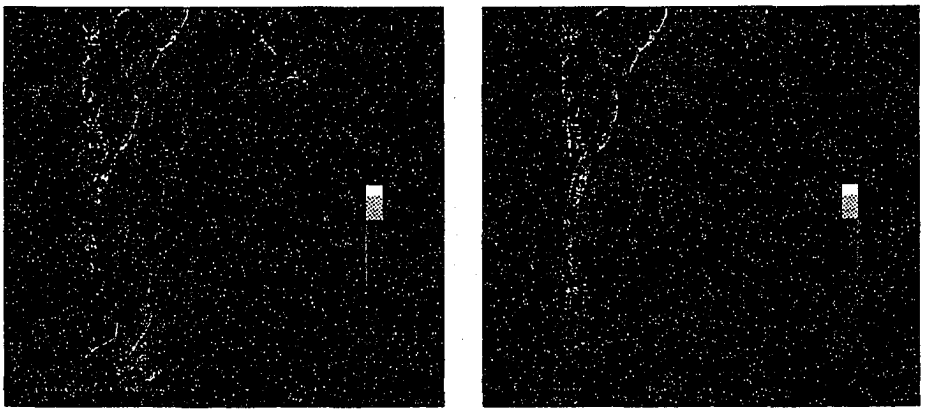

a27. 10 November, 1992.

a28. 6 December, 1992.

Figure 18: Color plate showing SST images.

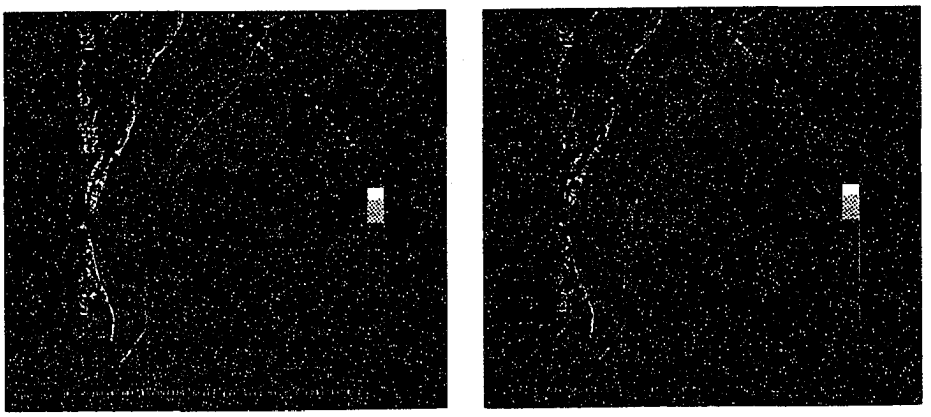

b01. 24 January, 1993.

b02. 3 February, 1993.

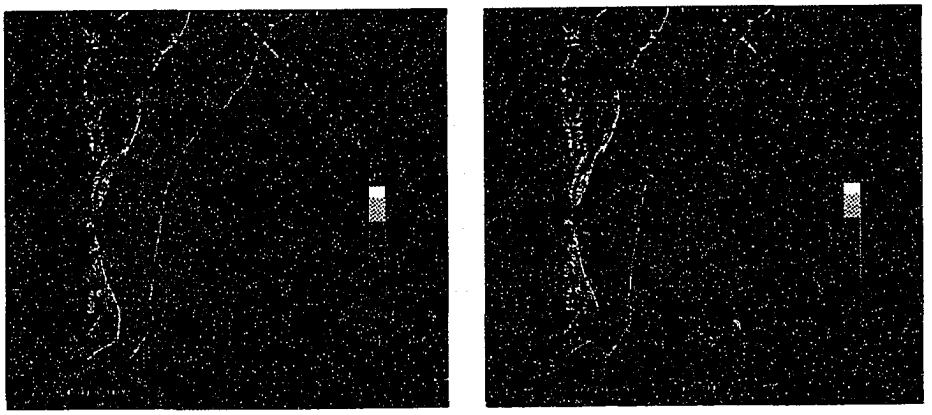

b03. 15 February, 1993.

b04. 19 February, 1993.

Figure 19: Color plate showing SST images.

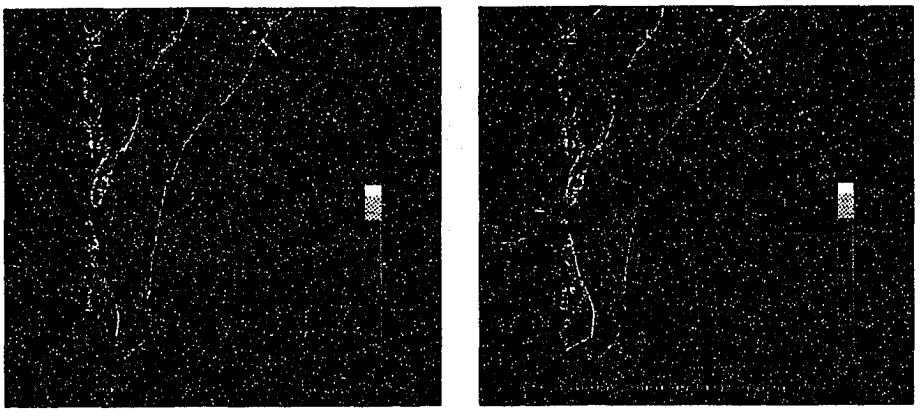

b05. 12 March, 1993.

b06. 22 March, 1993.

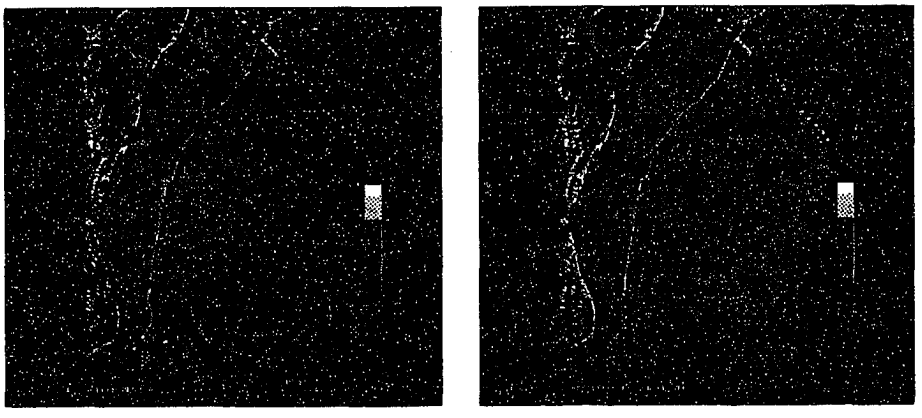

b07. 4 April, 1993.

b08. 8 April, 1993.

Figure 20: Color plate showing SST images.

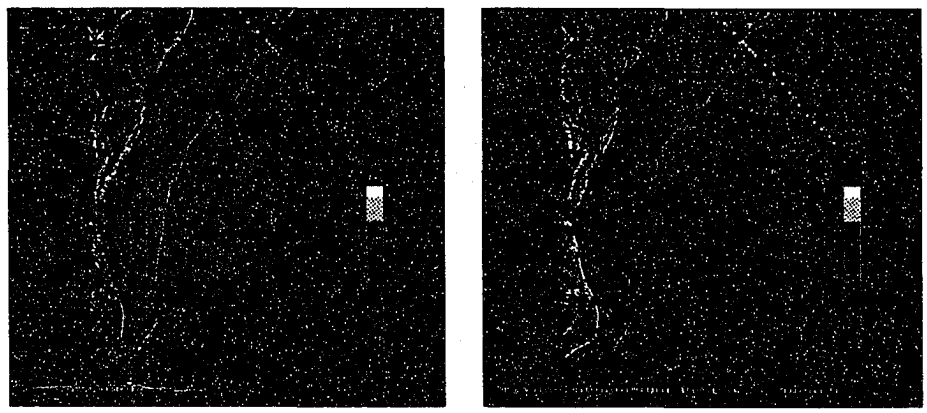

b09. 23 April, 1993.

b10. 8 May, 1993.

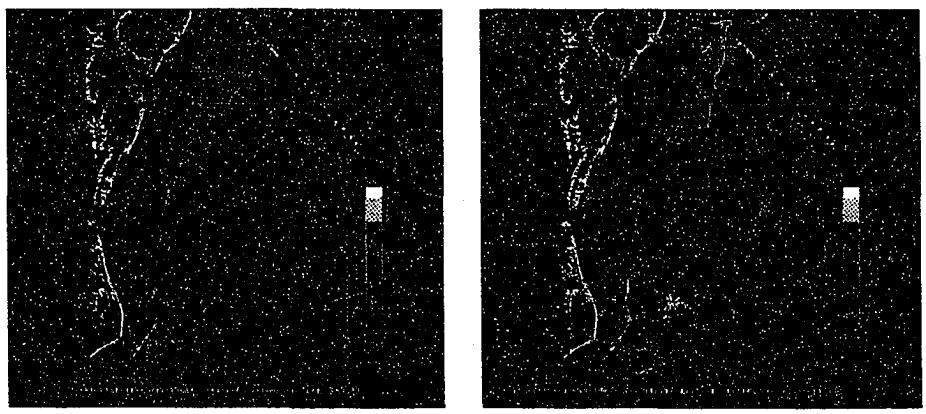

b11. 10 May, 1993.

b12. 11 May, 1993.

Figure 21: Color plate showing SST images.

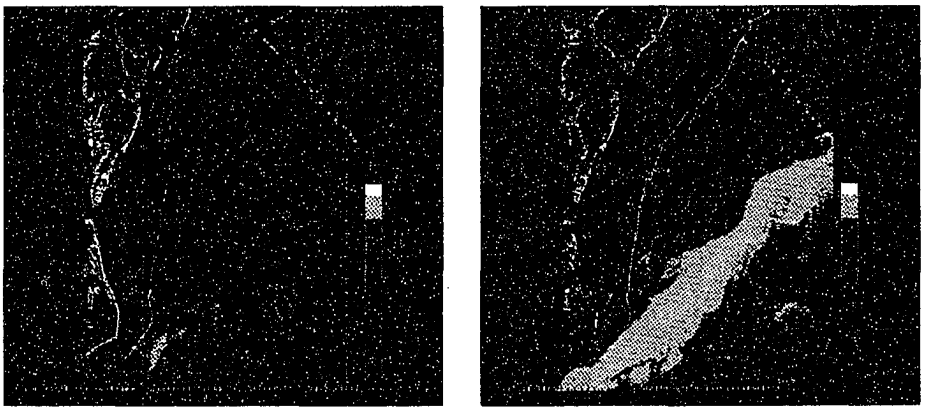

b13. 16 May, 1993.

b14, 4 October, 1993.

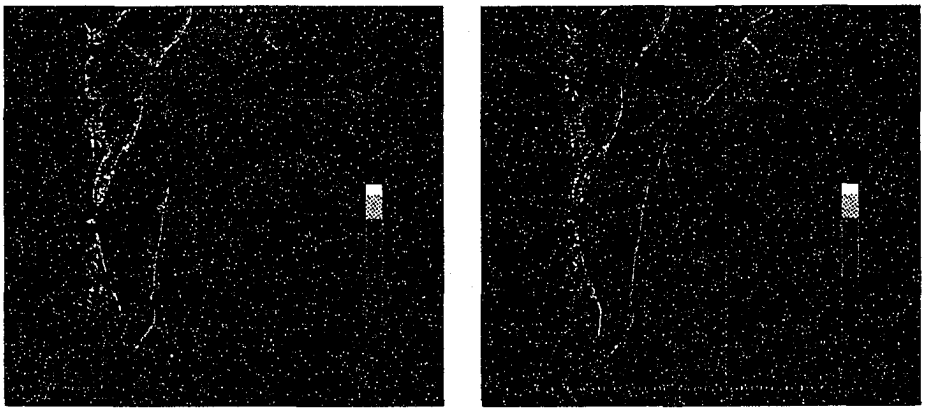

b15, 21 November, 1993.

b16, 31 December, 1993.

Figure 22: Color plate showing SST images.

The temperatures off the coast of New Jersey and Virginia are the first regions to cool to temperatures of 16°C in October, decreasing to 12°C in November and 6°C by December. The surface temperatures decrease systematically offshore. A Gulf Stream filament is seen to curl anticyclonically off Chesapeake Bay on 21 November. By the end of December, this filament has pushed up to the Delaware Bay along the outer shelf. The thermal contrast between the shelf, slope and Gulf Stream waters reappear due to cooling especially by winter storms.

Thus the SST images reveal interesting features during its seasonal progression in the MAB. Among the main features are the seasonal cooling and heating of the coastal and shelf waters. The advection of cool water on the outer shelf in summer. During the early part of the year the shelf water expands and overruns the slope region. The overrun shelf water is entrained by the western wing of the Gulf Stream between Chesapeake Bay and Cape Hatteras and appears lost to the Gulf Stream. Later in the year slope water and Gulf Stream water intrudes onto the outer shelf.

4.3 Time history of surface temperature

We further analyzed the SST images by constructing time series of surface temperatures. First four surface temperature profiles, T(x) at four transects labeled A, B, C, D were extracted from each image stretching across the shelf and slope region in the southern MAB. The location of the transects is shown in Figure 23.

Some sample profiles are shown in Figure 24– 27. A time sequence of SST was extracted from the profiles at fixed distances, representing the inner-shelf (20 m isobath), mid-shelf (40 m isobath),shelf-break (100 m isobath) and slope regions, marked on the profiles (Figure 28 to Figure 35). These time sequence portrays the seasonal variation of surface temperature in the shelf and slope region during 1992

and 1993 of the southern MAB. The blank spaces in some of the line plots are due to missing data caused by clouds in the image.

There is a clear seasonal cycle in the SST time series for the inner, mid and outer shelf regions. The surface temperature during both the years gradually decrease from 10°C in early January to about 5°C in late January. This temperature is maintained for approximately 100 days and falls occasionally to 3–4°C during February and March. The surface temperature then starts to warm up rapidly until it reaches a maximum of 25°C around day 200. From then on the SST starts to decrease and by December the shelf water temperature reaches about 10°C. The inner shelf regions tend to warm and cool more rapidly than the mid and outer shelf due to its shallower depth. Surface temperature also appears noisy along the southernmost transect (D) on the outer and slope regions. The temperature fluctuation, especially during the period between day 100 to day 200 shows evidence of Gulf Stream discharged water over the outer shelf and slope regions as discussed by [*Churchill and Cornillion*, 1991].

The warming trend of surface temperature in the outer shelf is broken during some days for a period between day 130 and day 170. This is noticeable by the periodic fall in temperature across the mid and outer shelf regions. The decrease in temperature is illustrated by a band of cool water advecting along the mid and outer shelf in SST images and represents the signature of the outer shelf current.

The mean temperature of the slope water mass during winter is in the range between 10–15°C. But lower temperatures of 4–9°C are observed frequently during certain periods. This temperature corresponds to shelf water temperature of the same period and again suggest overrunning of slope water by shelf water mass during the early part of the year.

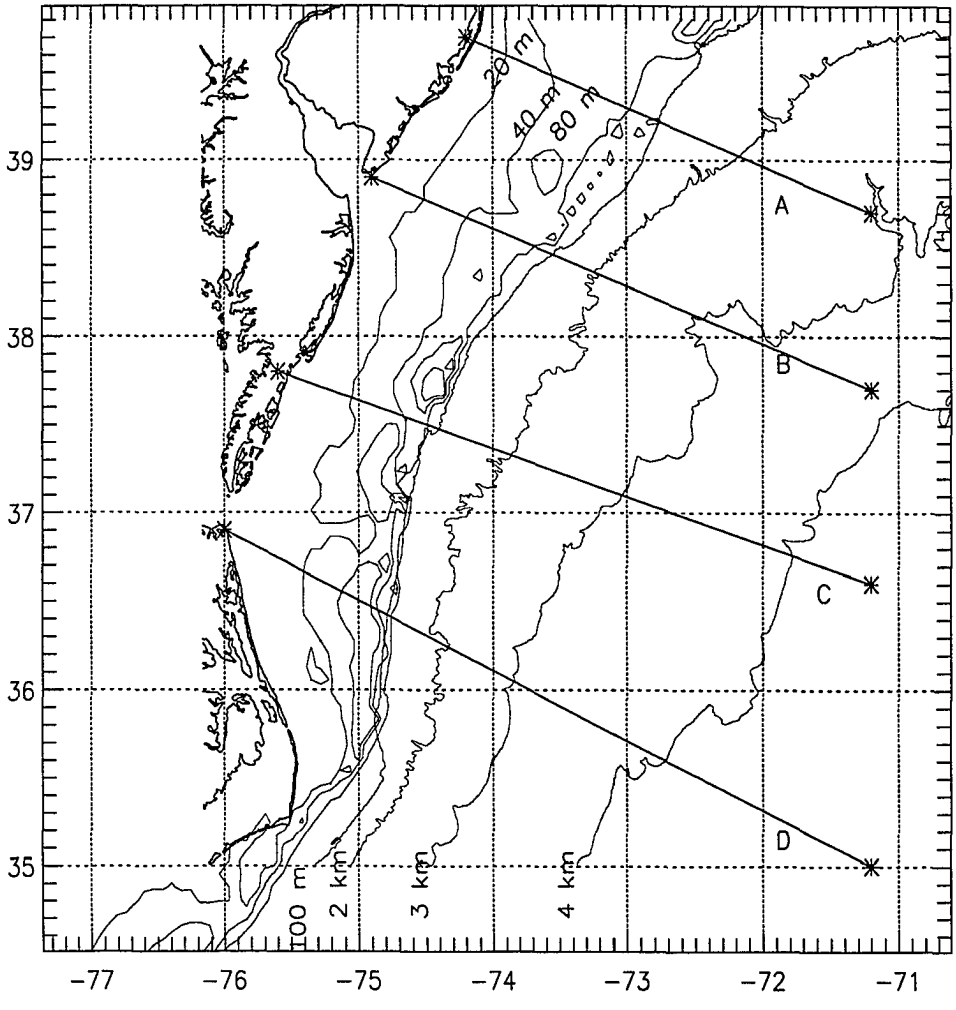

Figure 23: The MAB region showing the four SST transects.

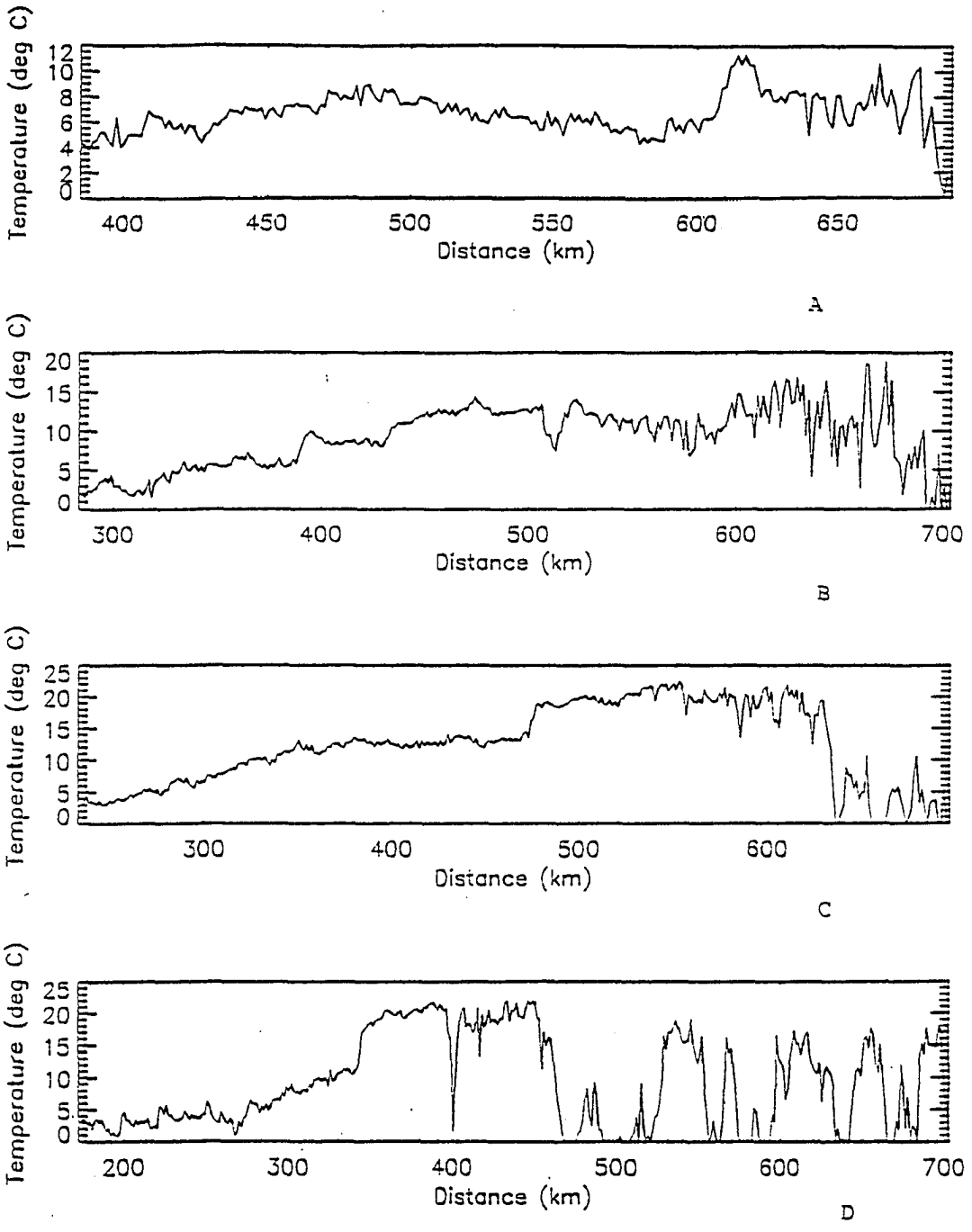

Figure 24: Sample of profiles extracted from a SST image.

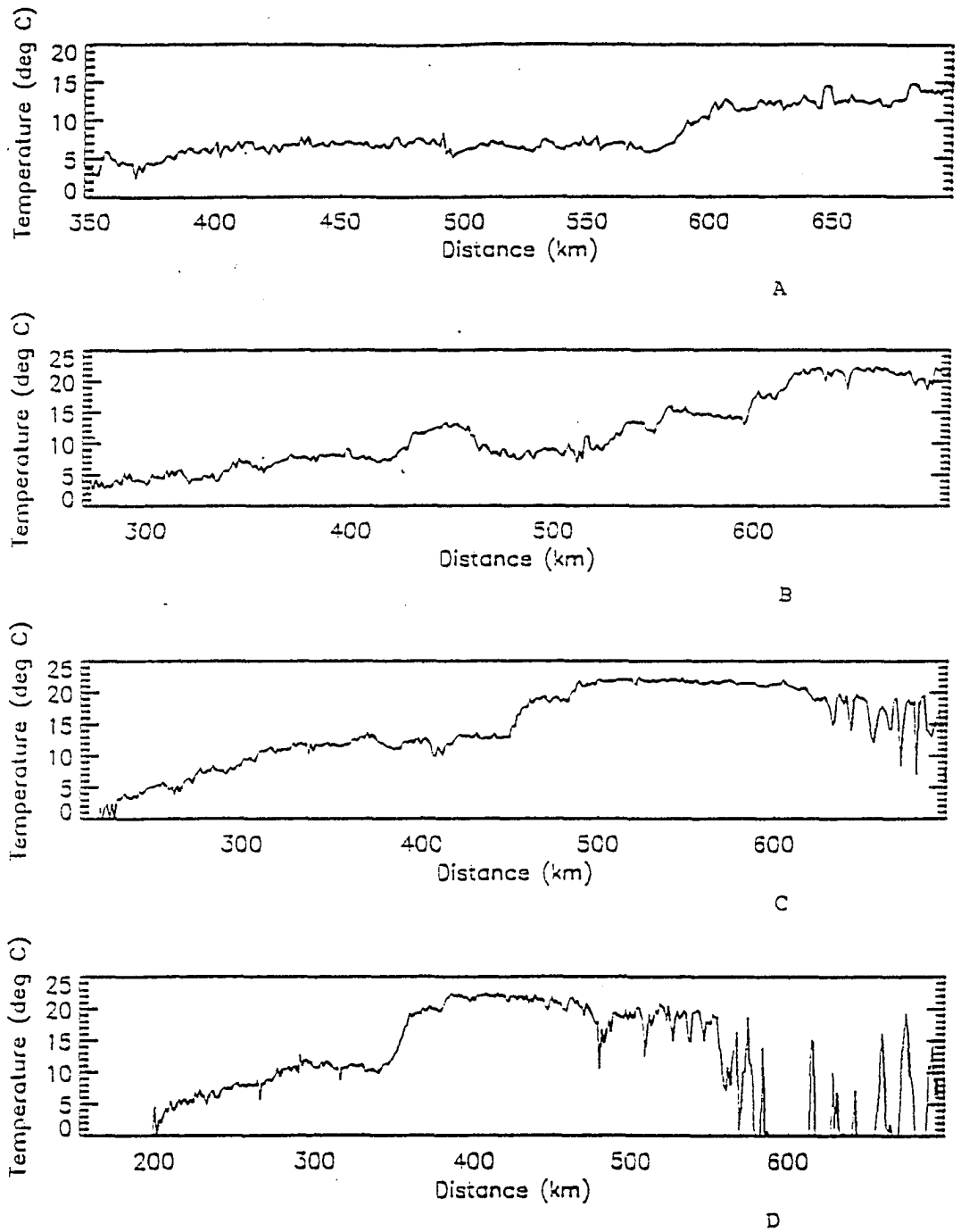

Figure 25: Sample of profiles extracted from a SST image.

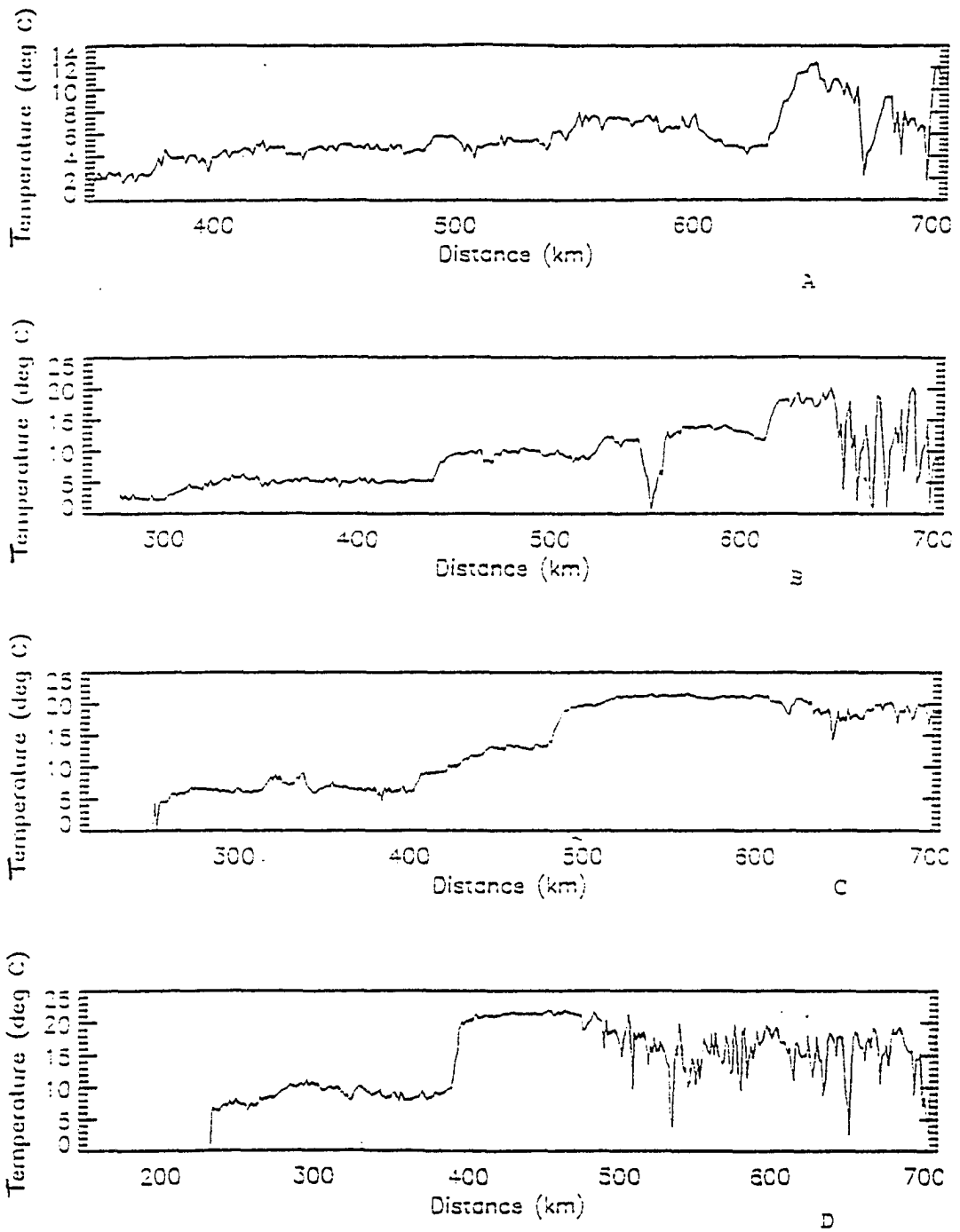

Figure 26: Sample of profiles extracted from a SST image.

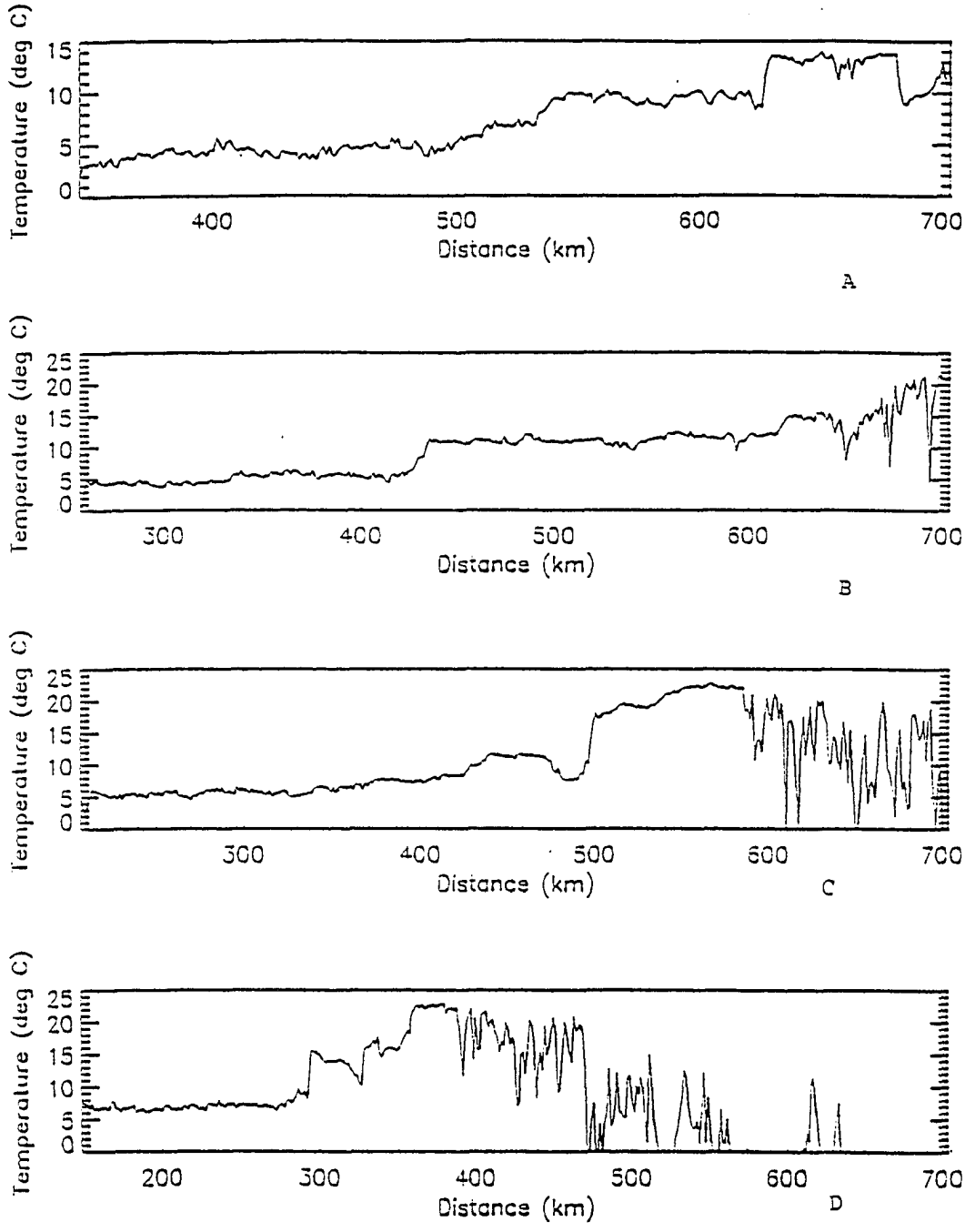

Figure 27: Sample of profiles extracted from a SST image.

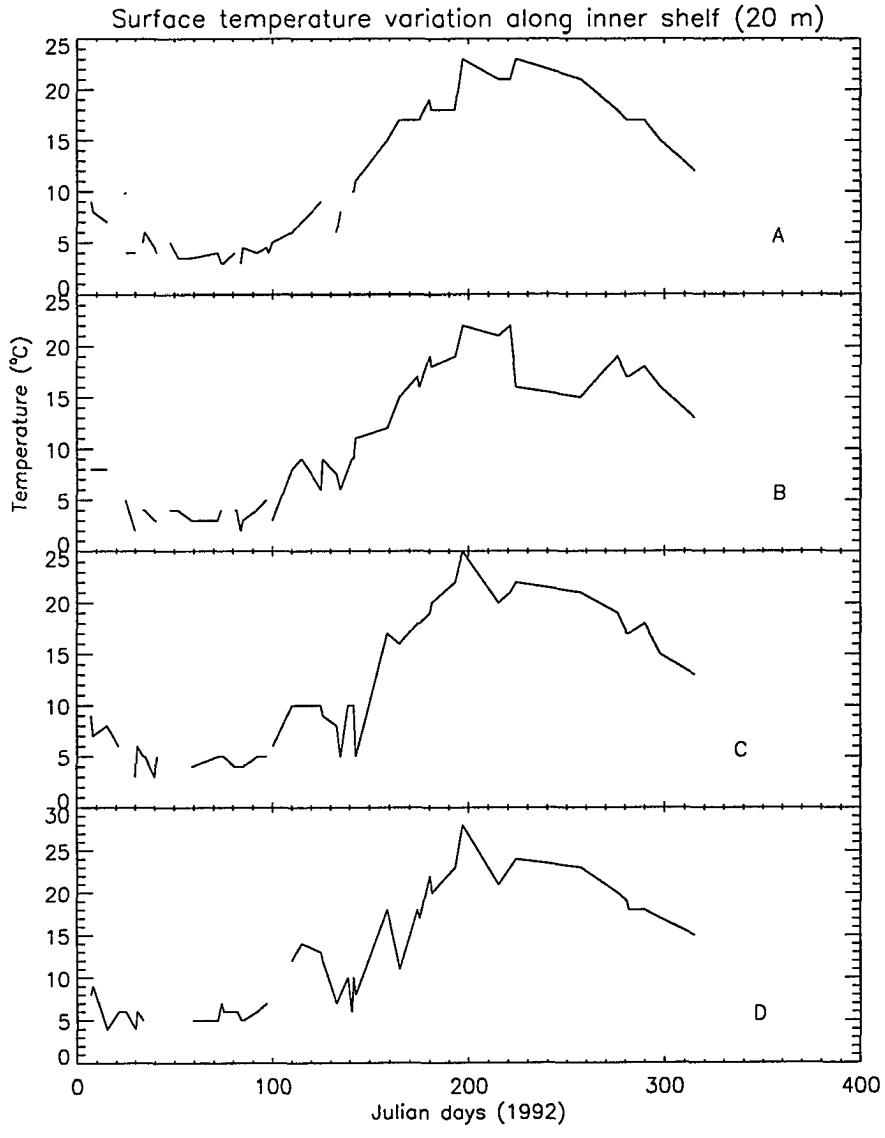

Figure 28: Time series of surface temperature on the inner shelf extracted from SST profiles along the four Transects (1992).

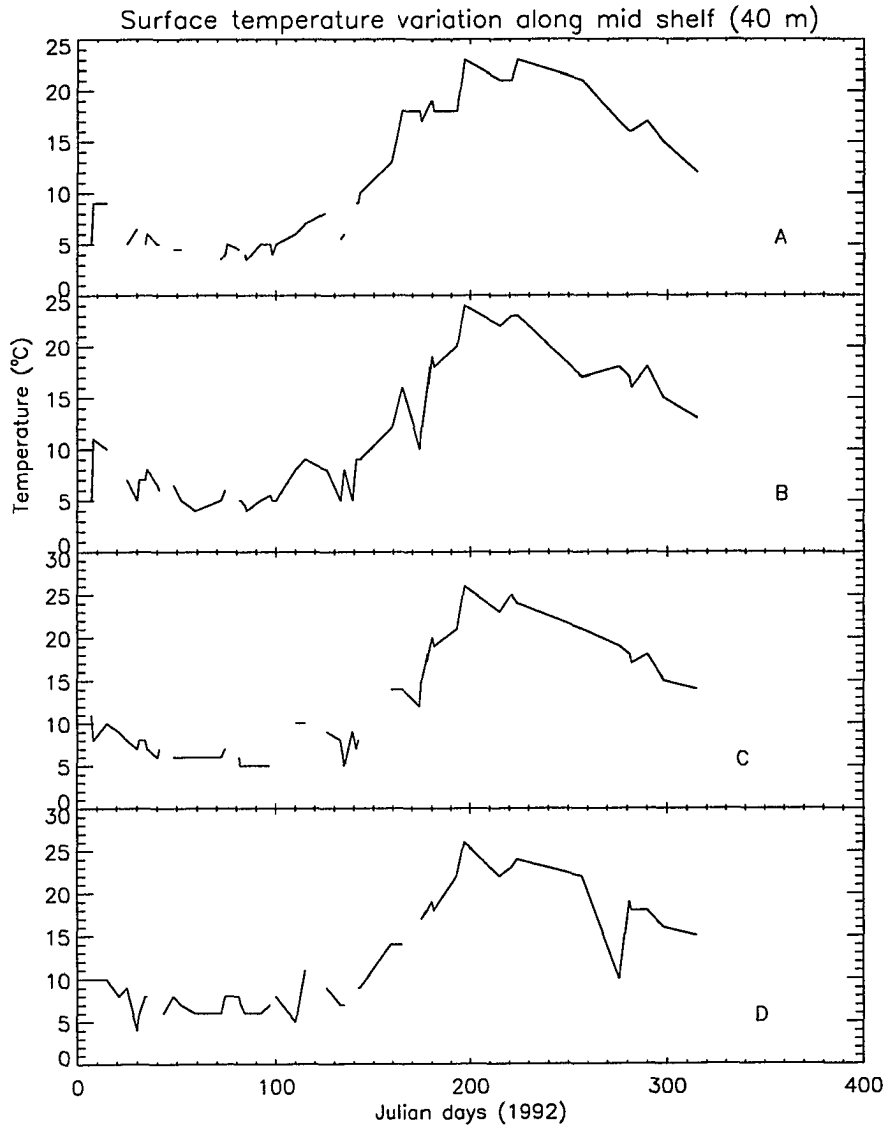

Figure 29: Time series of surface temperature at the mid shelf.

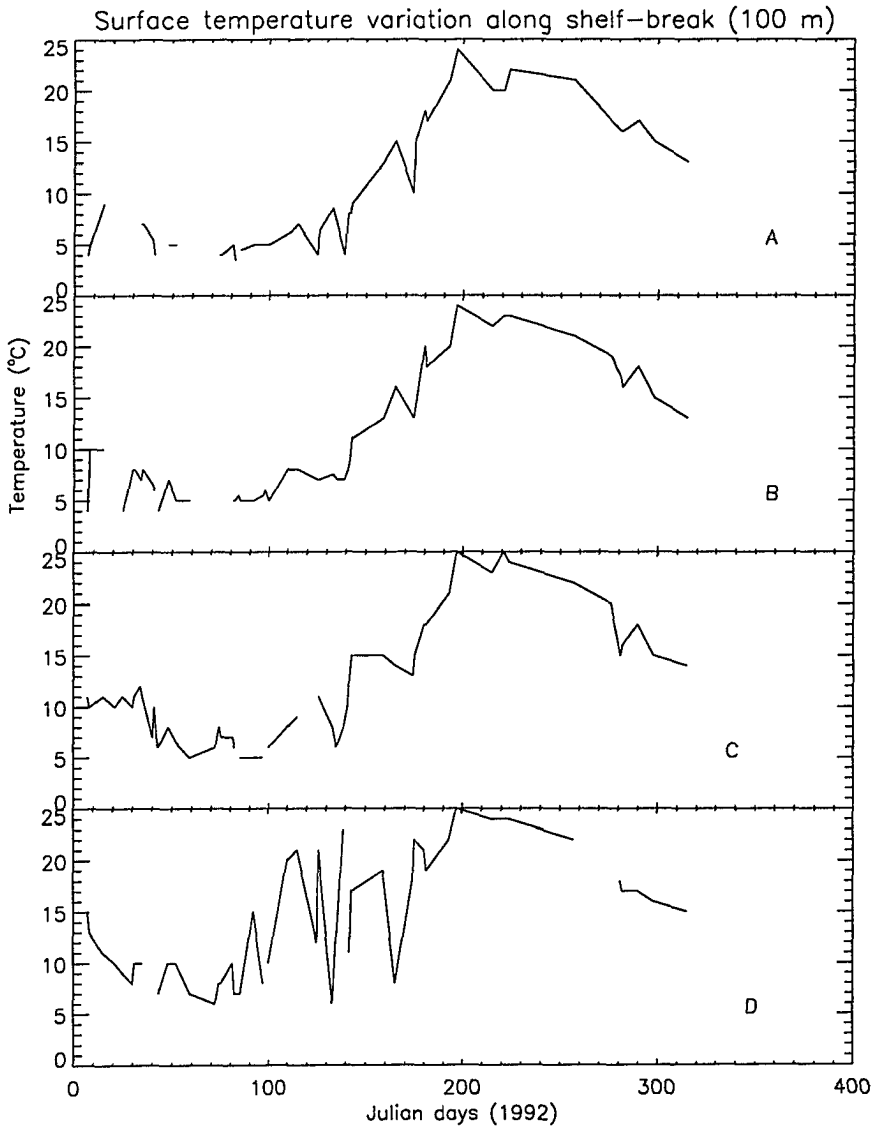

Figure 30: Time series of surface temperature on the outer shelf.

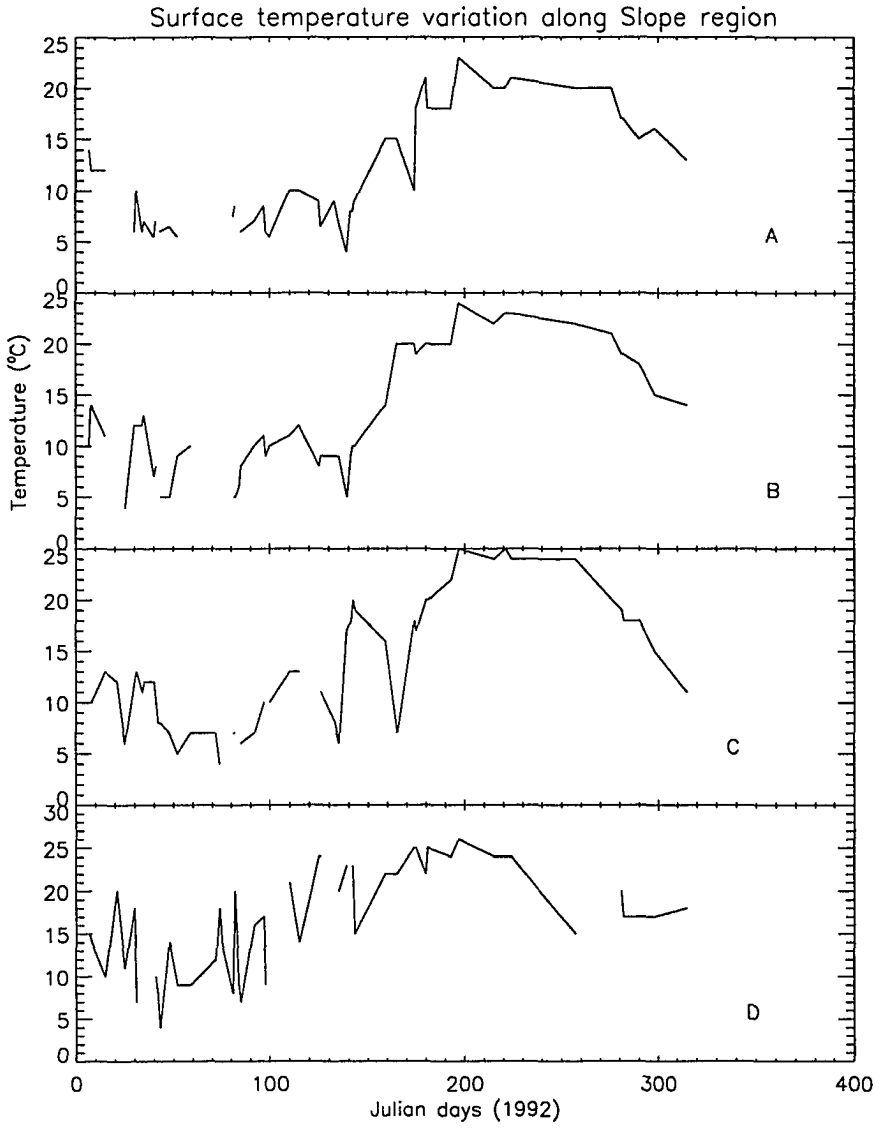

Figure 31: Time series of surface temperature in the slope region.

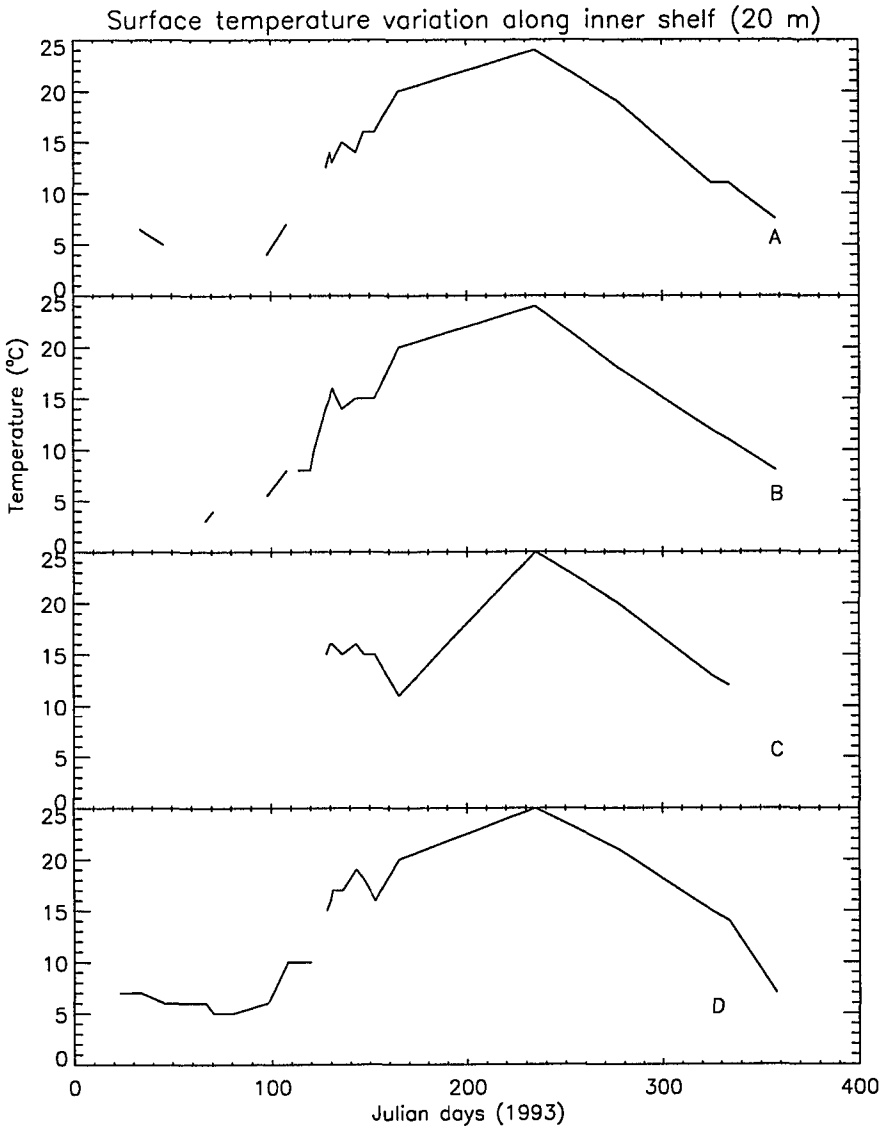

Figure 32: Time series of surface temperature on the inner shelf extracted from SST profiles along the four transects (1993).

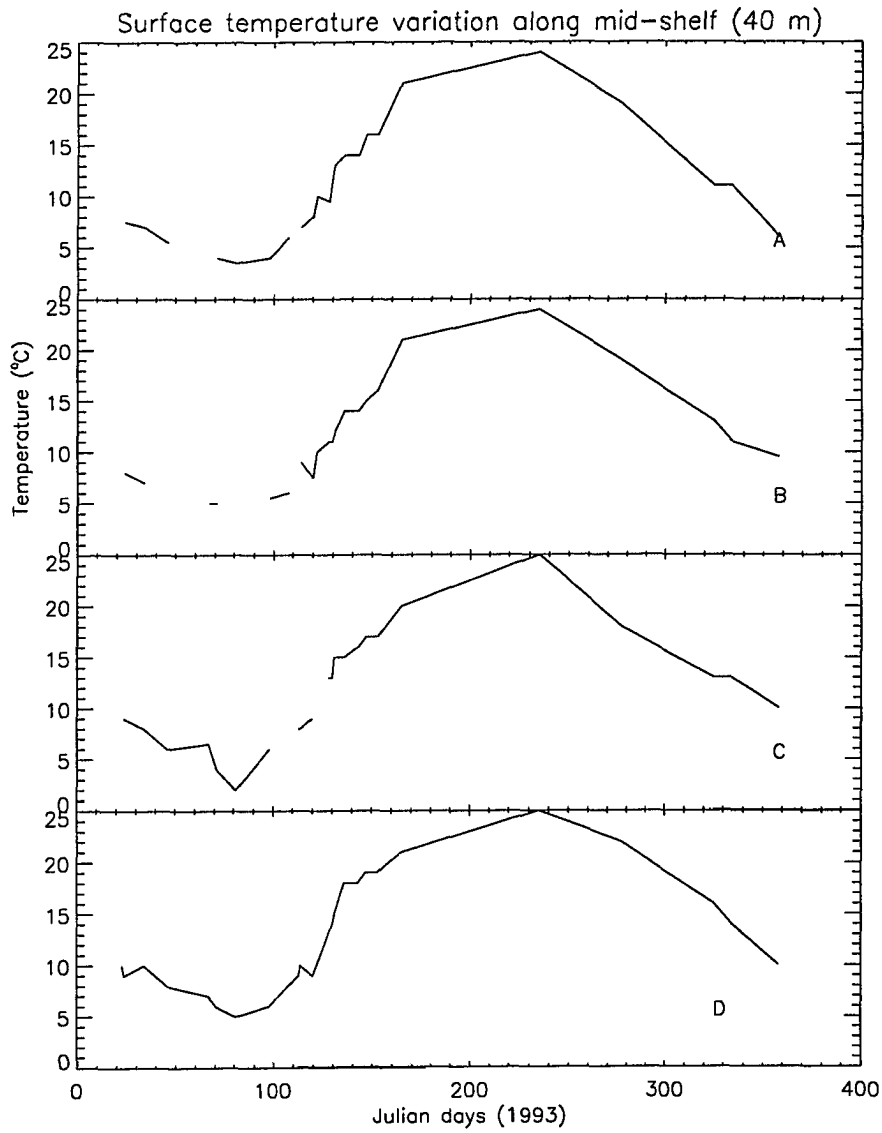

Figure 33: Time series of surface temperature at the mid shelf.

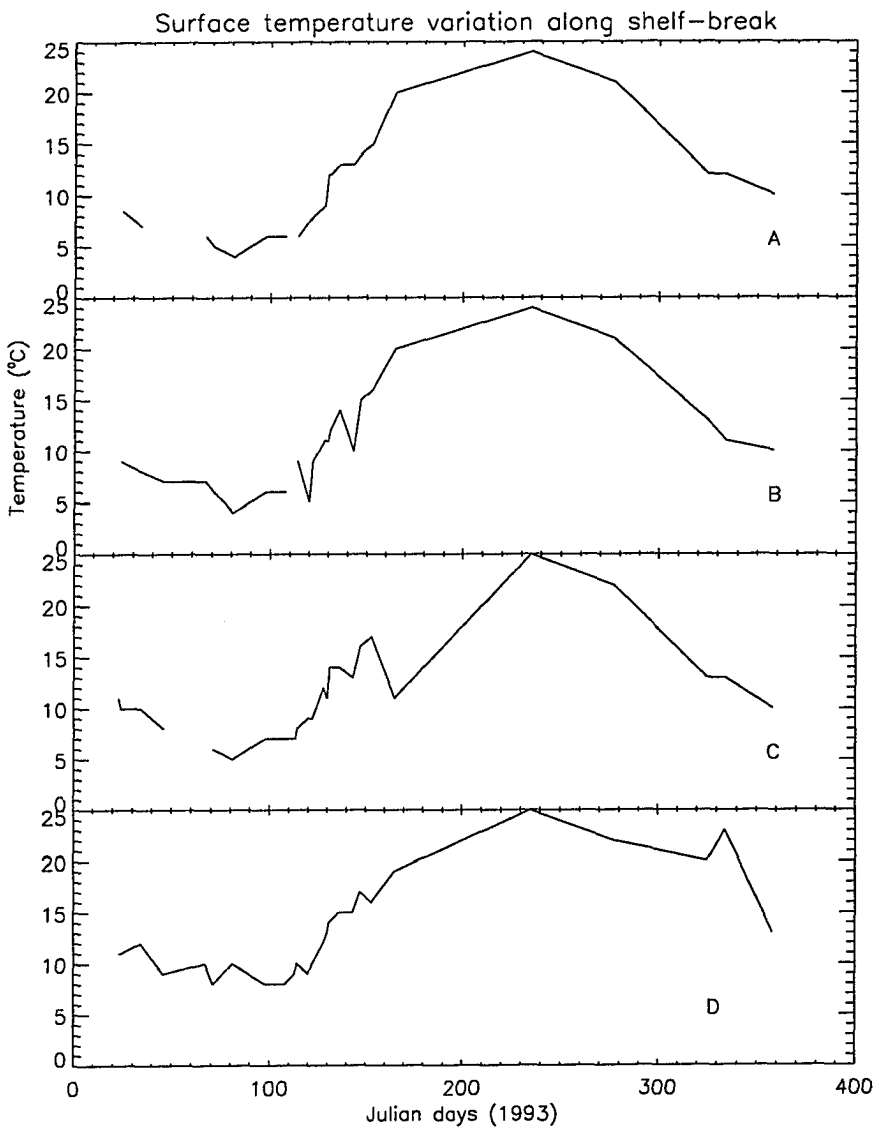

Figure 34: Time series of surface temperature on the outer shelf.

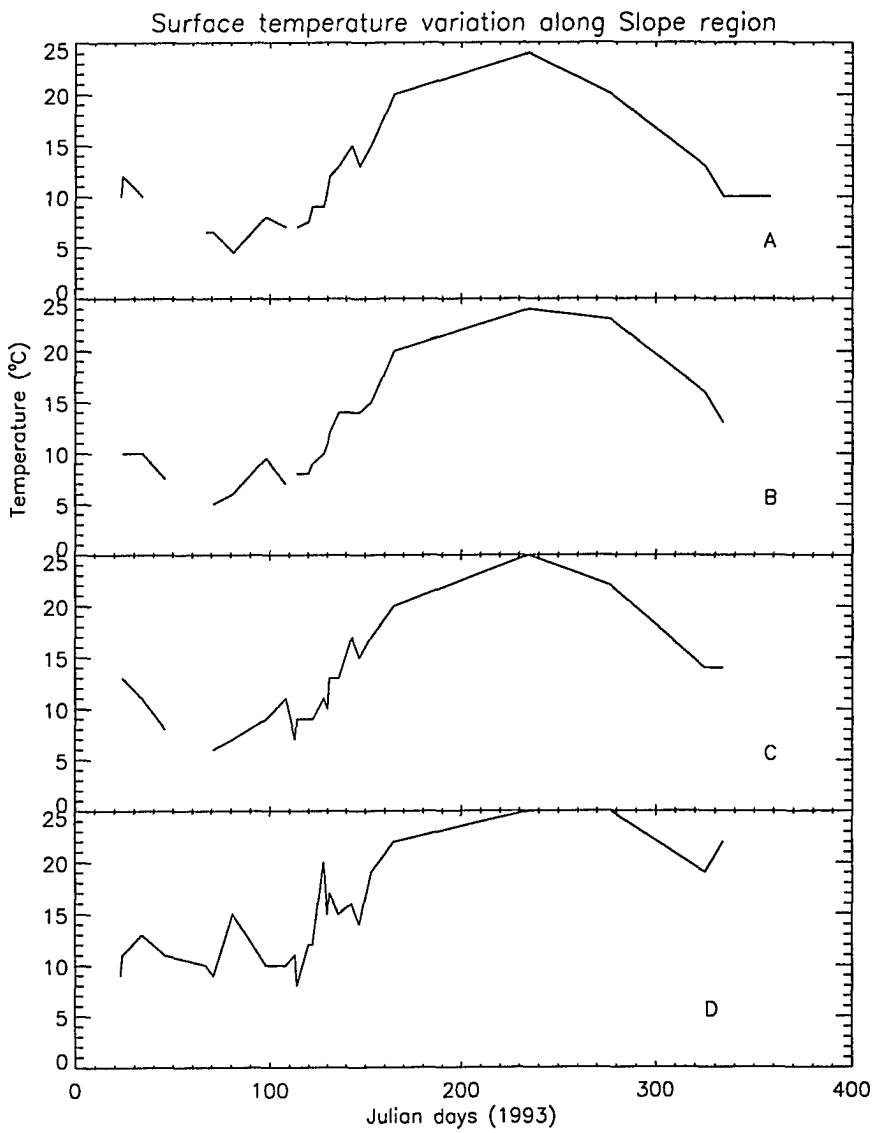

Figure 35: Time series of surface temperature in the slope.

5 RELATIONSHIP BETWEEN SATELLITE SST AND *in situ* DATA

In the previous Chapter, satellite infrared images were used to describe the seasonal evolution of the surface temperature field in the southern MAB. The images also revealed certain dynamic features, notably the overrunning shelf water over the Slope Sea and its subsequent entrainment by Gulf Stream, as well as advection of cooler water by the outer shelf current from the north during late spring early summer. The satellite derived data provided a synoptic coverage in both space and time. Hydrographic data, both coincident with satellite data and historical, are now examined to relate surface features with hydrographic cross–sections in the vertical dimension.

5.1 Data

Surface temperature, salinity and XBT profiles are routinely collected from the "ship of opportunity" R/V Oleander in a NY–Bermuda transect. The data are obtained from National Marine Fisheries Service, NOAA for comparison with coincident satellite imagery. The transect, acquired once or twice a month, are shown as **** in SST images (Figures 36 to 46 (except 42 and 43)).

The upper panel of Figures 36 to 46 (except 42 and 43) show shipboard surface salinity and temperature along with temperature extracted from satellite infrared images for approximately the period of each cruise. The satellite derived and *in situ* surface temperature profiles demonstrate that both data records are in good agreement. However, the satellite profiles show greater variation and underestimate the surface temperature in some cases. The difference between satellite and *in situ* estimates is due to two reasons. First, the satellite measurements lag or precede the *in situ* observations by a few days. Clouds in satellite measurements that appear along the transect or near it can cause substantial underestimation. This is evident

in Figure 37, 38 and 46. Second, *in situ* surface temperatures are sampled in discrete intervals few kilometers apart, whereas the satellite gives a continuous record showing finer–scale variations.

The shelf–slope front is represented by the 10°C isotherm in SST images and can be identified by the thermal gradient between shelf (7°C) and slope (12°C) waters in *in situ* data during winter and early spring. The shelf–slope front signature can be observed in salinity profiles by the gradient between shelf water ($33^o/oo$) and slope water ($35.3^o/oo$). There is remarkable agreement between the satellite derived position of the front with that of *in situ* temperature and salinity profiles. This boundary between shelf and slope waters will be used later to determine the offshore limit of shelf waters in the MAB.

The lower panel of Figures 36 to 46 (except 42 and 43) show vertical cross–sections from XBT data along the same NY–Bermuda transect. The interesting feature about these cross–sections is that the location of the shelf–slope front in XBT data corresponds with that observed in surface satellite derived and *in situ* temperature and salinity data (compare locations with upper panel). The relationship between surface features and vertical cross–sections is discussed below.

The historical data set consists of cross–sections taken during the SEEP I and II and the National Marine Fisheries Service Marine Resources Monitoring, Assessment and Prediction (MARMAP) programs to the MAB [*Walsh et al.,* 1988; *Biscaye et al.,* 1994; *Mountain,* 1991]. In addition, a compilation of hydrographic transects of the MAB shelf–break front that describes the variability of the physical conditions in this region and the shelf–slope front in particular are also used in the analysis [*Lyne and Csanady,* 1984].

5.2 Observations

At least three distinct water masses could be related to surface SST images in our discussion in the previous chapter. The shelf water mass was identified by shades of green (3–10°C), the darkest shade representing cold coastal waters. Shades of blue (11–14°C) were associated with slope water masses with the darkest shade illustrating slope waters furthest offshore. The Gulf Stream was marked by shades of red (18–26°C) to white (30°C), the lighter shades showing mixed slope water and Gulf Stream water.

The winter time cross–sections are best illustrated in Figure 36 to Figure 40. In general, the shelf waters are well mixed vertically and the shelf–slope front extends offshore into slope waters. The Oleander section of February, 1992 (Figure 36) shows that the front extends into the slope water about 150 km from the shelf break. This can also be seen on the SST image of February 3rd (see SST image a03 in chapter 4). The base of the front intersects the 80 m isobath. In addition, the front encloses shelf water to a depth of $\sim$ 60 m offshore of the shelf break. The shelf water properties are vertically uniform down to 60 m. Lenses of 13^0 water are observed from the surface to a depth of 200 m and appear intruding onshore over the continental slope. The Oleander data therefore illustrates that the shelf water mass (shades of green) observed on the SST image of February 3rd can reach depths of up to 60 m offshore of the shelf break.

Another winter time section during February of 1993 (Figure 37) shows a weak contorted (deformed) front with active exchange taking place on either side of the front. The contorted nature of the XBT contours can also be noticed by the shades of blue and green on the SST image of February 3rd (SST image b02). From the coast to the inshore edge of the front, the waters are vertically well mixed and cross–shore

temperature gradients increase offshore. Here again the front extrudes into the Slope Sea, sweeping shelf water $\sim$ 150 km offshore of the shelf break to a depth of $\sim$ 60 m. The base of the front intersects the bottom at about 200 m. Slope Water of 13^0C protrudes upward and inshore over the continental slope from a depth of $\sim$ 150 m.

The transect in March, 1992 (Figure 38) shows the shelf–slope front $\sim$ 50 km offshore of the shelf break and extending to a depth of $\sim$ 50 m. The position of the front correlates well with surface measurements. The satellite derived surface temperature profile shows a noisy appearance due to the presence of clouds in the SST image (image a08). The XBT contours show steeply sloped isotherms that suggest strong southwestward flow. In the slope region, the 13^o thermostad reaches to a depth of 150 m. Once again the shelf is vertically well mixed at this period of the year mainly due to strong mixing by wind and weak buoyancy input.

The Oleander section in April, 1992 (Figure 39) shows the shelf–slope front about 50 km offshore from the shelf edge (see image a09). The shelf water is well mixed and reaches a depth of $\sim$ 60 m bounded by the front beneath and offshore. The isotherms are steeply inclined suggesting strong southwestward flow near the junction of the shelf–slope front. The bottom of the front intersects the continental shelf at about 100 m. The XBT transects also illustrate a diffused front about 150 km offshore from the shelf break (between 300 and 350 m along transect) and a 12^o thermostad at a depth of 200 m in the slope region.

In comparison, the April 1993 (Figure 40) section shows a diffused and contorted front that extrudes offshore $\sim$ 150 km from the shelf break. (Not clearly visible on SST image (b07) due to clouds). The bottom of the front is unresolved. Relative homogeneous conditions prevail across the shelf up to the inshore side of the shelf–slope front.

The Oleander cruise of May 1993 (Figure 41) shows a surprising contrast to the homogeneous shelf conditions observed in April. Shelf water is highly stratified and spring time warming and development of a thermocline are evident shore–ward of the shelf break region. The shelf–slope front appears to have bounced back to its position over the shelf break. The 13° thermostad in the slope region has decreased to a depth of about 100 m.

The SST image (Figure 42) shows a band of cool water advecting from the north over the shelf break during early May. This band of cooler surface temperature represents advection of shelf water from further north by the outer shelf current. This signature lasts for about 25 days (from analysis of images in Chapter 4.) before the contrast between different water masses decreases in SST images to be identified further (see images in Chapter 4.) The SST images also reveal the entrainment of this cold water mass just off Cape Hatteras. The outer shelf current signature is clearly observable in another cross–section taken in May (Figure 43). It shows a band of cool water 8–10°C at the surface shore ward of 10°C plus water extending beyond the 100 m isobath. The cool band is about 50 km wide (off New Jersey) and narrows down considerably as it approaches Cape Hatteras and reaches depths of $\sim$ 50 m. It advects southwestward with a velocity of 0.3 m s^{-1}as measured along the same transect at a depth of 48 m (Glenn Gawarkiewicz, personal communication).

The summer time variation of the shelf and slope waters are best described by cross–sections during June to August. The June, 1992 (Figure 44) section shows the stratification of the surface shelf and slope regions and the strong seasonal thermocline that establish isopycnal contact between shelf and slope waters in the MAB. Note the excellent agreement between the surface location of the shelf–slope front and temperature field with the depth contours from XBT data. The 13° thermostad is still present in the slope region between 80 and 150 m. The slight depression of the

surface isotherms just offshore of the shelf break suggest the signature of the outer shelf current. The 7°C over the bottom shelf region is the remnant of winter cooled water called the 'cold pool'.

The Oleander section of August, 1992 (Figure 45) shows a strong thermocline stretching from the shelf to the slope region. The surface waters are again stratified to a depth of about 40 m. The 'cold pool' over the bottom shelf is clearly noticeable, although reduced in volume from June. The temperature contrast in SST images decrease during summer making it difficult to observe strong gradients.

By late fall, a combination of winter cooling and wind mixing help to re–establish the thermal gradient between shelf, slope and Gulf Stream waters (images a21 to a28). A typical fall cross–section is illustrated by the November, 1992 (Figure 46) section of Oleander which shows a relatively well mixed upper shelf region. The shelf break is poorly resolved and deep slope waters are still stratified. The mixing also helps to remove the 'cold pool' feature that persisted all summer.

In conclusion, the shelf–slope front observed on SST images are in good agreement with coincident Oleander XBT vertical sections. The position of shelf–slope front in SST images is determined by the 10° C isotherm. The outer shelf current signature is illustrated in early May cross–sections and satellite imagery. It is denoted by the advection of cool shelf water from the north and reaches a depth of $\sim$ 50 m. The overrunning of the Slope Sea by the shelf water mass observed in shades of green in winter SST images varies from about 40–60 m in depth near the shelf break and narrows at the offshore edge as shown by vertical XBT sections.

The focus of this section was to illustrate, using hydrographic cross–sections from Oleander combined with earlier evidence (eg. historical data), that overrunning of the slope region by shelf water observed in SST images reach depths of 40–60

m. The overrun shelf water, bounded by the shelf break and the shelf–slope front offshore enclose a large portion of the total shelf water volume in the MAB. When the shelf water overruns the slope region, it advects nutrients and other organic and inorganic matter offshore. The resultant production and carbon export from the shelf is important and should be taken into account for shelf water budgets.

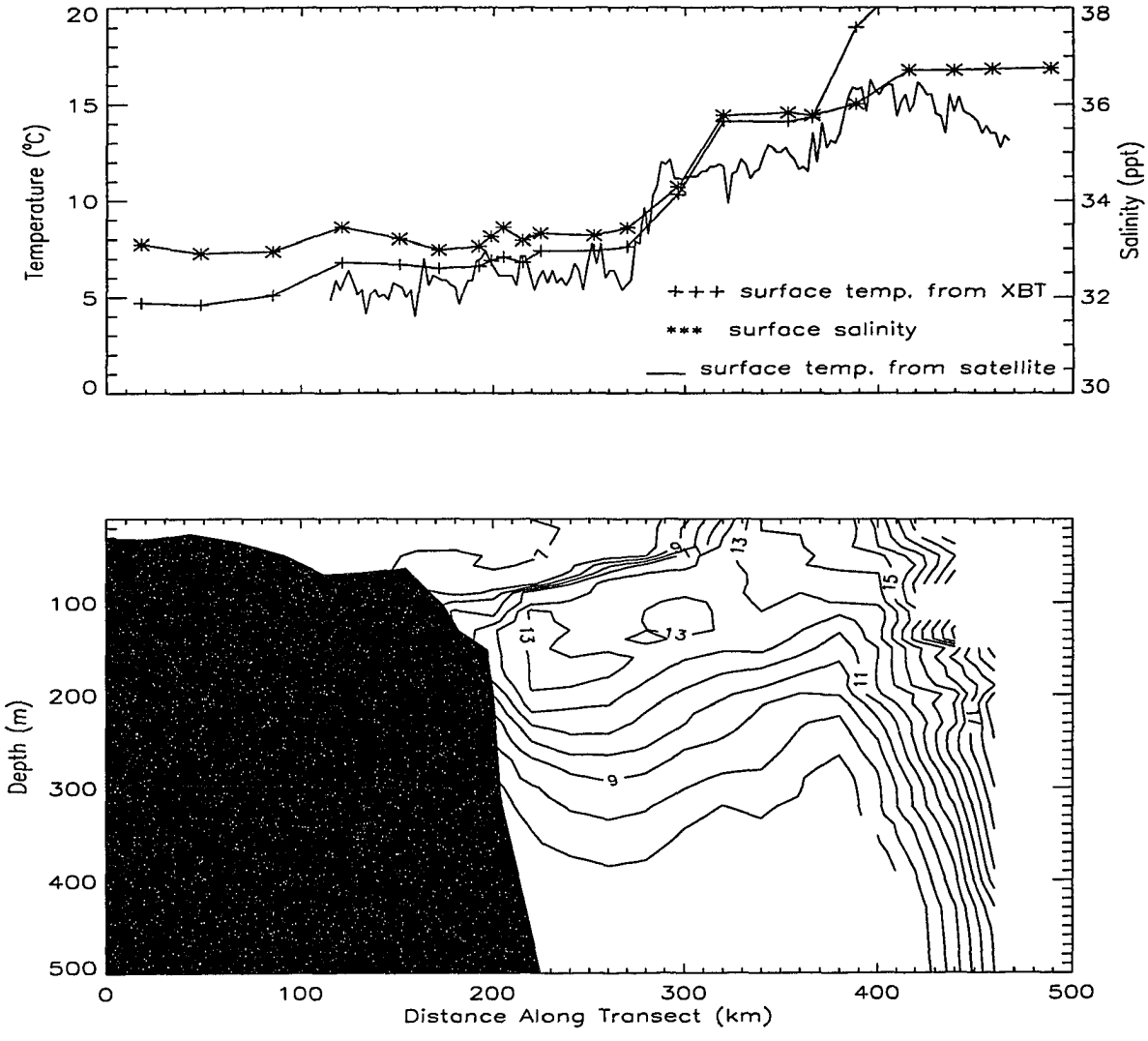

Figure 36: The surface temperature, salinity and satellite extracted temperature across a transect from NY to Bermuda during February, 1992. The bottom section shows temperature contours constructed from XBT data in the underlying water mass. The full lines with rapid variation is satellite SST.

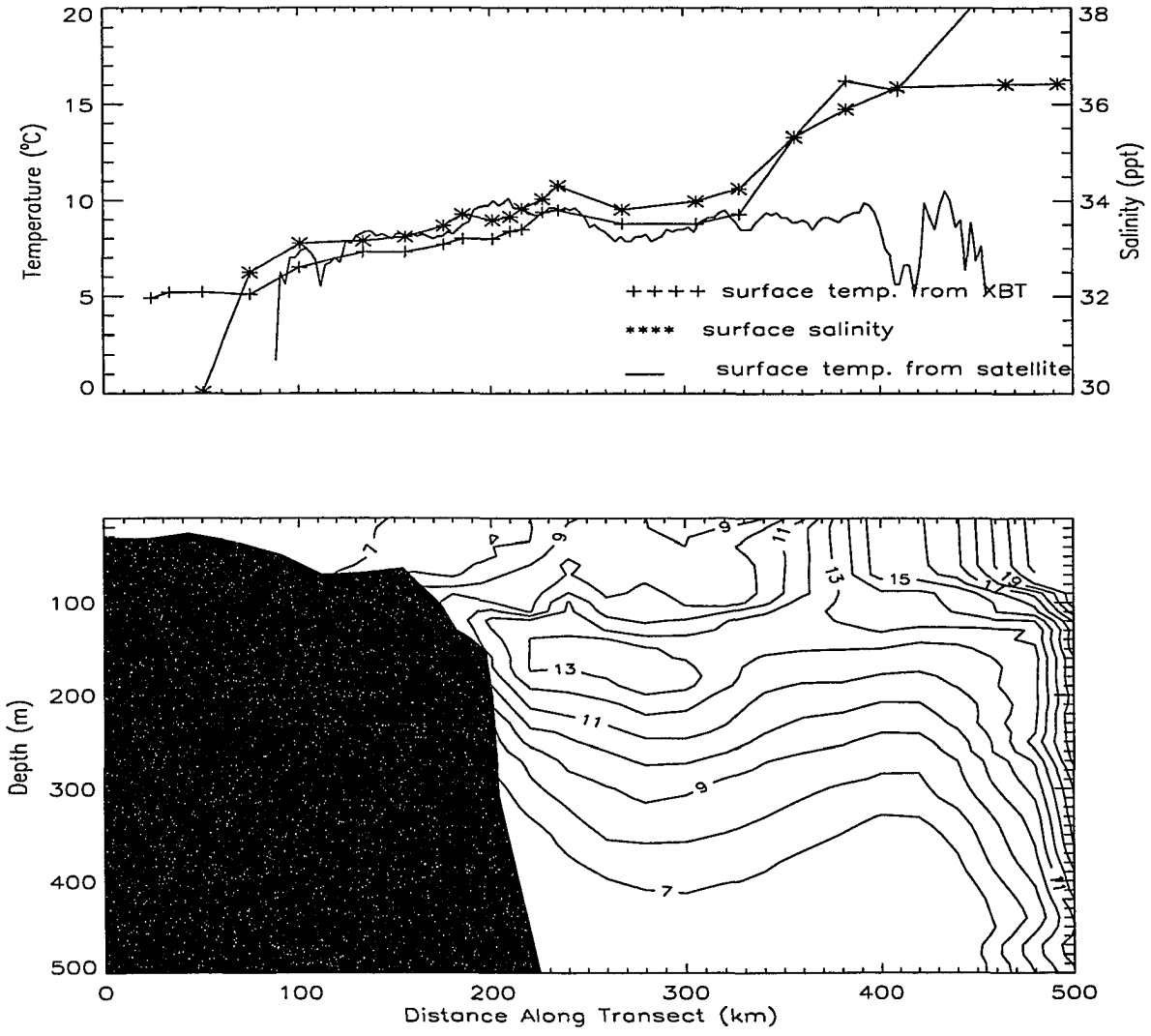

Figure 37: As in Figure 36 but for February, 1993

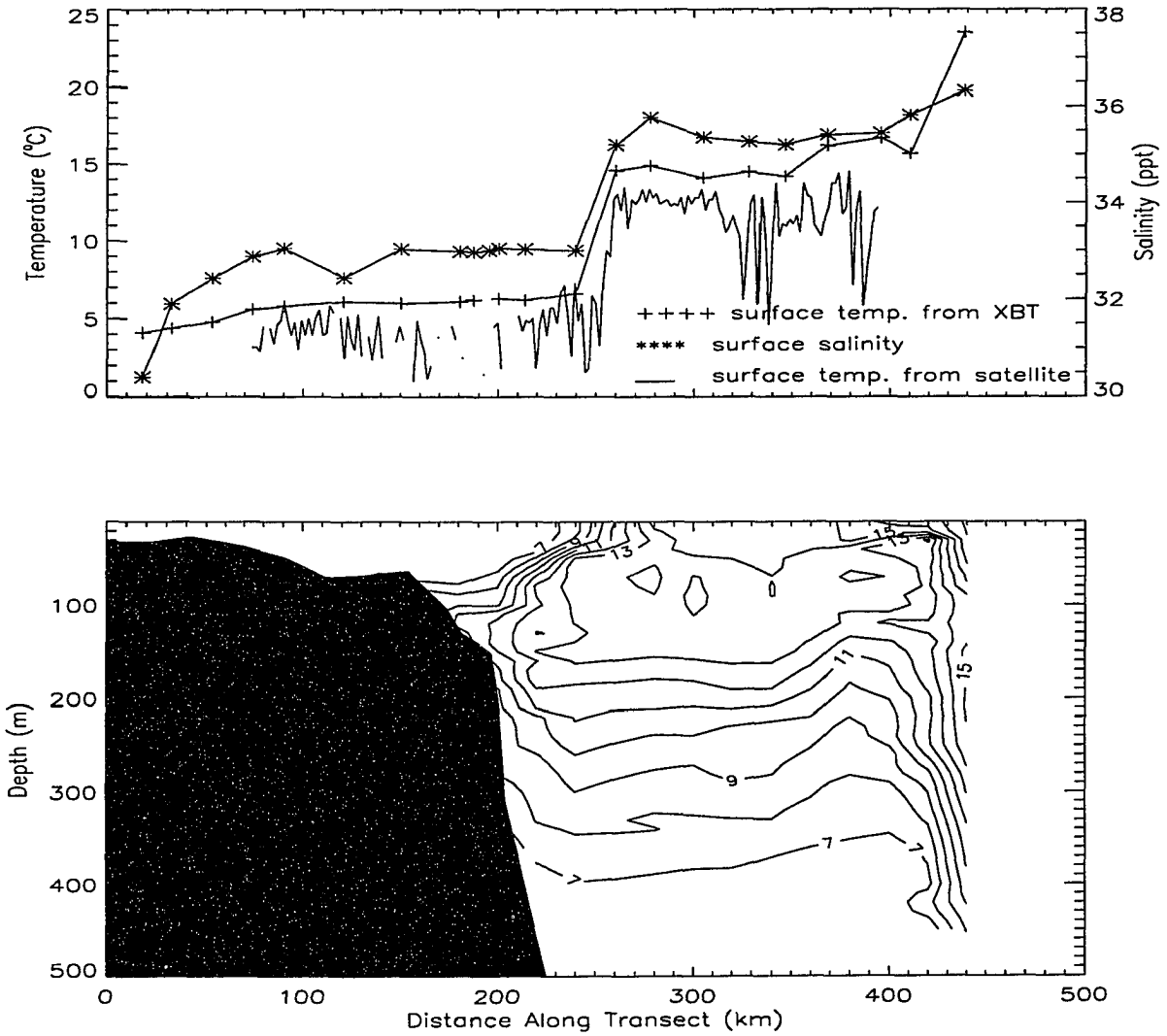

Figure 38: As in Figure 36, but for March, 1992

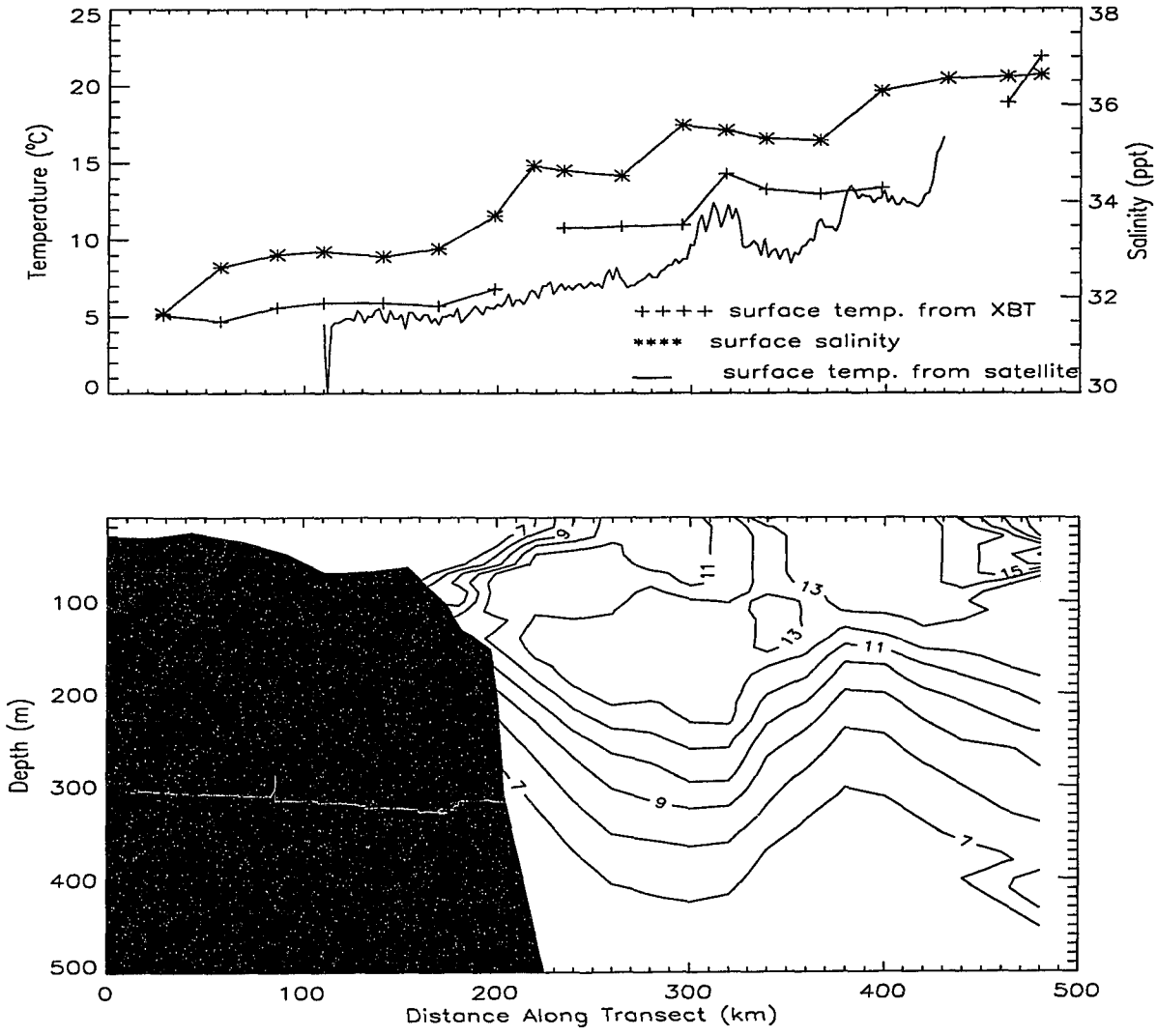

Figure 39: As in figure 36, but for April 1992.

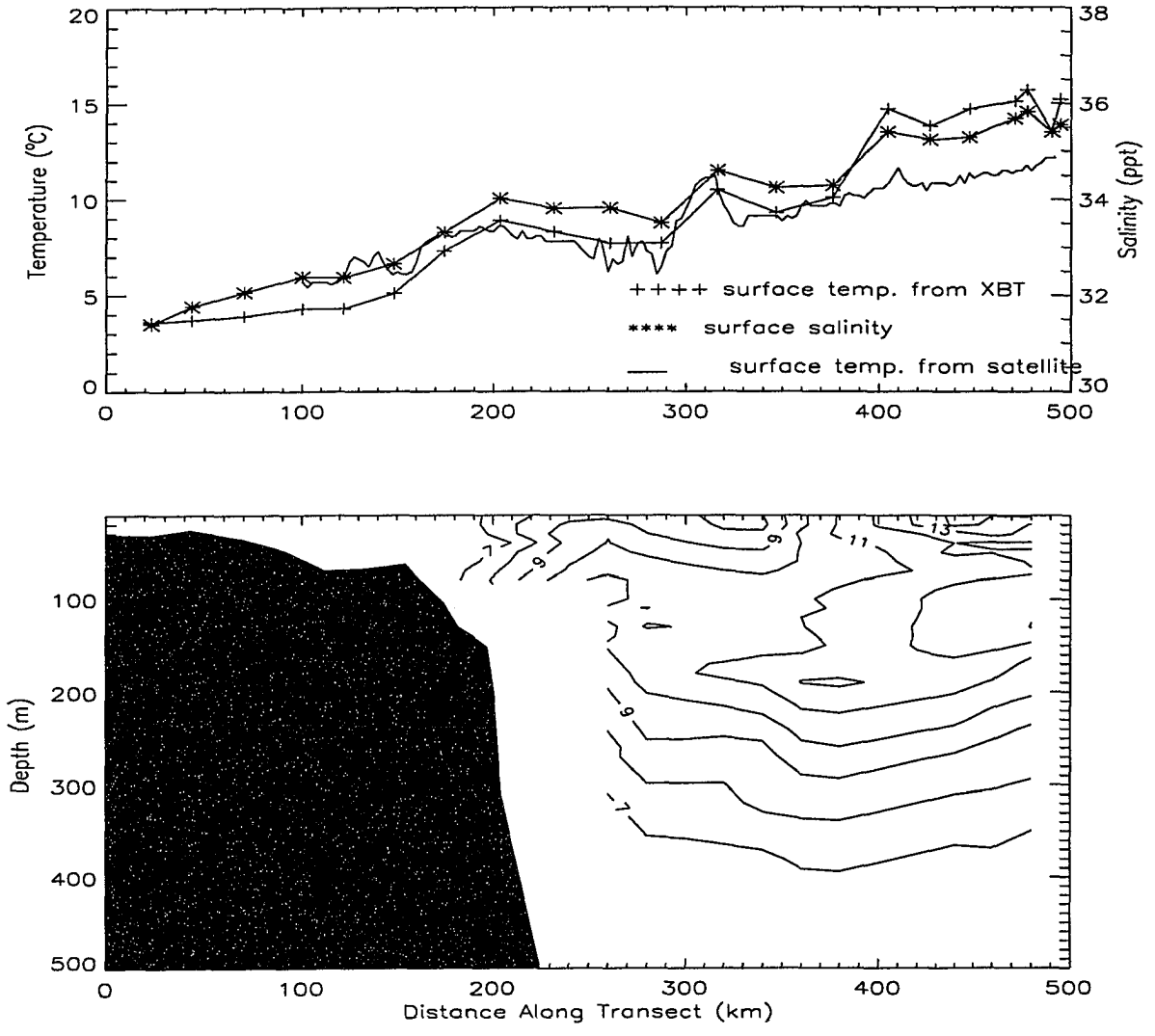

Figure 40: As in figure 36, but for April, 1993.

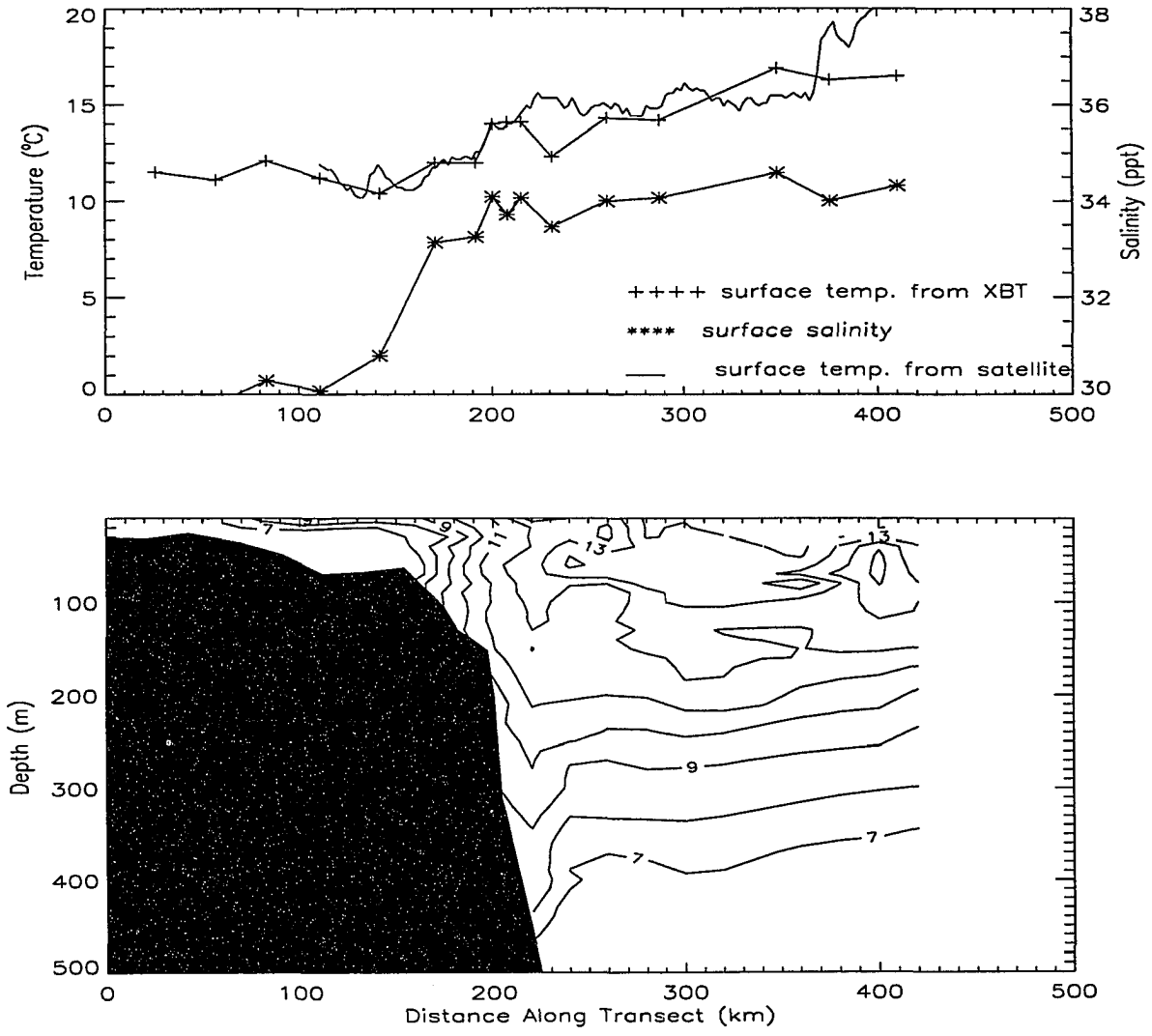

Figure 41: As in figure 36, but for May, 1993.

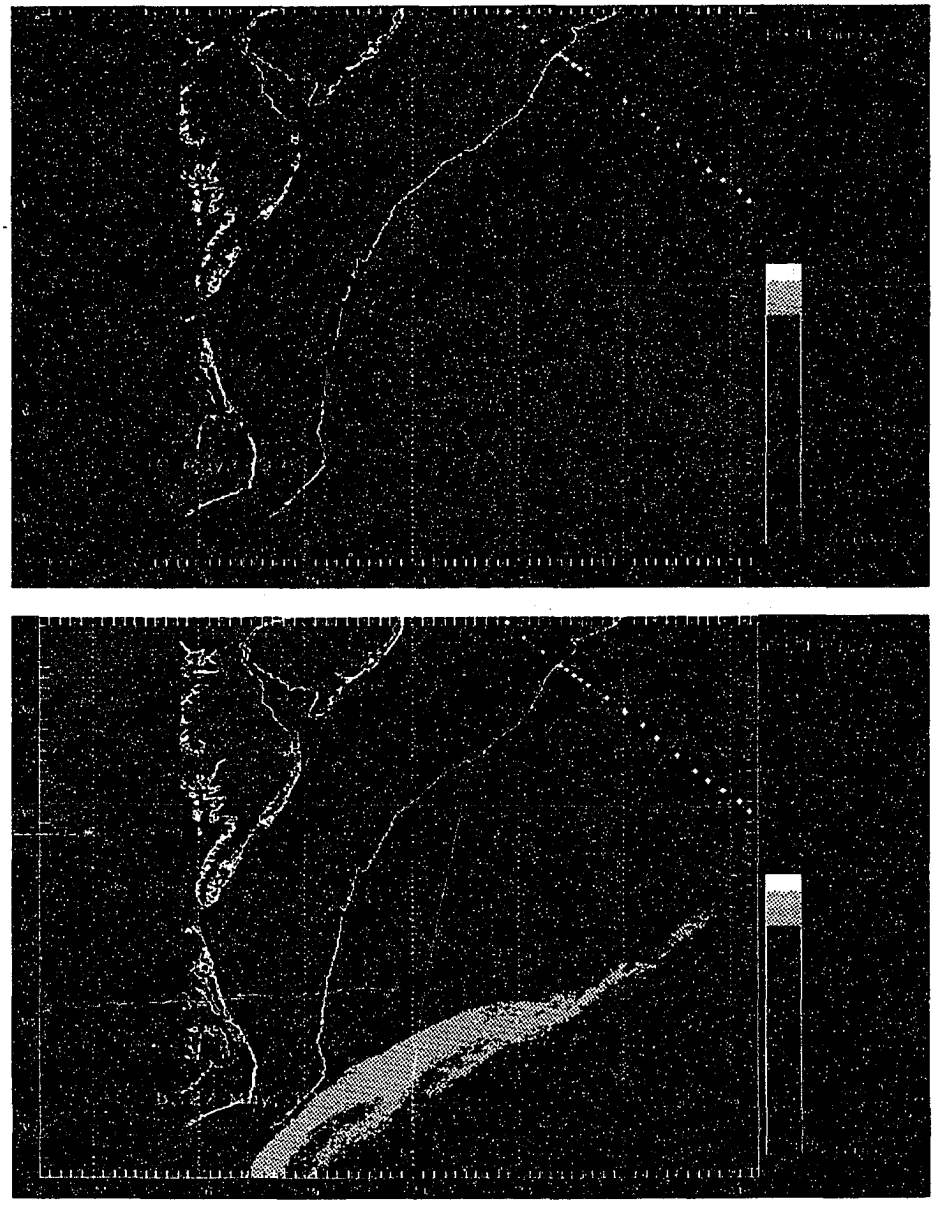

Figure 42: Color plate showing SST image

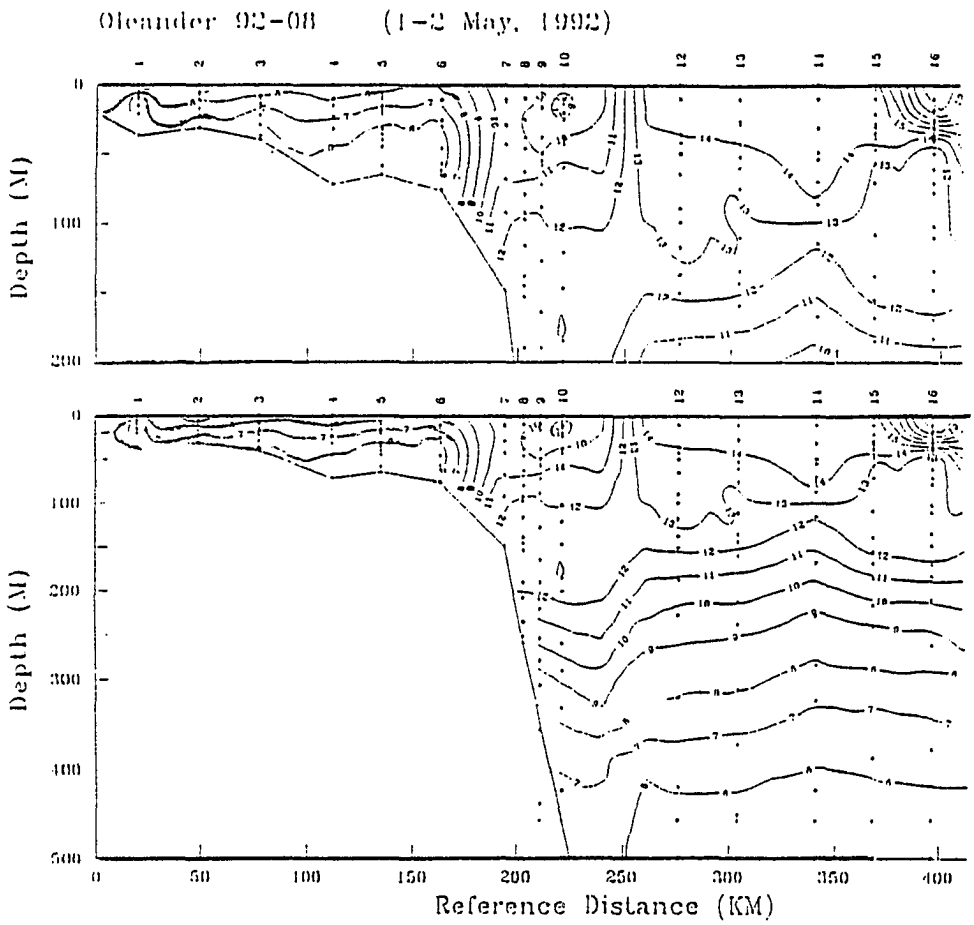

Figure 43: Oleander transect on 1–2 May showing the signature of the Outer Shelf Current

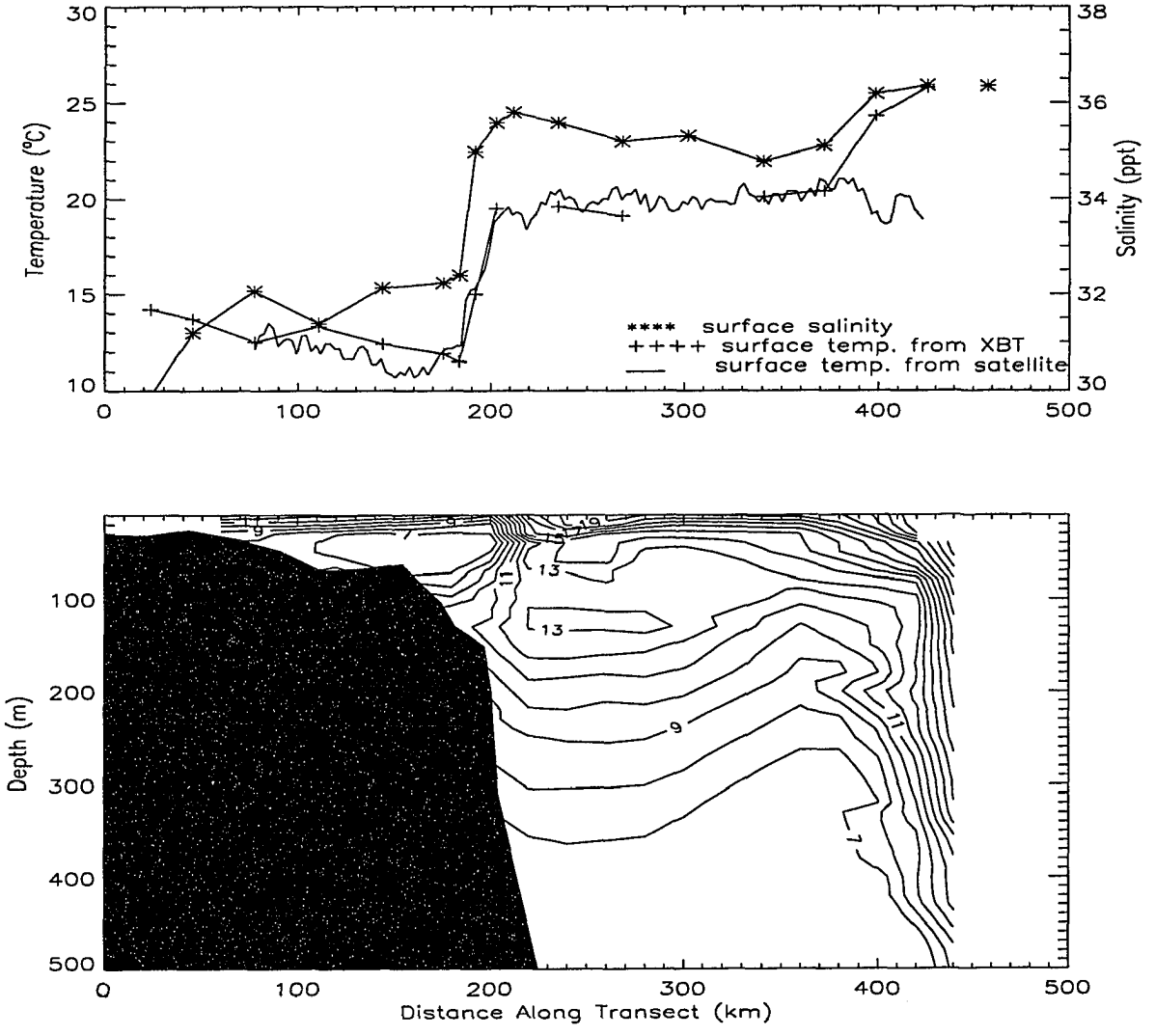

Figure 44: As in figure 36, but for June, 1992

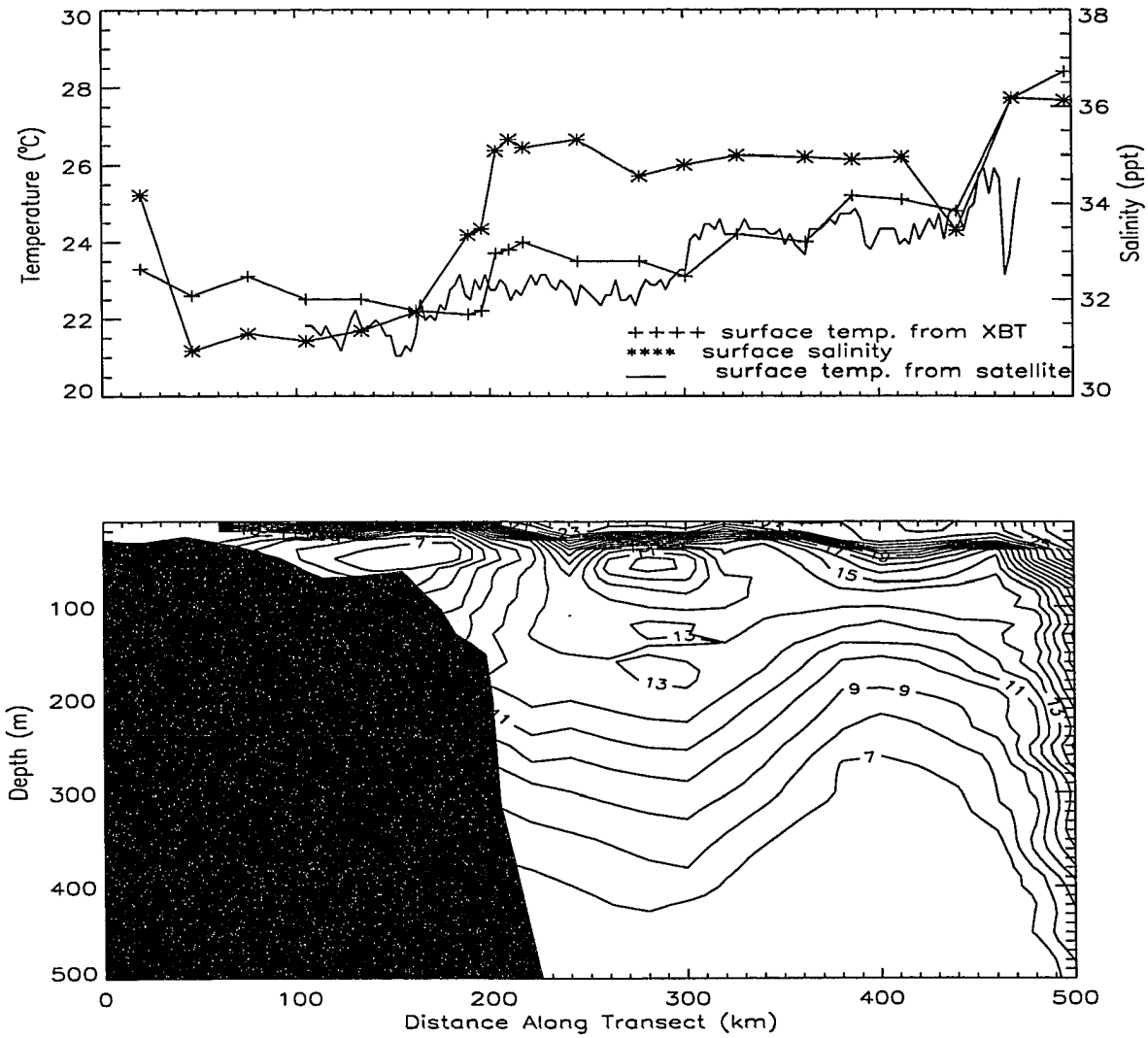

Figure 45: As in figure 36, but for August, 1992

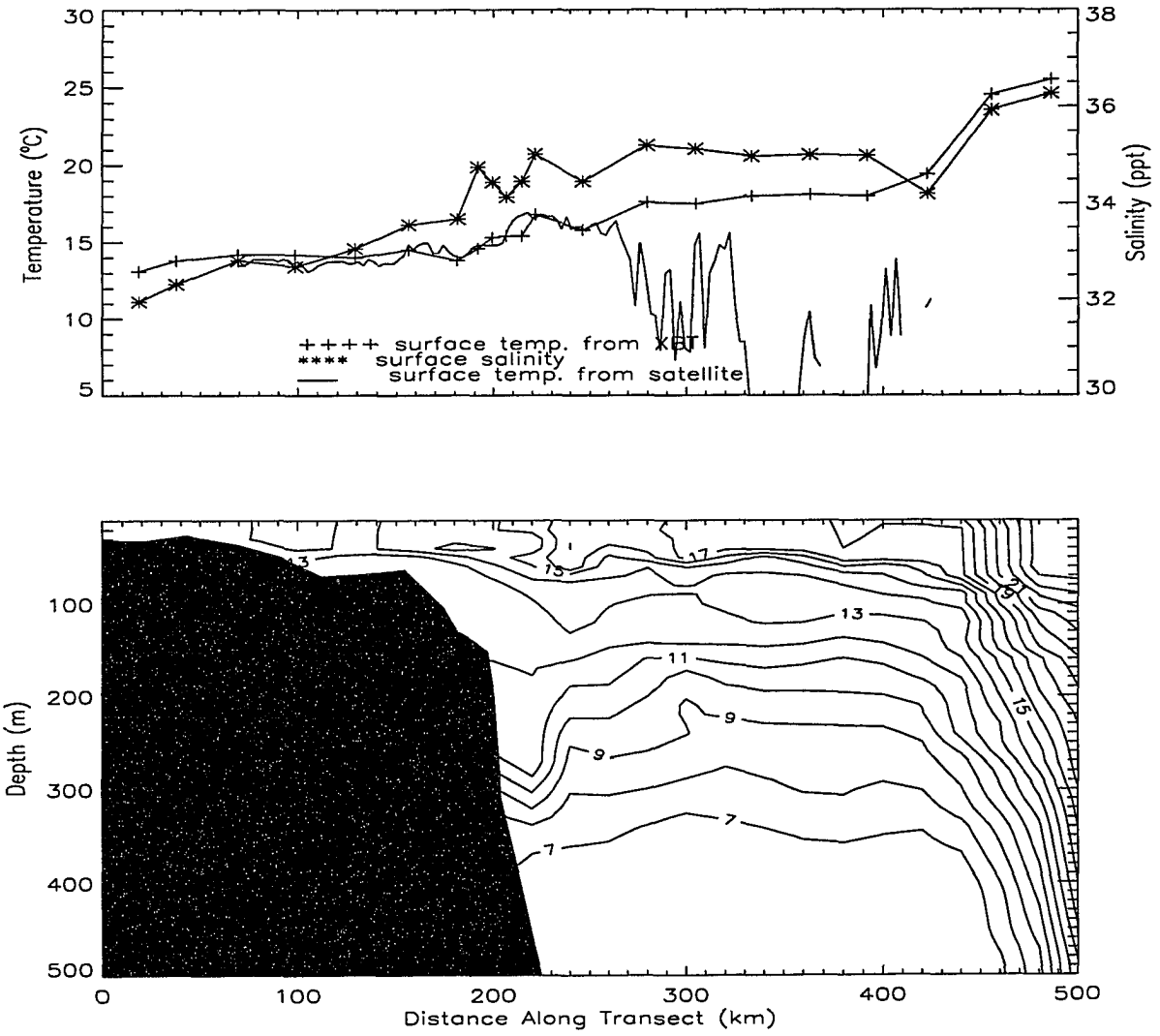

Figure 46: As in figure 36, but for November, 1992

6 ANALYSIS OF SHELF WATER OVERRUNNING IN THE SOUTHERN SLOPE SEA

During the early months of the year, SST images show large volumes of shelf water stored over the slope region in the southern MAB. This excess amount of shelf water, or overrunning, is responsible for a massive southward transport of shelf water along the Slope Sea. In this chapter, satellite derived quantities and hydrographic sections are used to estimate the speed, volume, and transport of overrunning shelf water. The speed of shelf water advected southwestward over the upper slope is determined with "feature tracking" in successive temperature fields. The transport is estimated from the hydrographic cross–sections and the speeds determined with feature tracking. Possible generation of overrunning by winter storms, freshwater discharge or pressure gradient effects are examined.

6.1 Estimation of alongshelf velocity

The velocity of shelf water overrunning the slope region is determined from sequential satellite imagery using the method described in *Breaker et al.* [1994]. This method calculates the velocity of a particle given its displacement between two successive images and the time interval between the two images assuming that the motion of the particle is linear. The above technique has been used extensively in meteorology for the last 25 years to estimate low–level winds from geostationary satellite data. It has also been used to estimate the surface circulation in such regions as the California Current, the Gulf Stream, in and around the Kuroshio Current, the Gulf of Mexico, the English Channel, off the west coast of Ireland, and over the Chatham Rise off New Zealand [*Breaker et al.,* 1994]. In the Slope Sea off the East coast of North America, case studies of surface currents using the above technique have been shown

to be quite reliable [*(Breaker et al.,* 1994; *Cornillon et al.,* 1989] used the same technique to estimate the surface velocity of the slope waters off North America and the translational velocity of Warm Core Rings.

In this study, pairs of SST images that are less than 24 hours apart are selected to determine surface current vectors. Several constraints are placed on the selection of the thermal features to ensure that the same features are identified. The features had to be defined by closed thermal contours; kinks and cusps are excluded. The features are subjectively digitized and their center positions are located. Small features are selected as they best represent the velocity of the surface slope water [*Cornillon et al.,* 1989]. First, a thermal feature is identified and its position obtained from image1. The same feature is located in image2, that is less than 24 hours apart and its position obtained. The difference between these positions gives the distance traveled by the thermal feature from image1 to image2. The velocity is then calculated for this thermal feature from the distance and time interval between the images. In this way, a number of features are subjectively digitized between pairs of images. Most of the features chosen are located in the slope region and helps to determine the rate of advection of the shelf water that has overrun the Slope Sea.

An example of feature tracking using SST images in the MAB is shown in Figure 47. The vectors in the figure illustrate the general circulation features of shelf and slope waters in the MAB. The shelf water that overruns the slope region advects southwestward as part of the mean circulation with velocities ranging from 0.05 m s^{-1} to a maximum of 0.2 m s^{-1}. Near Cape Hatteras the surface velocity vectors obtained from feature tracking show the entrainment of shelf water mass and its northeastward advection as part of the western edge of the Gulf Stream. A sequence of SST images with velocities obtained from feature tracking superimposed are then used for the analysis of shelf water overrunning the southern Slope Sea.

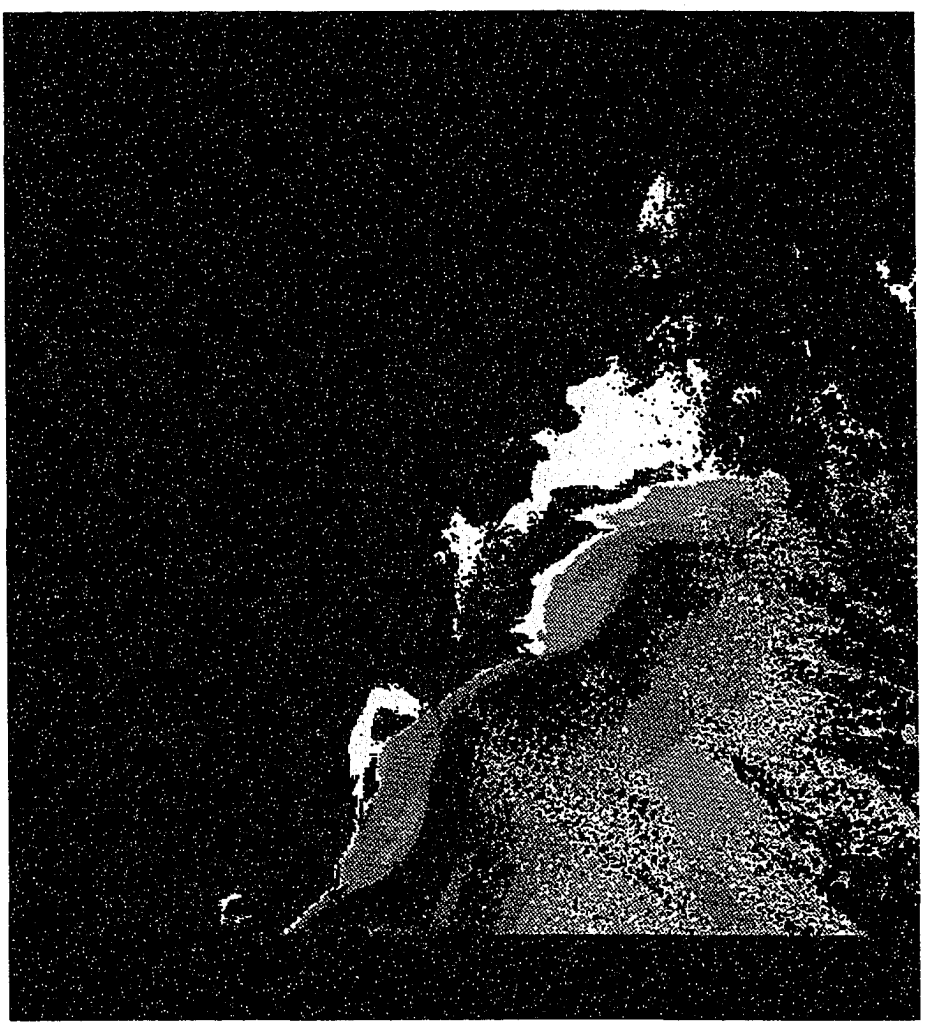

Figure 47: SST image with velocity vectors obtained from feature tracking superimposed in the image. The shades of red represent Gulf Stream water. Shades of yellow and green the slope water mass and shades of blue the shelf water mass. The red arrows represent surface velocity determined from feature tracking. The arrow shown in a box on the right hand side shows a scale of 0.20 ms^{-1} for the surface velocity

From the satellite imagery, which comprises 18 usable images for the two years, the shelf water overrunning and advecting along the Slope Sea are observed to occur in pulses one after the other (the images are explained in detail in Chapter 4 and hence not repeated here for brevity). When one pulse of shelf water leaves NJ, it is tracked all along in a sequence of successive SST images until it entrains eastward between Chesapeake Bay and Cape Hatteras. The time interval from its inception to when it turns eastward is defined here as an episode.

The first episode of overrunning of shelf water during 1992 started around January 31 (see images in Chapter 4). The feature tracking showed persistent velocities of 0.2 m s^{-1} just off New Jersey in the southwestward direction. The shelf water then appears to slow down with velocities of 0.05 m s^{-1} probably due to the motion of an anticyclonic eddy. The anticyclonic eddy entrains and wraps cold shelf water as it advects southwestward. The sequence of other SST images revealed that the first overrunning episode lasted about 34 days. Velocities of 0.2 m s^{-1} are also observed near the southern most tip of the Slope Sea probably due to the influence of the Gulf Stream.

The next episode of overrunning originates off New Jersey on February 17th (see image a05). The influence of the second episode on the shelf water mass can be recognized in successive images until the 28th of March especially on the 15th and 22nd of March, lasting for about 39 days. The shelf water advection is again southwestward along the upper slope region and often reaches velocities of 0.2 m s^{-1}, especially off New Jersey.

The third episode is observed to begin around the first of April and by the 15th of April it has reached off the coast of Delaware. Unlike the earlier episodes, the shelf water mass appears to get entrained much earlier by the western edge of the Gulf Stream and does not reach Cape Hatteras. The shelf water again advects along

the upper slope region with velocities ranging from 0.05 m s^{-1} to nearly 0.2 m s^{-1}. The images from this date become too cloudy to follow the shelf water mass in a recognizable configuration.

The overrunning episodes in 1993 began earlier than in 1992 (see images in Chapter 4). The first episode started around January 24th. The shelf water had a maximum velocity of $\sim$ 0.20 m s^{-1} near New Jersey and advected southwestward. The progression could be followed to March 1st, before it entrains in the vicinity of Cape Hatteras, lasting $\sim$ 35 days.

The next episode started on March 1st before the end of the first episode and is clearly observable on the image of 12th March. The entrainment of this episode occurs much earlier off Chesapeake Bay and does not appear to advect to Cape Hatteras. This shorter episode lasted around 22 days with a maximum velocity of $\sim$ 0.20 m s^{-1} occurring off New Jersey.

The third episode began around March 22nd and could be followed upto April 8th. The image on the 8th shows possibly another episode off New Jersey. The third overrunning episode lasted until April 23rd for about 31 days. The shelf water in the slope region off New Jersey again showed a persistent southwestward velocity of $\sim$ 0.20 m s^{-1}.

The two year analysis showed that (three to four) episodes can be identified during a period of approximately three months during winter and early spring. Each episode lasted about 30 days. The episodes of shelf water overrunning the Slope Sea appeared to originate off New Jersey (at the New York Bight apex) around the end of January and advected southwestward along the upper slope region. The maximum velocities($\sim$ 0.20 m s^{-1}) were recorded off New Jersey and decreased slightly as the event advected towards Cape Hatteras. The entrainment of shelf water to the Gulf

Stream or the Slope Sea appeared to take place anywhere between Cape Hatteras and off Chesapeake Bay and advected eastward along the western wing of the Gulf Stream.

The shelf water traveled a distance of $\sim$ 500 km in the slope region from New Jersey to near Cape Hatteras in about 30 days. This gives a mean velocity of $\sim$ 0.19 m s^{-1} which is consistent with the mean velocity estimated from feature tracking of $\sim$ 0.20 ms^{-1} obtained between two successive images less than 24 hours apart.

The velocity estimate by feature tracking can be affected due to a number of reasons. First of all it is assumed that sea surface temperature serves as a conservative passive tracer. Secondly, it is assumed that the changes seen are solely advective when they could be due to surface heat exchange or diffusion. Propagating waves (eg. on the northern wall of the Gulf Stream) tend to interfere with advective motion in places where both are present. Furthermore, the motion of the particles are assumed rectilinear when in fact they could be rotational. The time separation between images is also an important criterion. If the time difference between images is too small, there may be lack of features to track. If it is too long, features begin to loose their identity and it becomes difficult to assign a displacement. *Svejkovsky* [1988] found that periods greater than 12 hours but not more than 24 hours between images produces the best results. Another problem associated with satellite feature tracking is precise navigation, lack of which can cause errors of 0.02–0.03 m s^{-1} in estimating the surface velocity. Procedures such as those developed by *Krasnopolsky and Breaker* [1994] typically reduce this error by a factor of 4. Landmarks are often useful in reducing these errors over coastal areas. In this study all the images are registered to a common coastline therby reducing the error due to navigation.

An uncertainity in the velocity estimate from feature tracking can arise from the error in determining the accurate distances between particles on two different images.

The resolution of the sensor is about 1.47 km^2 giving a diagonal distance of $\sim$ 1.71 km for each pixel. This gives an uncertainity in the distance of $\pm$3.42 km for an error of one pixel or $\pm$6.84 km if the error is two pixels. Since the time interval between two images is kept a constant (86400 s), the uncertainity in the velocity estimate for feature tracking in this study for an average velocity of 0.2 m s^{-1} ranges from $\pm$0.04 m s^{-1} to $\pm$0.08 m s^{-1} for one and two pixels respectively. The velocity estimate from feature tracking is almost twice the mean velocity ($\sim$ 0.10 m s^{-1}) observed in the outer shelf region of the MAB [*Beardsley and Boicourt,* 1981]. This suggest that the advection of shelf water over the upper slope region may be linked with the circulation of the Slope Sea. The mean southwestward velocity of the upper slope current off New Jersey is about 0.15 m s^{-1} [*Csanady and Hamilton,* 1988]. The relative velocity by geostrophic calculation of shelf water layer is about 0.1 m s^{-1}. This gives a good reason to believe that the overrun shelf water motion over the upper slope region, bounded by the front offshore and to a depth of $\sim$ 50 m, is carried southward by the upper slope current.

6.2 Volume calculations

To estimate the volume of shelf water overrunning in the southern MAB, the offshore extent of shelf water is determined from the position of the shelf-slope front in each SST image. Previous studies have shown that the location of the shelf-slope front from the surface as determined by satellite imagery could account for about 50% of the variance in the shelf water volume in the MAB [*Mountain,* 1991]. In this study, offshore limit of shelf water extends from the shelf break (100 m isobath) along the shelf–slope boundary represented by the 10°C contour line , and back to the shelfbreak. This area from the shelf break to the 10°C contour line is used to estimate the volume of shelf water that overruns the slope region in the southern

MAB.

To quantify the area of shelf water in the slope region from satellite SST images, only those images that are completely cloud free in the shelf-slope region are used. This rules out errors due to cloud contamination. The perimeter of the area bounded by the shelf break and the 10°C contour is obtained by determining the coordinates of each pixel in the image along this line. This is done by subjectively moving the cursor along this line and extracting the pixel positions. The coordinates, in latitude and longitude, of each point on the perimeter of the area are converted to x and y distances (km) with respect to the origin of each image. The area is then calculated using the formula;

$$AREA = 0.5[X_1(Y_2 - Y_n) + X_2(Y_3 - Y_1) + X_3(Y_4 - Y_2) + ...X_n(Y_1 - Y_{n-1})]$$

where n is the number of points extracted, and $X_1, X_2, ..., X_n$, and $Y_1, Y_2, ..., Y_n$ are the x and y coordinates of pixel position on the perimeter.

The depth of the shelf water in the Slope Sea varies generally from 40–60 m. The Oleander cruise track (marked as '***' in SST images above) showed the overhang in February 1992 to be 60 m deep and in March 1992 to be 50 m. In February 1993, the depth of the overhang was 60 m and in April of the same year it was 50 m deep. Sections from SEEP programs taken off New Jersey and off Delaware also showed the depth of the overhang to vary between 40–60 m. Historical transects and cross–sections taken from "A compilation and Description of Hydrographic Transects of the Mid-Atlantic Bight Shelf–Break Front" atlas [*Lyne and Csanady,* 1984], which span more or less the whole of the MAB have also confirmed the depth of the overhang to vary within 40–60 m. *Mountain* [1991] used an average depth of 40 m in his calculation of the volume of shelf water from cruises between 1977–1987.

An uncertainty in the volume estimate can be induced by the constraint in assuming a constant depth of $\sim$ 40 m and the error in determining the area of the overrun shelf water. An error of about 10 pixels will give an uncertainity in the area of about $\pm$920 km^2. The volume unceratinity for depths of 40, 50 and 60 m are about $\pm$ 36, 45 and 55 km^3.

The volume of shelf water that overruns the slope region during four months; January to April is shown in Figure 48. The top panel displays a time series of shelf water volume during 1992. The differently shaded portion in the diagram are used to show the volume of each of the three overrunning episodes separately The shelf water volume shows a general increase from late January to a maximum of $\sim$ 2000 km^3 on day 80. In addition there was another peak at about day 100. This shows up as a complex double frontal structure in the cross–section of 3-4th April, 1992. The shelf water volume steadily decrease until end of April as the shelf–slope front retreats back to its normal position over the shelf break.

The volume of shelf water for the three episodes for 1992 are also shown in Figure 48 as the shaded regions. The first episode of overrunning reached a maximum of about 1000 km^3. The volume of shelf water for the second episode reached a maximum of about 1100 km^3 around day 80, after which it decreased steadily until about day 100. The second episode thus lasted longer and contained slightly more volume than the first episode. A feature in the third episode is the patchiness in the shelf water mass that has overrun the slope region. This is noticeable by the presence of slope water in the region off New Jersey and below it. This large estimate is partly due to the stagnant shelf water mass in the slope region as seen in the SST images.

The volumes of the overrun shelf water mass for 1993 are also shown in Figure 48 (lower panel). Although the overrunning started slightly earlier, the volume was considerably less than in 1992. The maximum volume (2000 km^3) again occurred at

the end of March which may be due to the accumulation of shelf water in different episodes as in 1992. Thereafter, the shelf water volume decreased steadily to about 1000 km^3 in late April.

The mean volume of the overrun shelf water (between the shelf break and the location of the shelf–slope front) is about 1600 $\pm$55 km^3 for 1992 and 900 $\pm$55 km^3 for 1993. The mean shelf water volume in the MAB is about 3600 km^3. This shows that about 25–45% of the volume of shelf water in the MAB lies offshore of the shelf break during these episodes. *Wright and Parker* [1977], have also observed that about 50% of the volume of shelf water in the MAB lie in the outer wedge between the shelf break and the shelf–slope front. The large variation in volume between 1992 and 1993 ($\sim$ 70%) may be associated with increase in the flow into the Gulf of Maine and later into the MAB. *Mountain* [1991], in his ten year analysis of the volume of shelf water in the MAB has observed interannual changes of 60–90% from the mean volume in the MAB.

6.3 Transport

The transport of the overrun shelf water just off New Jersey can be roughly estimated from the Oleander cross–sections and the velocity determined from feature tracking. On the 8th of February, 1992, the shelf water extends $\sim$ 100 km offshore. Taking an average depth of about 40 m and $\sim$ 0.2 m s^{-1} as the cross–sectional velocity, the transport is $\sim$ 0.8 Sv. Taking depth = 60 m, the transport = 1.25 Sv. Similarly, on the 11th of March, the shelf water extends about 60 km offshore and the transport associated with it is $\sim$ 0.5 Sv and 0.7Sv for h = 60 m. During 1993, the transport estimate from 6th February and 8th April is again $\sim$ 0.8 Sv. This gives an average of $\sim$ 0.725 Sv for one third of a year for two episodic events or the episodic annual average may be about 0.12 Sv. The high transport estimate suggests that the transport of

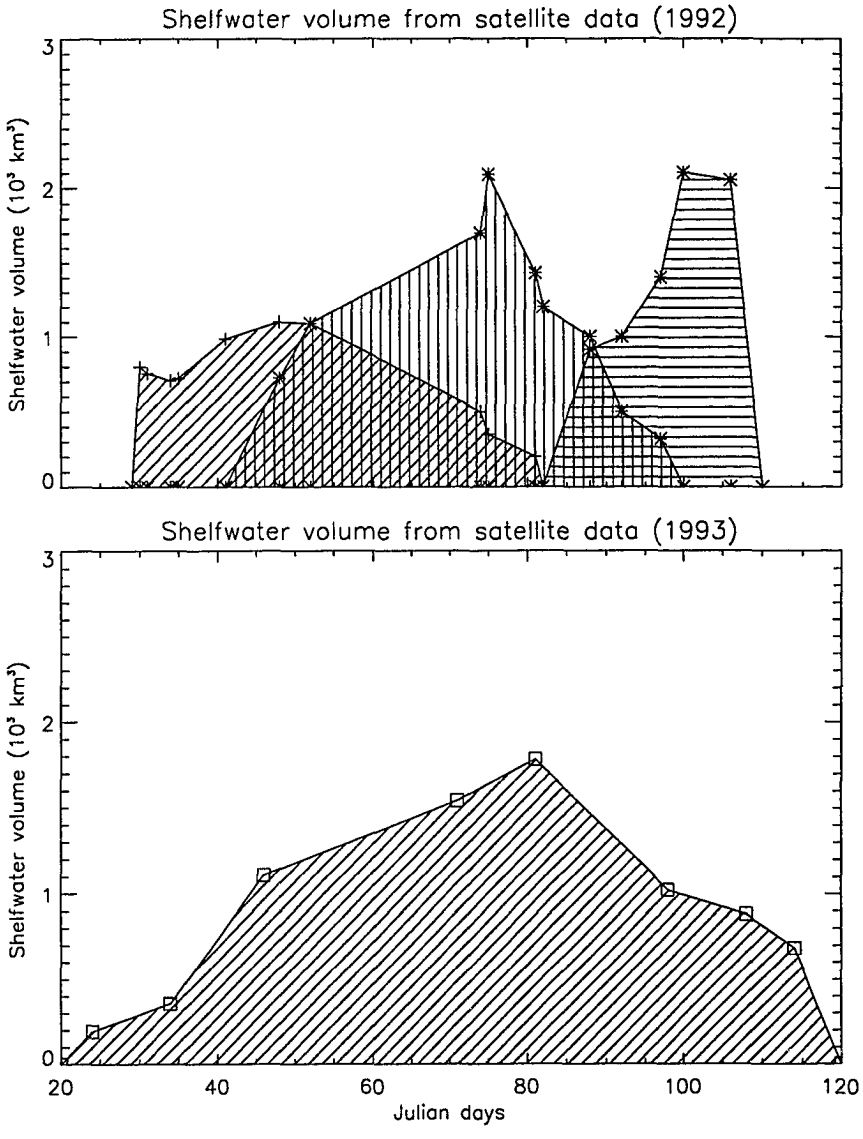

Figure 48: Cummulative shelf water volume between the 100 m isobath and the satellite determined position of the shelf–slope front. The three shaded portions during 1992 represent the shelf water volume during the three overrunning episodes of 1992.

the overrun shelf water is large and cannot be ignored. The uncertainty associated with this transport is the constrain due to the velocity measurements and the depth of the overrun shelf water as discussed before. For a maximum offshore distance of $\sim$ 100 km the uncertainity in the transport estimate is ± 0.64 Sv.

The fate of the overrun shelf water is largely influenced by the circulation of the Slope Sea and the entrainment processes off Cape Hatteras [*Csanady and Hamilton,* 1988]. The transport of the overrun shelf water is always southwestward. The shelf water mass keeps its distinct identity and does not mix with the slope water or retreat back on to the shelf. The SST images in this study show that the shelf water is entrained intermittently into the Slope Sea at various locations between 38° N and Cape Hatteras and eventually drains eastward into the western edge of the Gulf Stream. This agrees with the observed circulation in this region [*Ford et al.,* 1952; *Kupferman and Garfield,* 1977; and *Fisher,* 1972].

6.4 Potential Forcing Mechanisms

In this section we are concerned with identifying forcing mechanisms responsible for overrunning events. Potential forcing include wind stress, freshwater discharge, pressure gradient effects, baroclinic or barotropic instability, and various oceanic forcings such as topographic Rossby waves, Gulf Stream meanders, warm-core rings, and local mixing. We confine our attention to the winter–spring period, January to April 1992 and 1993, when the frontal boundary is well defined.

6.4.1 Effect of windstress

Hourly wind data, obtained from NODC buoys located in the MAB (Figure 8) are used to analyze the shelf water response to wind stress. Alongshore and offshore

stress components are computed by rotating the coordinate system 30° clockwise so that the alongshore direction was aligned with the large–scale bathymetric contours. Time series of wind stress are computed from

$$\tau_{alongshore} = \rho_{air} C_D |W| V \tag{10}$$

$$\tau_{offshore} = \rho_{air} C_D |W| U \tag{11}$$

where U and V are offshelf and alongshelf components of wind and $| W | = (U^2 + V^2)^{1/2}$. C_D was computed according to Large and Pond (1981), ie

$$C_D = (0.49 + 0.065|W|) \times 10^{-3} \quad |W| > 10 m s^{-1} \tag{12}$$

$$C_D = 1.14 \times 10^{-3} \quad |W| \leq 10 m s^{-1} \tag{13}$$

where $| W |$ is in m s^{-1} and $\rho_{air} = 1.2 kg m^3$

Coherence squared and phase of east–west and north–south components are computed for each of the buoys for the four month period (January to April, 1992 and 1993) to show, in general, the uniformity of the wind field in all the buoy locations of the MAB. In all, data from five buoys are used to compare windstress in the northern and southern part of the MAB area. The coherence squared between the stresses at different locations is significant at the 95% confidence level at most frequencies (Figure 49). In addition, the phase is not significantly greater than zero at these frequencies most of the time. Therefore, data from buoy 44008 (for 1992) and 44014 (for 1993) are used to represent wind conditions for these two years in the MAB.

In (Figure 50, Figure 51) wind vectors are plotted for the four month period during 1992 and 1993. Wind vectors use oceanographic conventions. A northward wind blows towards the north. The winds during the four month period are generally towards the southeast for both the years. But considerable small scale wind reversals towards the northeast also exist. It will be noted that average climatological winter

winds in the southern MAB are everywhere to the southeast (see The Bunker Atlas of the North Atlantic Ocean). As spring approaches, there is a gradual decrease in wind magnitude and change in direction to the north.

To illustrate the major features of the magnitude of the stress, the east–west and north–south components are shown in (Figure 52 and 53). What is apparent from the figures is that maximum stresses occur during mid January and early February. In addition, the winter stress tend to be directed offshelf with brief wind reversals. *Saunders* [1977] reported that an offshore increase in stress was a dominant feature in the MAB and it approximately doubled 200 km offshore. The large stress values also arise principally because of frequent strong winds rather than because of the tendency of the winds to blow more frequently in a given direction.

There are two major offshelf stresses from 9–20 January and 2–10 February, with less intense ones on 25th January, 2,4, 12, 13, and 30th of March and on 5 and 6th of April 1992 (see upper panel on Figure 52). Strong onshelf stress are also observed on 4, 23 January, 8, 26 February, and on 8, 12 and 27th March. During 1993, the wind stresses are mostly offshelf and less frequent intense storms with the major ones recorded on 5 and 28th February and 11–15th March (upper panel on Figure 53).

The alongshelf wind stress is mainly southward with strong stresses during 4, 16, 17 and 26th January, 3, 4 and 25th February and 20th March, 1992 (see lower panel on Figure 52). During 1993, again the alongshelf winds are mostly southward, with intense ones recorded on 9, 10th January, 28th February, 18th March and 7th April. However, the striking feature of the wind stress in the MAB is its variability and there are periods of strong wind reversals during the entire four month periods with alongshelf winds to the north of greater than 0.1 Pa on 24, 25th January, 20th February and 12th March, 1992 and 2nd February and 12th March, 1993 (lower panel on Figure 53).

The work done by the north–south component of wind stress on the overrunning of shelf water in the MAB can be examined in terms of the time integral of the wind stresses ($\int \tau_y dt$) and the Bakun index. $\int \tau_y dt$ is the cummulative sum of the magnitude of hourly wind stress vectors, where τ_y is the kinematic wind stress ($\frac{m^2}{s^2}$) in the alongshore direction. The Bakun index is based on Ekman transport derived from surface winds [Bakun, 1973]. The Ekman transport is calculated from ($\frac{1}{f}\tau_y$) where f is the Coriolis parameter. The offshore displacement can be expressed as $\frac{1}{fD}\int \tau_y dt$ where D is the depth of shelf water. A comparison of time integral of the wind stresses ($\int \tau_y dt$) and SST images showed that cross–shelf motions of the front can be wind driven (Figure 54). A northward wind starting on 5th January and another on 23rd January, moved shelf water and the shelf–slope front upto the slope region as seen in images a01 and a02 (see chapter four). The most intense ocean response to strong northward windstress from day 40 to around day 61, produced a displacement of $\sim$ 4 km for a depth of 50 m and $\sim$ 20 km if only 10 m of the water column is taken into account. The displacement determined from satellite imagery (images a05, a06 and a07) is greater than 50 km. The intense storm from day 70 to around day 80 again moved shelf water offshore all along the shelf–slope front (image a8) with an offshore displacement in the range of 6–30 km for depths 50 m and 10 m respectively. The image on 22 March shows offshore displacement greater than 50 km. The less intense northward winds from day 90 onwards also helped in driving shelf water into the slope region(image a9 and a10). The most energetic northward wind events for 1993 occurred from day 60 to day 75 and from day 97 onwards (images b05, b06–b09). The wind induced displacement per unit length of coastline during these periods of $\sim$ 8 km and 40 km with depths ranging from 50 to 10 m respectively. These observations illustrate that although northward winds move shelf water offshore, the displacements measured from satellite imagery are probably greater than those determined from wind stress only.

Another observation that can be made from satellite imagery and the wind data is that the ocean response to periods of strong southward wind stress does not appear to always displace the shelf–slope front significantly onshore of the shelf break as observed in SST images. The shelf water that was transported offshore to the slope region moves southwestward and entrains off Cape Hatteras as discussed in detail in chapter four. For example, the strong southward winds during 1–10 February did not move the shelf–slope front or for that matter, shelf water significantly onshore (see images a03 and a04). During SEEP I and II, the sequence of northward and southward events on the shelf produced large fluctuations of the shelf–slope front and the front rapidly returned to its equilibrium position. But this was not always the case at the shelfbreak [*Houghton et al.,* 1988; *Houghton et al.* , 1994]. Hence, one can conclude that northward winds, as has been noted above, appeared to help in shelf water overrunning slope water in the MAB.

6.4.2 Effect of Freshwater Discharge

The volume changes of shelf water in the MAB also appear to originate as a result of changes in the major inflows to the Gulf of Maine [*Mountain,* 1991]. A simple thermohaline model of the Gulf of Maine requires an input of surface colder and less saline Scotian shelf water, which is then mixed at mid-depths during winter with warmer and more saline slope water flowing into the Gulf of Maine at depth through the Northeast Channel to produce the intermediate salinity water leaving the Gulf of Maine and flowing into the MAB. Factors controlling the amount of shelf water available for flow into the Gulf of Maine during early winter–spring may include the magnitude of the St. Lawrence River discharge during the previous spring. An increase in the St. Lawrence discharge, would result in an excess quantity of shelf water (after mixing with slope water in the Gulf of Maine) flowing into the MAB.

To examine whether freshwater discharge from the St. Lawerence River produced the flooding of shelf water observed off New Jersey, the monthly-averaged St. Lawerence River discharge data measured at "LaSalle" (station no. 020A016) for 1991 and 1992 and also multi-year long-term monthly averages (computed from the beginning of 1955 through the end of 1992) are shown in Figure 55 [*Bisagni* personal communication]. The cummulative freshwater discharge from the St. Lawrence increased by 15.1 km^3 during the first five months of 1991 relative to the long term mean (115.17 km^3). The freshwater mixes with more saline slope water in the Gulf of Maine and results in $\sim$ 225 km^3 increase in shelf water (see Note below) entering the MAB by late January 1992. The time lag between the St. Lawerence discharge and the inflow into the MAB, about nine months, is sufficient for the excess outflow to reach the vicinity off New Jersey. Therefore, the shelf water flooding the Slope Sea off New Jersey during late January appears related to excess discharge from the St. Lawerence.

To examine if the outflow from the Chesapeake Bay can cause any significant contribution to the overrunning of shelf water, the monthly averaged discharge from all the rivers that flow into the Chesapeake Bay along with a long–term mean (computed from the beginning of 1950 to the end of 1988) are shown in Figure 56. During spring of 1993 an anomalous large freshwater discharge from the Chesapeake Bay of about 10000 m^3 (an increase of about 6000 m^3 from the mean) is observed. Since the discharge from the Chesapeake Bay occurs further south it could not have contributed to the overrunning of shelf water off New Jersey. However, as shown by *Ketchum* and *Keen* [1955] the changes in the outflow from the Bay can account for the increased volume of shelf water further south in the MAB.

Note: The mean salinity of shelf water and slope water for the winter period are taken as 33 and $35.3^o/oo$ respectively [*Biscaye*, 1994]. To get one part of shelf water

with salinity $33.0°/oo$, the ratio of slope water to freshwater is $\sim$ 15. In other words, the freshwater volume has to be multiplied by $\sim$ 15 to produce the shelf water of required salinity($33°/oo$).

6.4.3 Pressure Gradient Effect

The alongshelf pressure gradient in the MAB is an important force in the shelf circulation [*Stommel and Leetmaa,* 1972; *Csanady,* 1976]. The mechanism that creates the pressure gradient has been suggested to originate in the open ocean. It is interesting to examine how remote offshore forcing, such as the Gulf Stream can alter the pressure gradient and what effect it can have on the shelf water circulation.

The instantaneous path of the Gulf Stream in this region may be complex. Several mechanisms cause the path to move laterally and can induce shifts of 100 km or more in the Stream's path in a few days. Such shifts in the path of the Gulf Stream have shown to discharge fluid from the Stream into the shelf and slope region in the MAB [*Churchill and Cornillon,* 1991]. *Bane et al.* [1988], have also shown that such onshore movements of the Stream strongly increase the mean monthly shelfbreak currents southwestward in the MAB.

Satellite-derived information on the position of the Gulf Stream's shoreward surface thermal front (Figure 8) and the offshore limits of shelf water in the slope region off New Jersey suggest a relationship between the overrunning events and the Stream's position. Figure 57 shows the four-month-long time series(for 1992 and 1993) of the surface position of the Gulf Stream and shelf water on a line extending directly offshore from the shelf break (100 m isobath). Both positions are shown in Figure 8. Since the shelf water overrunning was maximum off New Jersey, this location was used for the offshore position of shelf water. Negative distances for the

Gulf Stream position indicate water onshore of the shelfbreak. Note that the Gulf Stream position varies from -20 to 60 km, whereas the shelf water distances vary from 0 to 140 km from the shelfbreak.

The agreement between the two time series appears good. These data suggests that the shelf water overrunning the Slope Sea off New Jersey was extensive when the Gulf Stream was nearer the shelfbreak in the vicinity of Cape Hatteras and decreased as the Stream veered offshore. This relationship demonstrates that a change in the Gulf Stream position may have a blocking effect on the shelf circulation causing shelf water to overrun the shelf break and move offshore into the slope region.

The water level variation measured at a tide gauge near Duck, North Carolina indicate the presence of Gulf Stream as it veers shoreward. A time series of sea level variation (observed - predicted) is shown in Figure 58 and Figure 59. The straight lines in the figures illustrate the periods when the Gulf Stream was nearer (less than 10 km) the shelf break as determined from satellite data.

In summary, the shelf water overrunning the slope region of the southern MAB is a complex interaction of various forcings which include wind stress, freshwater discharge and the remote offshore forcing from the Gulf Stream.

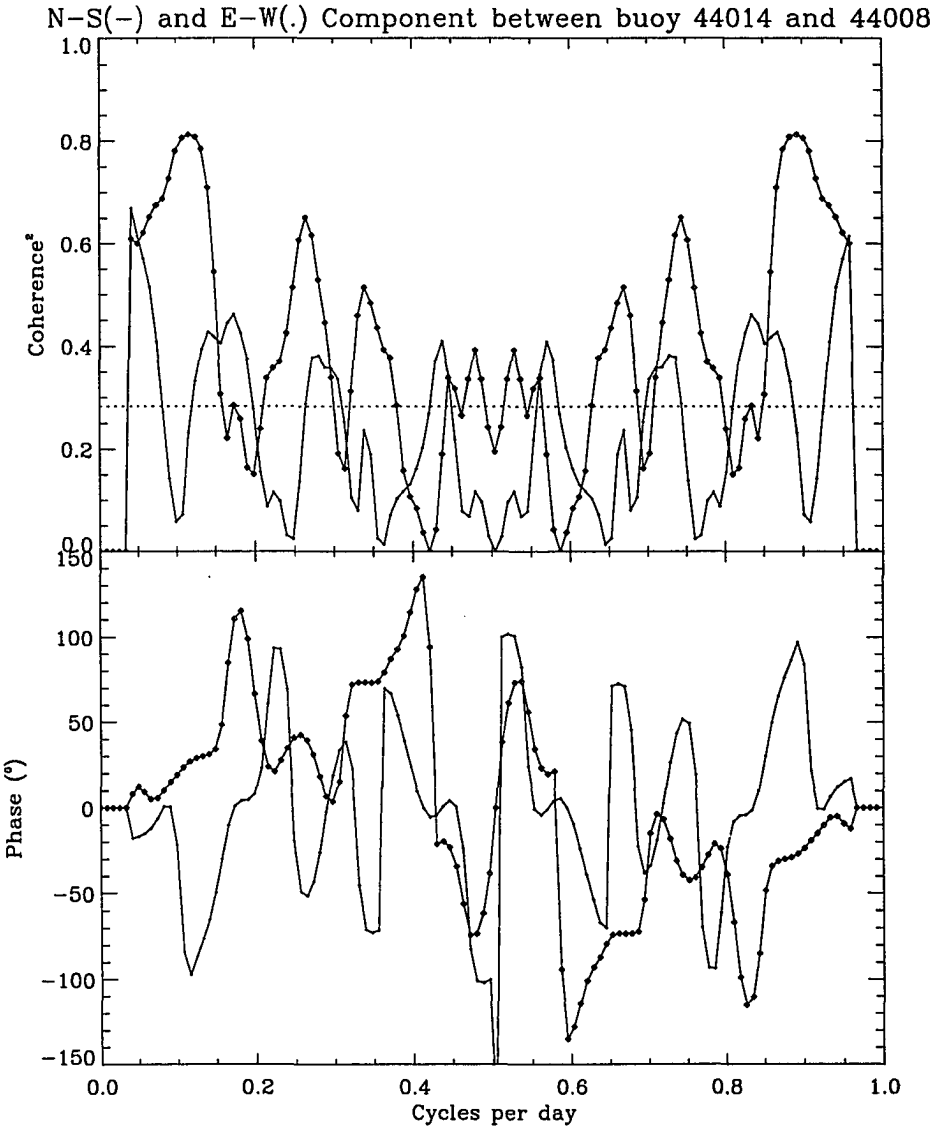

Figure 49: Coherence^2 and Phase of wind stress

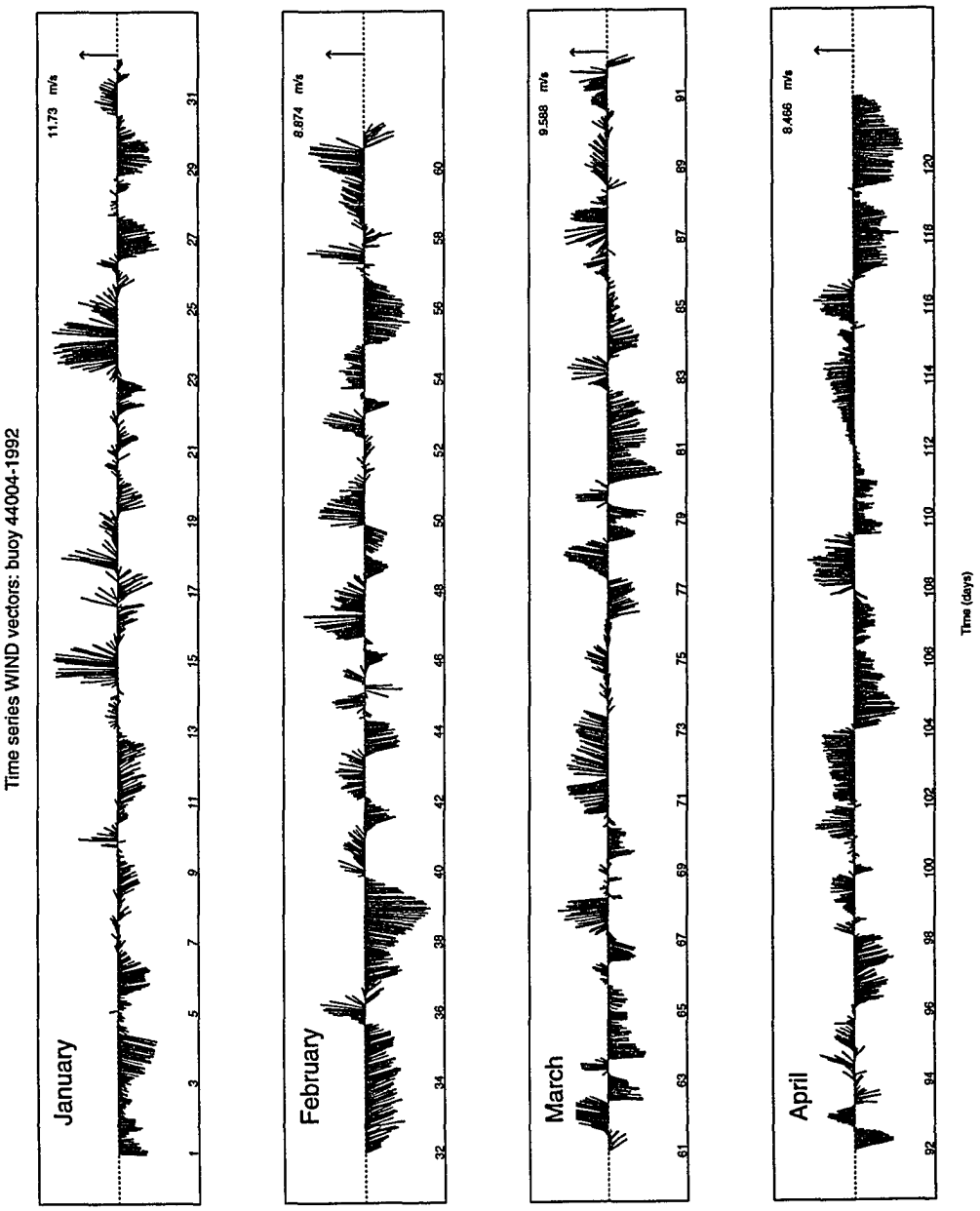

Figure 50: Time series Wind Velocity for buoy 44008, 1992. The velocity on the right hand corner represents the largest magnitude of the wind measured for the month.

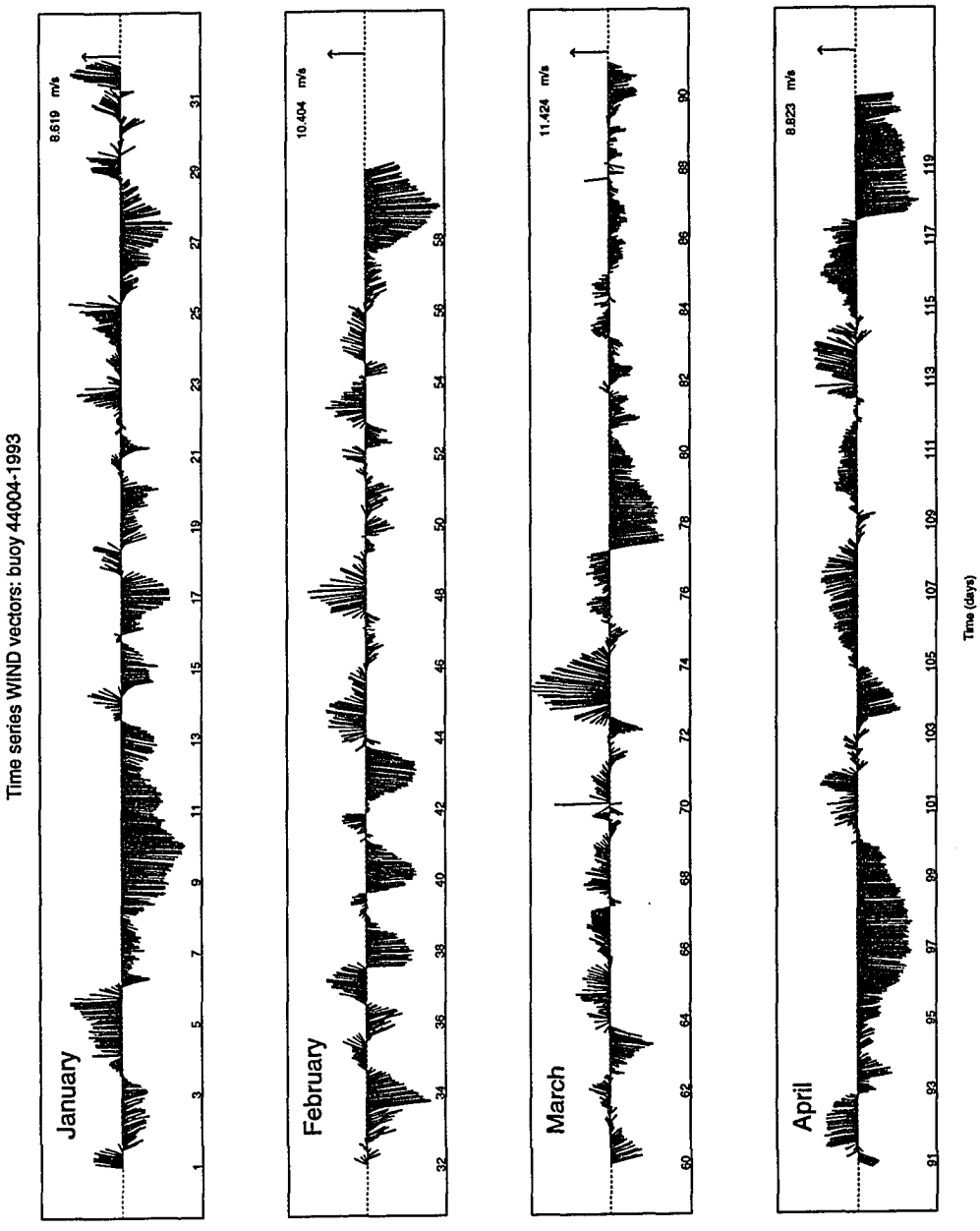

Figure 51: Time series Wind Velocity for buoy 440014, 1993. The velocity on the right hand corner represents the largest magnitude of the wind measured for the month

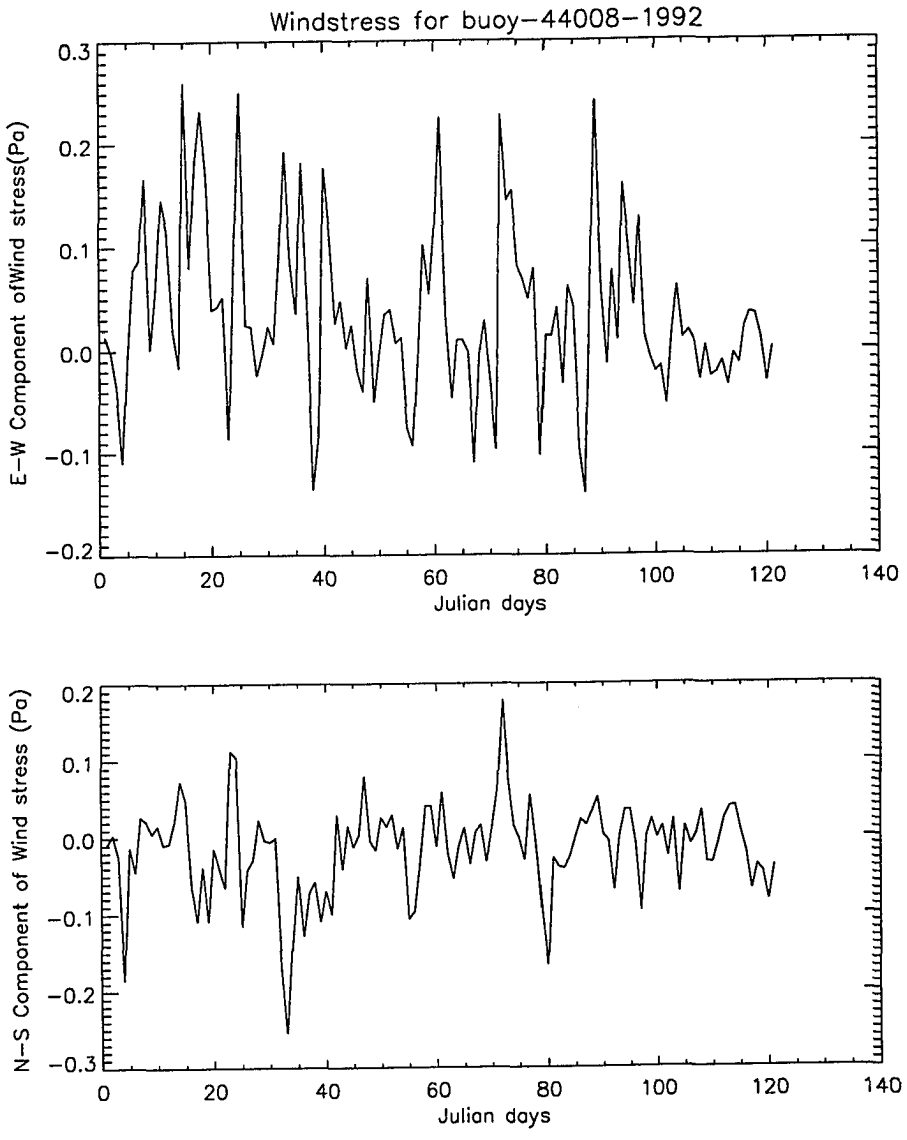

Figure 52: Time series wind stress for buoy 44008, 1992

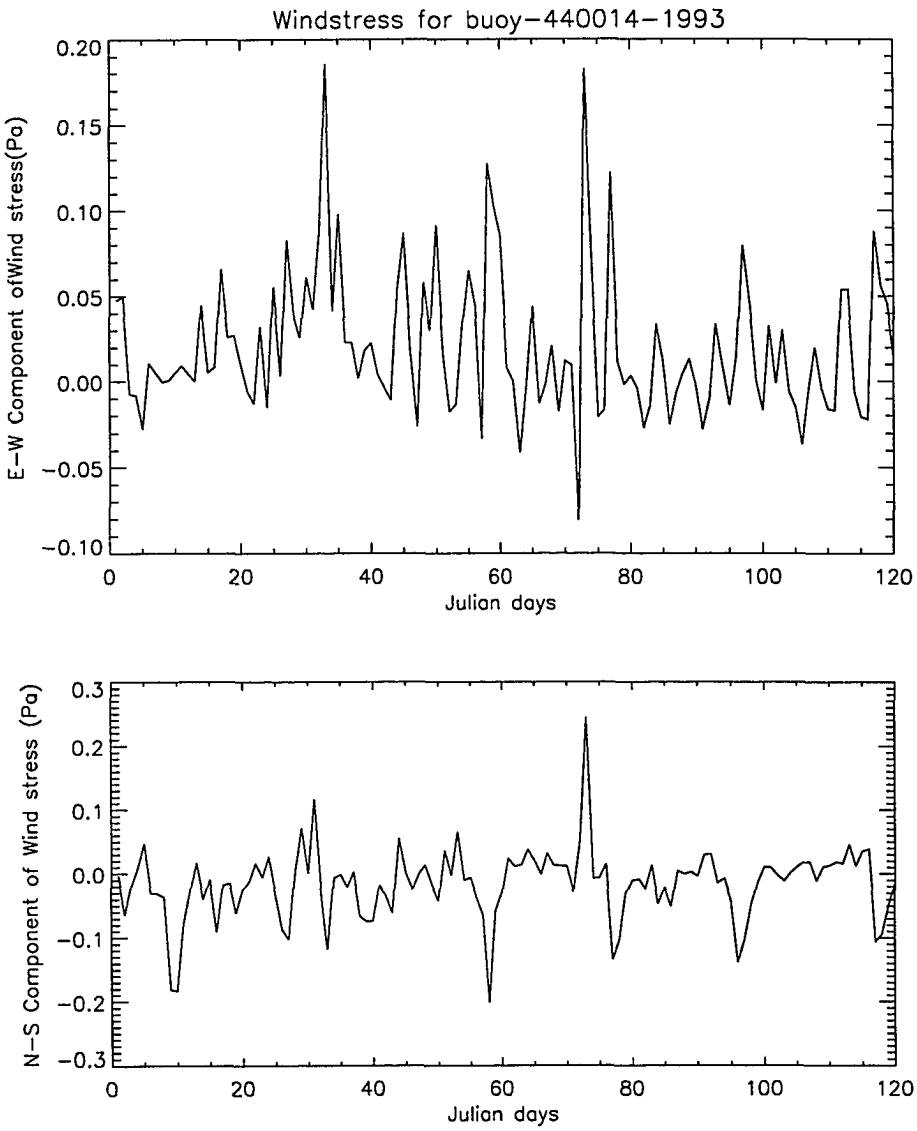

v

Figure 53: Time series wind stress for buoy 44014, 1993

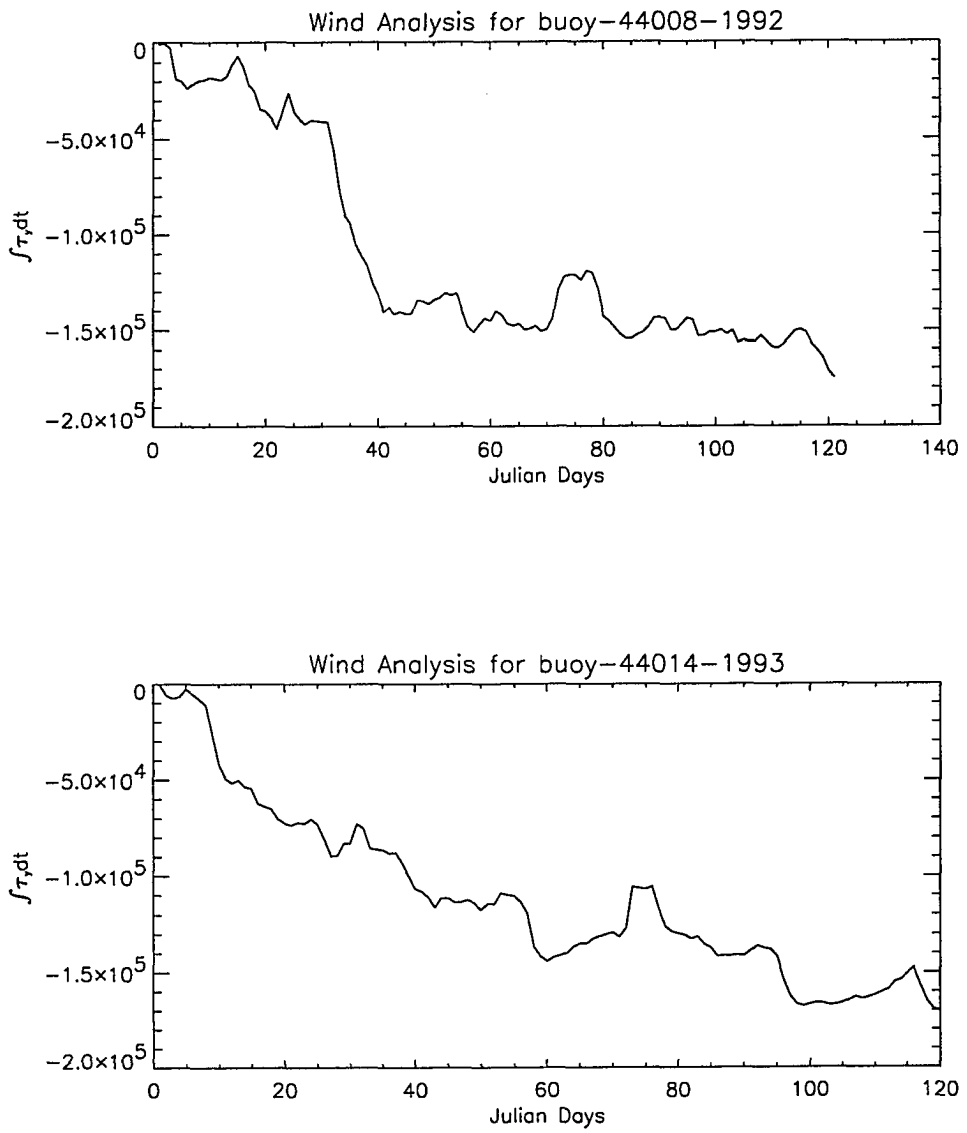

Figure 54: Wind induced Ekman transport for 1992 and 1993

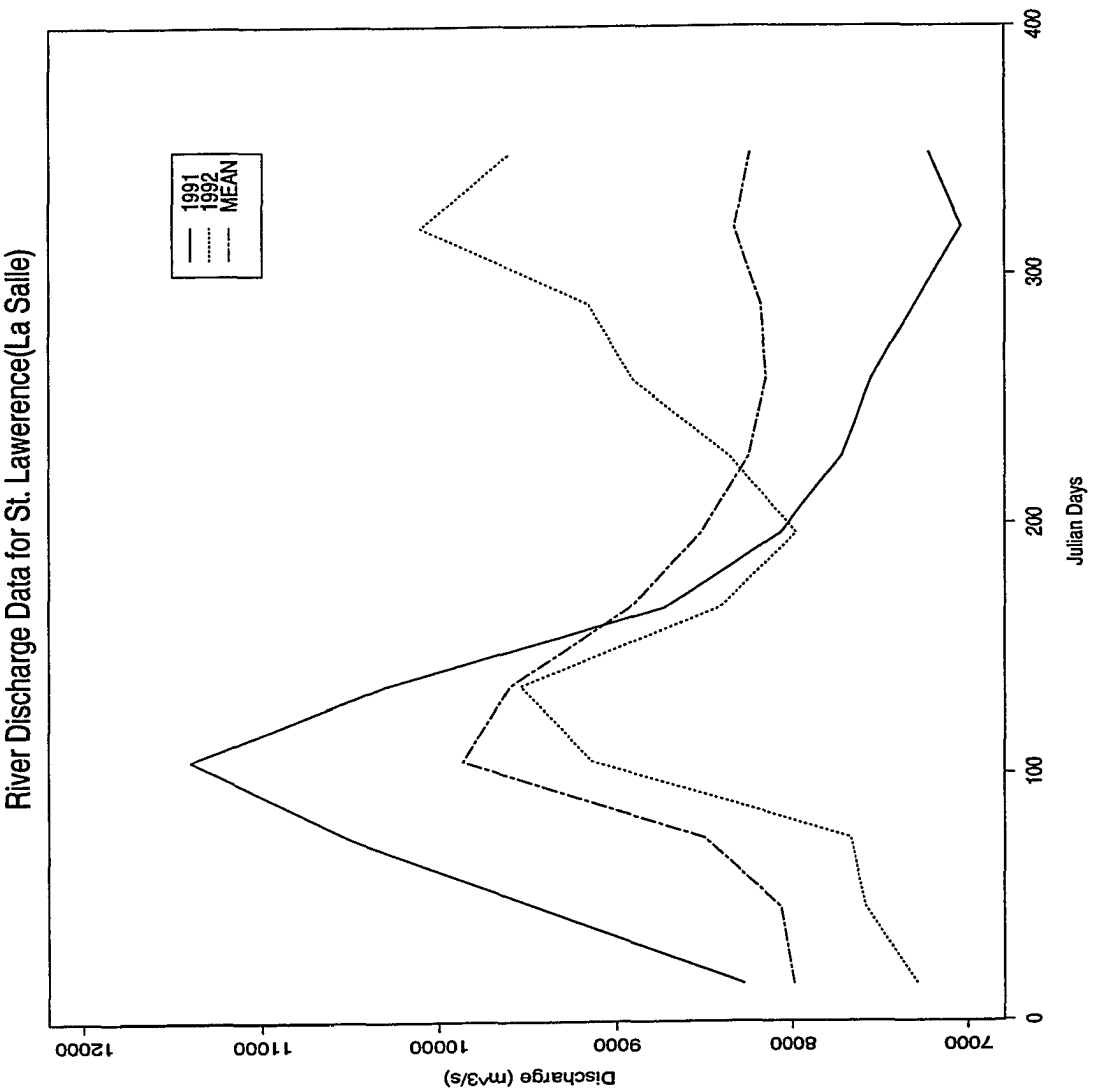

Figure 55: St. Lawerence River discharge

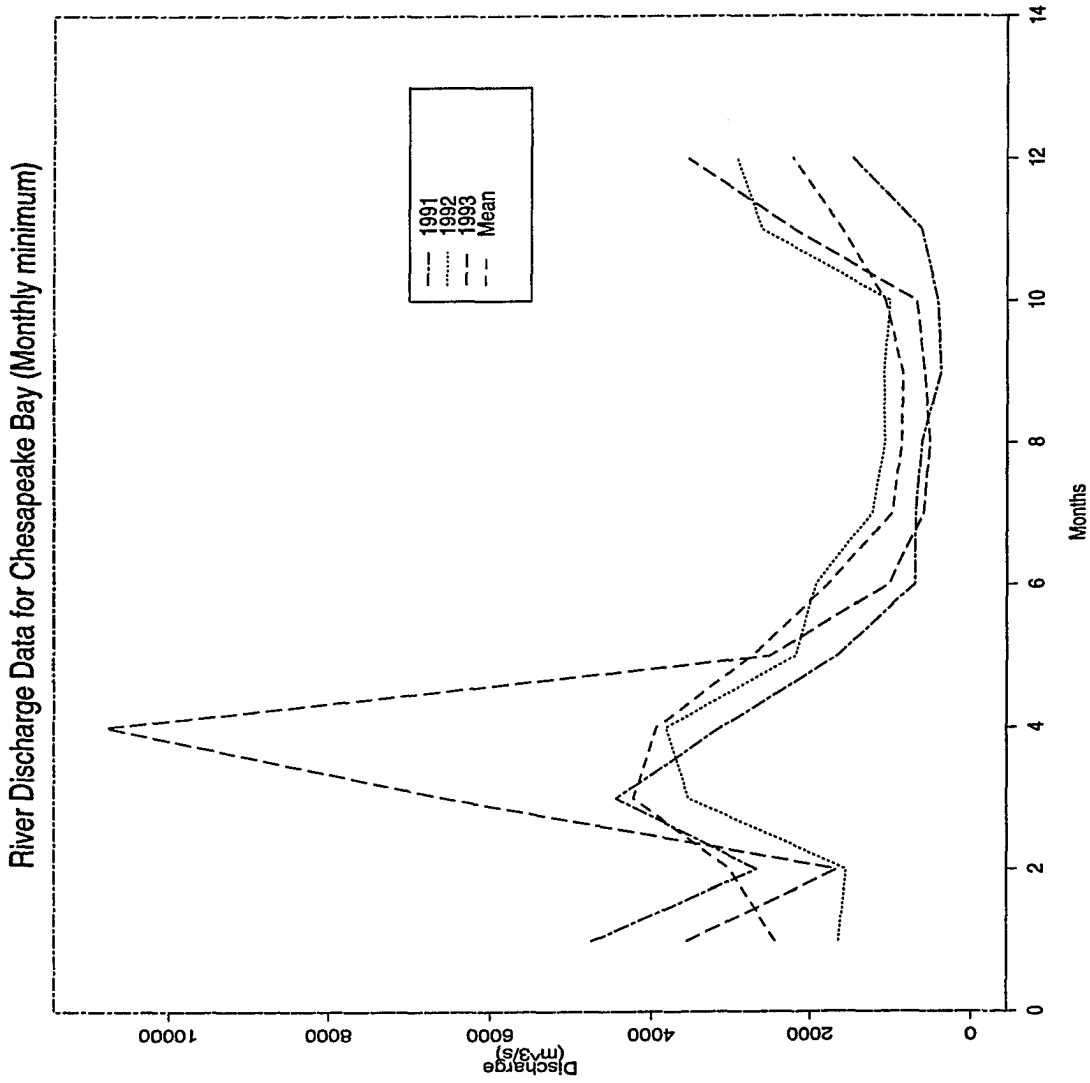

Figure 56: Chesapeake Bay discharge

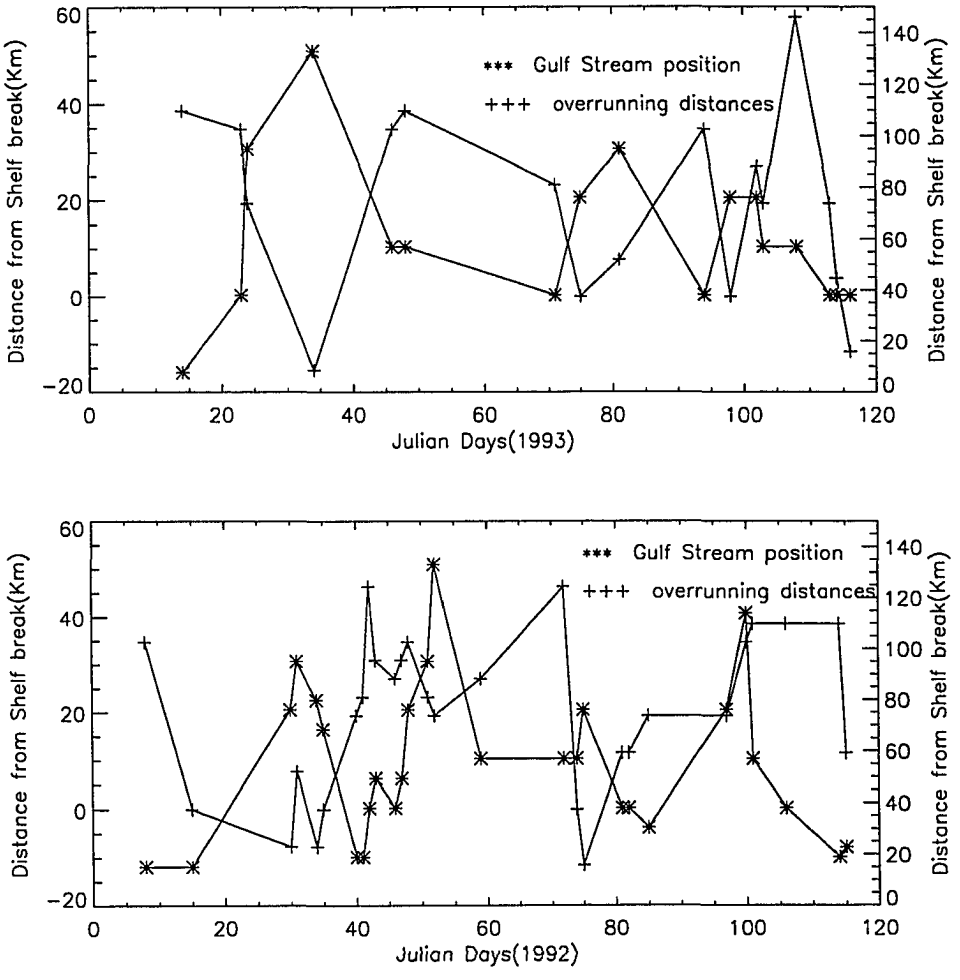

Figure 57: A four-month-long time series(for 1992 and 1993) of the surface position of the Gulf Stream and shelf water on a line extending directly offshore from the shelf break(100 m isobath)

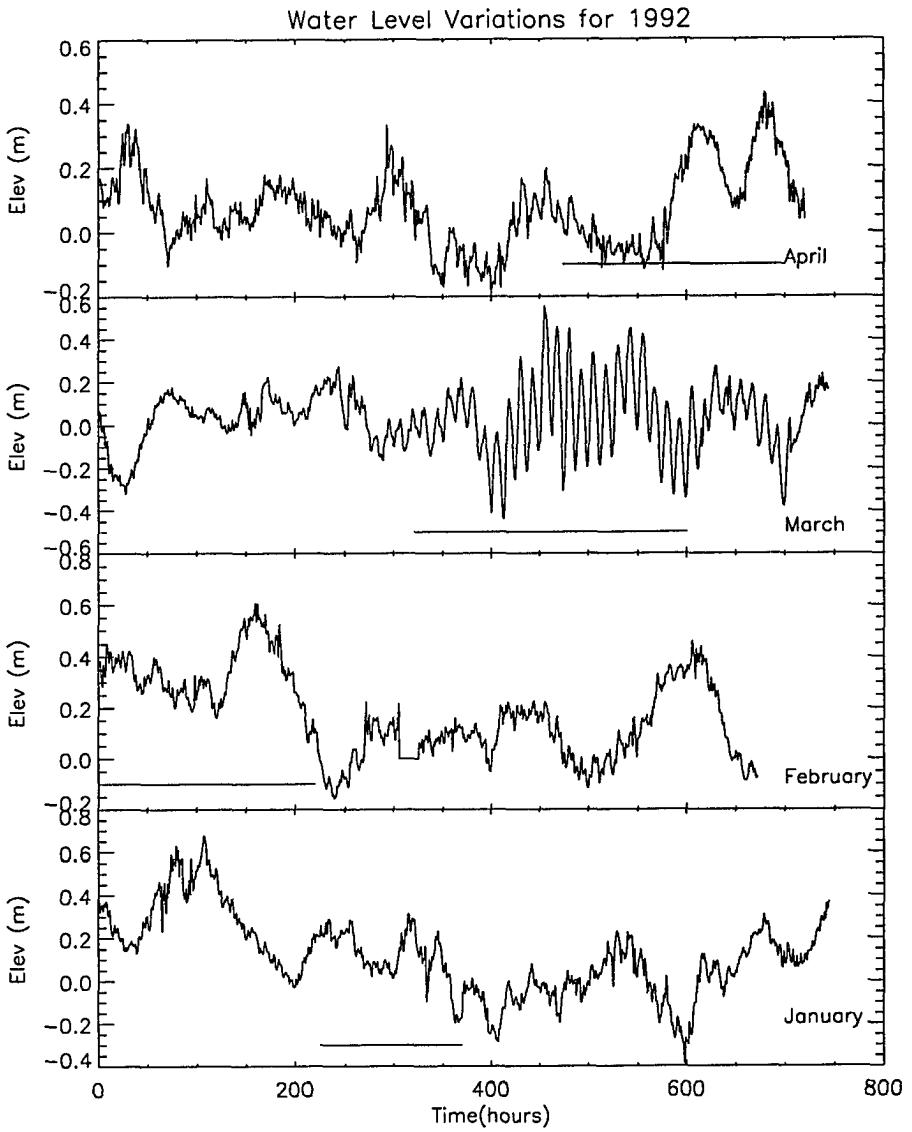

Figure 58: A four-month-long time series of Sea level variation measured at Duck, North Carolina for 1992. The straight lines represent periods when the thermal position of the Gulf Stream was near (less than 10 km) from the shelf break.

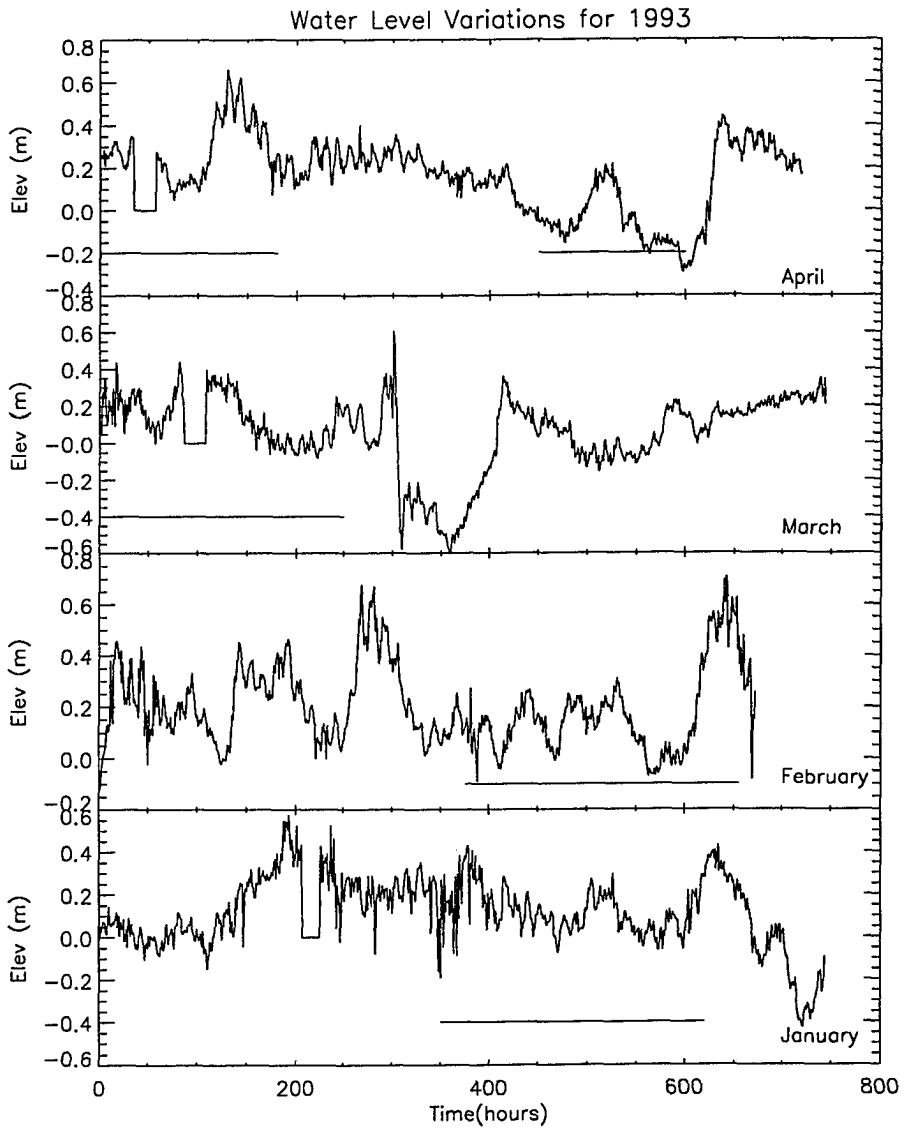

Figure 59: A four-month-long time series of Sea level variation measured at Duck, North Carolina for 1993

7 CONCLUSIONS

This study examined the seasonal variation of shelf and slope waters in the MAB using two years of high resolution (1.47 km^2) sea surface temperature (SST) data derived from NOAA satellites. Additionally, Oleander transects that coincided with the satellite images combined with earlier data (eg. historical data) were used in the analysis of the images.

The two–year (1992 and 1993) SST analysis revealed extensive overhang of shelf water into the slope region. These protrusions of shelf water occurred episodically and coherently along shelf distances of several hundred kilometers. The satellite images combined with *in situ* data further illustrated that the overrun shelf water, bounded by the shelf–slope front offshore and beneath, enclose a large volume of shelf water. The shelf water was advected southwestward in several episodes and caused extensive overrunning of the Slope Sea. The large shelf water volume produced by overrunning events was transported southwestward along the upper slope and later accounted for the entrainment of shelf water by the eastward flowing Gulf Stream in the vicinity of Cape Hatteras.

The focus of this work was on estimation of the velocity, volume and transport of the overrun shelf water from satellite images and *in situ* data. The velocity of shelf water overrunning the slope region was determined from sequential satellite imagery using the feature tracking method. The satellite feature tracking showed a maximum velocity (~ 0.20 m s^{-1}) off New Jersey which decreased slightly as the episodic events advected towards Cape Hatteras. On the average, three to four episodes could be identified during a period of approximately three months from winter to spring. The episodes of shelf water overrunning the Slope Sea originated off New Jersey (at the New York bight apex) around the end of January and was advected southwestward

along the upper slope region. Each episode lasted about 30 days. The high rate of advection of the overrun shelf water over the upper slope region suggested that the shelf water, bounded by the front offshore and to a depth of $\sim$ 50 m, could be carried southwestward with the help of the upper slope current along the western flank of the Slope Sea.

The volume of shelf water that overrun the slope region showed a general increase from late January to a maximum of $\sim$ 2000 km^3 on day 80 during 1992. In addition there was another peak at about day 100. During 1993, although the overrunning started earlier, the volume was considerably less than in 1992. The maximum volume ($\sim$ 2000 km^3) again occurred during end of March which may be due to the accumulation of shelf water in different episodes as in 1992. The shelf water volume uniformly decreased until end of April as the shelf–slope front retreated back to its normal position over the shelf break. The mean volume of the overrun shelf water (between the shelf break and the location of the shelf–slope front) was about 1600 km^3 for 1992 and 900 km^3 for 1993. This volume comprised between 25–45% of the total volume of the MAB and showed that an important component of the shelf water volume in the MAB actually lies offshore of the shelf break.

A rough estimate of the transport yielded an episodic annual average of about 0.12 Sv. This large episodic shelf water was transported along and across the Slope Sea and its fate was largely influenced by the gyre circulation in the vicinity of Cape Hatteras. The SST images showed that the overrun shelf water was entrained intermittently into the Slope Sea at various locations between 38°N and Cape Hatteras and eventually drained into the eastward flowing branch of the Gulf Stream.

Potential forcing of the shelf water, causing it to overrun the slope region were also examined. Northward winds appeared to force the shelf water offshore to distances of $\sim$ 10 km to 40 km. However, the satellite determined offshore extent of the

overrun shelf water was greater than that produced by wind events. This showed that wind forcing of shelf water was not solely responsible for large overrunning events. The fresh water discharge from the St. Lawerence was linked to the inflow of shelf water into the MAB. Interannual variations of St. Lawerence discharge related to the shelf water flooding of the Slope Sea off New Jersey. Another likely mechanism that could contribute to the overrunning events is the onshore displacement of the Gulf Stream in the vicinity of Cape Hatteras. The fluid discharged by the Gulf Stream did increase the sea level near Cape Hatteras, causing a blocking effect on the shelf circulation. This resulted in shelf water overrunning the slope region especially off New Jersey. In conclusion, the shelf water overrunning the slope region in the southern MAB appears to be a complex interaction of various forces including wind stress, fresh water discharge and the blocking effect on shelf circulation due to the onshore veering of the Gulf Stream.

REFERENCES

Allen, J. S., R. C. Beardsley, J. O. Blanton, W. C. Boicourt, B. Butman, L. K. Coachman, A. Huyer, T. H. Kinder, T. C. Royer, J. D. Schumacher, R. L . Smith, W. Sturges and C. D. Winant, Physical Oceanography of Continental shelves, *Reviews of Geophysics and Space Physics*, 21, 1149-1181, 1983.

Atkinson, L. P., J. O. Blanton, and E. B. Haines, Shelf Flushing Rates based on the Distribution of Salinity and Freshwater in the Georgia Bight, *Estuarine and Coastal Marine Science*, 7, 465-472, 1978.

Atkinson L. P., Hydrography and nutrients of the southeastern U. S. continental shelf, in *Oceanography of the Southeastern U. S. Continental Shelf, Coastal and Estuarine Sciences*, 2, edited by L. P. Atkinson , D. W. Menzel, and K. A. Bush, 77-92, AGU, Washington, D. C., 1985.

Bane Jr. J. M., O. B. Brown, R. H. Evans and P. Hamilton, Gulf Stream Remote Forcing of Shelf Break Currents in the Mid-Atlantic Bight, *Geophysical Research Letters*, 15, 13065-13087, 1990.

Bakun, A., Coastal upwelling indices, west coast of North America, 1946-71, *NOAA Tech. Rep., NMFS SSRF-671*, U. S. Dept. of Commerce, 103 pp.

Beardsley, R. C. and C. N. Flagg, The water structure, mean currents, and shelf-water/slope-water front on the New England Continental Shelf, *Memoires Societe Royale des Sciences de Liege,* tome X, 209-225, 1976.

Bigelow, H. B., Studies of the waters on the Continental shelf, Cape Cod to Chesapeake Bay. 1. The cycle of temperature, *Physical Oceanography and Meteorology*, 2(4), 135 , 1933.

Bisagni, J. J., Lagrangian current measurements within the eastern margin of a warm-core Gulf Stream ring, *Journal of Physical Oceanography*, 13(4), 709-715, 1983.

Biscaye, P. E., C. N. Flagg and P. G. Falkowski, The Shelf Edge Exchange Processes experiment, SEEP-II: an introduction to hypotheses, results and conclusions, *Deep-Sea Research Part II*, 41, No. 2/3, 231-252, 1994.

Blanton J. O., J. A. Amft and D. K. Lee, Windstress and heat fluxes Observed during winter and spring 1986, *Journal of Geophysical Research*, 94, 10,080–10,098, 1989.

Bower A. S. and T. Rossby, Evidence of cross-frontal exchange processes in the Gulf Stream based on isopycnal RAFOS float data, *Journal of Physical Oceanography*, 19, 1177-1190, 1989.

Breaker L. C., V. M. Krasnopolsky, D. B. Rao and X.-H. Tan, The Feasibility of Estimating Ocean Surface Currents on an Operational Basis Using Satellite Feature Tracking Methods, *Bulletin of the American Meteorological Society*, 75(11), 2085-2095, 1994.

Brink, K. H., Coastal Ocean Physical Processes, *Reviews of Geophysics*, 25, 204-216, 1987.

Brown, W. S., and R. C. Beardsley, Winter circulation in the western Gulf of Maine, 1. Cooling and water mass formation, *Journal of Physical Oceanography*, 8, 265-277, 1978.

Chapman, D. C., A simple model of the formation and maintenance of the shelf/slope front in the Middle Atlantic Bight, *Journal of Physical Oceanography*, 16, 1273-1279, 1986.

Chapman, D. C. and R. C. Beardsley, On the Origin of Shelf Water in the Middle Atlantic Bight, *Journal of Physical Oceanography*, 19, 384-391, 1989.

Chern, C.-S., J. Wang and D.-P. Wang, The exchange of Kuroshio and East China Sea Shelf Water, *Journal of Geophysical Research*, 95, 16017-16023, 1990.

Churchill, J. H., P. C. Cornillon and G. W. Milkowski, A Cyclonic Eddy and Shelf-Slope Water Exchange Associated With a Gulf Stream Warm-Core Ring, *Journal of Geophysical Research*, 91, 9615-9623, 1986.

Churchill, J. H., P. C. Cornillon and P. Hamilton, Velocity and Hydrographic Structure of Subsurface Shelf Water at the Gulf Stream's Edge, *Journal of Geophysical Research*, 94, 10791-10800, 1989.

Churchill, J. H. and P. C. Cornillon, Water Discharged From the Gulf Stream North

of Cape Hatteras, *Journal of Geophysical Research*, 96, 22227-22243, 1991.

Churchill, J. H. and P. C. Cornillon, Gulf Stream water on the shelf and upper slope north of Cape Hatteras, *Continental Shelf Research*, 11, 409-431, 1991.

Churchill, J. H., E. R. Levine, D. N. Connors and P. C. Cornillon, Mixing of shelf, slope and Gulf Stream water over the continental slope of the Middle Atlantic Bight, *Deep-Sea Research*, 40, 1063-1085, 1993.

Cochrane J. D., and F. J. Kelly, Low-Frequency Circulation on the Texas-Louisiana Continental Shelf, *Journal of Physical Oceanography*, 19, 1317-1332, 1989.

Cornillon,P. C., R. Weyer and G. Flierl, Translational velocity of warm-core rings relative to the Slope Water, *Journal of* , 91, 10645-10659, 1986.

Cresswell, G. H., Quasi-synoptic monthly hydrography of the transition region between coastal and slope water south of Cape Cod, Massachusetts, Ref. 67-35, Woods Hole Oceanographic Institution, Woods Hole, MA, 1967.

Csanady, G. T., Mean Circulation in Shallow Seas, *Journal of Geophysical Research*, 81, 5389-5399, 1976.

Csanady G. T., Circulation in the Coastal Ocean, Part 1, *EOS Transactions* , 62, 9-1, 1981.

Csanady, G. T. and P. Hamilton, Circulation of slopewater, *Continental Shelf Research*, 8, 565-624, 1988.

Davis, R. E., Drifter observations of coastal surface currents during CODE: The method and descriptive view, *Journal of Geophysical Research*, 90, 4741-4755, 1985.

Emery, W. J., and L. A. Mysak, Dynamical Interpretation of Satellite-Sensed Thermal Features off Vancouver Island, *Journal of Physical Oceanography*, 10, 961-970, 1980.

Evans, R. H., K. S. Baker, O. B. Brown, and R. C. Smith, Chronology of warm-core

ring 82B, *Journal of Geophysical Research*, 90, 8803-8811, 1985.

Fairbanks, R. G., The Origin of Continental shelf and slope water in the New York Bight and Gulf of Maine: Evidence from H_2^{18}/H_2^{16} O radio measurements, *Journal of Geophysical Research*, 77, 3248-3255, 1982.

Flagg, C., L. Vermersch and R. Beardsley, Report on the 1974 MIIT New England shelf dynamics experiment, Part 2; the moored array. Dep. Meteorol. Mass. Inst. Technol., Lab. Rep. (Unpublished), 1977.

Fisher, A., Entrainment of shelf water by the Gulf Stream northwest of Cape Hatteras, *Journal of Geophysical Research*, 77, 3248-3255, 1972.

Ford, W. L., J. R. Longard, and R. E. Banks, In the nature, occurrence and origin of cold low salinity water along the edge of the Gulf Stream, *Journal of Marine Research*, 11, 281-293, 1952.

Fuglister, F. C., Gulf Stream'60, *Progress in Oceanography*, 1, 265-373, 1963.

Garfield, N. III., and D. L. Evans, Shelf Water Entrainment by Gulf Stream Warm-Core Rings, *Journal of Geophysical Research*, 92, 13003-13012, 1987.

Garvine R. W., K. C. Wong., G. G. Gawarkiewicz., R. K. McCarthy., R. W. Houghton and Aikman III. F., The Morphology of Shelf Break Eddies, *Journal of Geophysical Research*, 93, 15593-15608, 1988.

Gordon, A. L.., A. F. Amos, and R. D., Gerard, New York Bight water stratification-October 1974, Special Symposia, Middle Atlantic Continental Shelf and the NYB, *The American Society of Limnology and Oceanography, M. Grant Gross, Ed.,*, Vol 2, 45-57, 1976.

Halliwell, G. R. and C. N. K. Mooers, The Space-Time Structure and Variability of the Shelf Water-Slope Water and Gulf Stream Surface Temperature Fronts and Associated Warm-Core Eddies, *Journal of Geophysical Research*, 84, 7707-7725, 1979.

Hood, R. R., M. R. Abbott, A. Huyer, and P. M. Kosro, Surface Patterns in Temperature, Flow, Phytoplankton Biomas, and Species Composition in the Coastal Transition Zone off Northern California, *Journal of Geophysical Research*, 95,

18081-18094, 1990.

Hopkins T. S., and N. Garfield, Gulf of Maine intermediate water, *Journal of Marine Research*, 37(1), 103-139, 1979.

Horne, E. P. W., Interleaving at the subsurface front in the slope water off Nova Scotia, *Journal of Geophysical Research*, 83, 3659-3671, 1978.

Houghton, R. W., R. Schlitz, R. C. Beardsley, B. Butman, and J. L. Chamberlin, The Middle Atlantic Bight cold pool: Evolution of the temperature structure during summer 1979, *Journal of Physical Oceanography*, 12, 1019-1029, 1982.

Houghton R. W. and J. Mara., Physical/Biological Structure and Exchange Across the Thermohaline Shelf/Slope Front in the New York Bight, *Journal of Geophysical Research*, 88, 4467-4481, 1983.

Houghton R. W. C. N. Flagg and L. J. Pietrafesa, Shelf–slope water frontal structure, motion and eddy heat flux in the southern Middle Atlantic Bight, *Deep-Sea Research, Part II*, 41, No. 2/3,273-306, 1994.

Iselin, C. O'D., A study of the circulation of the western North Atlantic, PPOM 4, *No. 4, MIT-Woods Hole Oceanographic Institution*, 110, 1936.

Joyce, T. M., J. K. B. Bishop and O. T. Brown, Observations of offshore shelf-water transport induced by a warm-core ring, *Deep-Sea Research*, 39, S97-S113, 1992.

Kawamura, H., K. Hanawa and Y. Toba, On The Characteristic Structure Of Horizontal Interleaving At The Northern Edge Of The Kuroshio And The Kuroshio Extension, *Ocean Hydrodynamics Of The Japan And East China Sea*, edited by T. Ichiye, 333-346, 1984.

Kupferman, S. L., and N. Garfield, Transport of low-salinity water at the slopewater-Gulf Stream boundary, *Journal of Geophysical Research*, 82, 3481-3486, 1977.

Large, W. G., and S. Pond, Open ocean momentum flus measurements in moderate to strong winds, *Journal of Physical Oceanography*, 11, 324–336, 1981

Lambert, R. B., Jr., Lateral mixing process in the Gulf Stream, *Journal of Physical Oceanography*, 12, 851-861, 1982.

Lillibridge III. J. L., G. Hitchcock., T. Rossby, E. Lessard , M. Mork and L. Golmen, Entrainment and Mixing of Shelf/Slope Waters in the Near-Surface Gulf Stream, *Journal of Geophysical Research*, 95, 13065-13087, 1990.

Loder J. W., B. Petrie and G. Gawarkiewicz, The Coastal Ocean off Northeastern North America: A Large–Scal View, submitted for publication in SEA, 1995.

Lyne V. D. and G. T. Csanady, A compilation and description of hydrographic transects of the Mid-Atlantic Bight shelf-break front, Woods Hole Oceanographic Institution, Technical Report, WHOI-84-19, 1984.

Manning J., Middle Atlantic Bight Salinity: Interannual Variability, *Continental Shelf Research*, 12, 123-137, 1992.

McLellan, H. J., On the distinctness and origin of the slope water off the Scotian Shelf and its easterly flow south of the Grand Banks, *Journal of the fisheries Research Board of Canada*, 14, 213-239, 1957.

Minnett P. J., Consequences of Sea Surface Temperature Variability on the Validation and Application of Satellite Measurements, *Journal of Geophysical Research*, 96, 18475-18490, 1991.

Morgan, C. W., and J. M. Bishop, An example of Gulf Stream eddy-induced water exchange in the Mid-Atlantic Bight, *Journal of Physical Oceanography*, 7, 472-479, 1977.

Mountain, D. G., The Volume of Shelf Water in the Middle Atlantic Bight: Seasonal and Interannual Variability, 1977-1987, *Continental Shelf Research*, 12, 251-268, 1991.

Njoku, E. G., T. P. Barnett, R. M. Laurs, and A. C. Vastano, Advances in Satellite Sea Surface Temperature Measurements and Oceanographic Applications, *Journal of Geophysical Research*, 90, 11,573-11,586, 1985.

Pelegri, J. L., G.T. Csanady, Nutrient Transport and Mixing in the Gulf Stream, *Journal of Geophysical Research*, 96, 2577-2583, 1991.

Ou H. W., Wind-driven motion near a shelf-front, *Journal of Physical Oceanography*, 14, 985–993, 1984.

Posmentier, E. S., and R. W. Houghton, Springtime Evolution of the New England Shelf Break Front, *Journal of Geophysical Research*, 86, 4254-4259, 1981.

Qiu, B., Toda and N. Imasato, On Kuroshio Front Fluctuations in the East China Sea Using Satellite and *in situ* Observational Data, *Journal of Geophysical research*, 95, 18191-18204, 1990.

Ramp, S. R., The interaction of warm core rings with the shelf water and shelf/slope front south of New England, Ph.D. thesis, 137 pp., Graduate School of Oceanography, University of Rhode Island, Kingston, 1986.

Rienecker M. M., C. N. K. Mooers, D. E. Hagan and A. R. Robinson, A cool anomaly off Northern California: an investigation using IR imagery and *in situ* data, *Journal of Geophysical Research*, 90, 4807-4818.

Richardson, P. L., On the crossover between the Gulf Stream and the Western Boundary Undercurrent, *Deep-Sea Research*, 24, 139-159, 1977.

Rossby, C. G., Dynamics of steady ocean currents in the light of experimental fluid mechanics, *PPOM, 5, Woods Hole Oceanographic Institution*, 1-43, 1936.

Shaw, P.-T., The Intrusion of Water Masses Into the Sea Southwest of Taiwan, *Journal of Geophysical Research*, 90, 18213-18226, 1989.

Shaw, P.-T., The Seasonal Variation of the Intrusion of the Philippine Sea Water Into the South China Sea, *Journal of Geophysical Research*, 96, 821-827, 1991.

Shaw, P.-T, Shelf Circulation Off the southeast coast of China, *Review of Aquatic Science*, 6, 1-28, 1992.

Svejkovsky, J., Sea surface flow estimation from Advanced Very High Resolution Radiometer and Coastal Zone Color Scanner Satellite Imagery: a verification study, *Journal of Geophysical Research*, 93, 6735–6743.

The Bunker Climate Atlas of the North Atlantic Ocean, Vol. 1: Observations, editors: Michael Ghil, Robert Sadourny and Jurgen Sundermann,*Springer-Verlag*, 1985.

The Bunker Climate Atlas of the North Atlantic Ocean, Vol. 2: Air Sea Interactions, editors: Michael Ghil, Robert Sadourny and Jurgen Sundermann,*Springer-Verlag*, 1987.

Wang D. -P, Effects of continental slope on the mean shelf circulation, *Journal of Physical Oceanography*, 12, 1524-1526, 1982.

Wright, W. R., The limits of shelf water south of Cape Cod, 1941 to 1972, *Journal of Marine Research*, 34(1), 1-14, 1976.

Wright, W. R. and C. E. Parker, A volumetric temperature/salinity census for the Middle Atlantic Bi9ght, *Limnol. Oceanogr.*, 21 (4), 563–571, 1976.

VanCamp, L., L. Nykjaer., E. Mittelstaedt and P. Schlittenhardt, Upwelling and boundary circulation off Northwest Africa as depicted by infrared and visible satellite observations, *Progress in Oceanography*, 26, 357-402, 1991.

Yoder, J. A., L. P. Atkinson, T. N. Lee, H. H. Kim and C. R. McClain, Role of Gulf Stream frontal eddies in forming phytoplankton patches on the outer southeastern shelf, *Limnology and Oceanography*, 26(6), 1103-1110, 1981.

AJOY KUMAR

941 Bolling Avenue, # 29
Norfolk, VA 23508
Phone(Res): (804)-489-1320
Phone(Off): (804)-683-4599
email : ajoy@ccpo.odu.edu

EDUCATION

Ph.D., Oceanography, Old Dominion University, Norfolk, VA, May, 1996
M.S., Physics, University of Madras, India, 1987
B.S., Physics, University of Madras, India, 1985

RESEARCH INTERESTS

Oceanographic Data Collection, Analysis and Interpretation,
Optical Oceanography, Remote Sensing of Ocean Temperature and Color.

EXPERIENCE

Graduate Student and Research Assistant, *Old Dominion University, 1991-1996.*
Senior Research Fellow, *National Institute of Oceanography, Goa, India, 1987-1990.*

PUBLICATIONS AND PRESENTATIONS

J. J. Goes, H. Do. R. Gomes, A. Kumar, A. H. Parulekar, A. Gouveia and L. V. G. Rao. Satellite and Ship Studies of Phytoplankton along the West Coast of India. Oceanography of the Indian Ocean, B. N. Desai (editor), 1992.

P. V. Sathe and Ajoy Kumar. Remote Sensing of Sea State by the Brewster's Angle Technique. Defence Science Journal, Vol 40, 2, 1990, pp 119-131.

S. K. Sasmal, Ajoy Kumar and L. V. G. Rao. Underwater irradiance in the Arabian Sea. (submitted to Indian Journal of Marine Science).

Ajoy Kumar, S. K. Sasmal and L. V. G. Rao. The inherent and apparent properties

in the Arabian Sea from irradiance measurements. (submitted to Indian Journal of Marine Science).

Ajoy Kumar and G. T. Csanady. Overrunning of Slope Sea by Shelfwater in the Southern Mid-Atlantic Bight. (manuscript in preparation).

Ajoy Kumar and L. P. Atkinson. Characterization of Water Circulation Over the Sandbridge Study Area Using CZCS imagery. (manuscript in preparation).

"Satellite Observation of Shelfwater Overflow in the Southern Mid-Atlantic Bight", at AGU Fall meeting, San Francisco, 1994.

"NASA Summer School for Earth Sciences, Processes of Global Change", August 9-13, 1993.